Sudan University of Science and Technology

College of Graduate Studies

Photo-Decolorization of Dyes in Water Using Titanium Dioxide Nanoparticles Under Solar Radiation

الإزالة الضوئية لألوان محاليل الأصباغ المائية بإستخدام جسيمات نانومترية لثاني أكسيد التيتانيوم تحت أشعة الشمس

A Thesis submitted in fulfillment of the requirements for the degree of Doctor of Philosophy in the chemistry

By

Yasmin Abd Elrazeg Ahmed Elhady

B.Sc. in chemical Laboratory – SUST (2001)

Post graduate Diploma in Chemistry - University of Gezira (2009)

M.Sc.in Chemistry - University of Gezira (2011)

Supervisor: Prof. Elmugdad Ahmed Ali

Co-supervisor: Dr. Adil Elhag Ahmed

2017

Dedication

I dedicate this work to all who stands with me to accomplish this work

To my mother,

Father,

Brothers and sisters,

and

All family and friends

With my best wishes.

Acknowledgements

First of all I thank Allah, after I feel grateful and indebted to my supervisor Prof. Elmugdad Ahmed Ali and Co-supervisor Dr. Adil Elahj, I would say that without their academic guidance, constant encouragement effort and revising the text. Special thanks go to Dr. Saleh Hamdato who built up the solar collector in his company. I would say without the solar collector it would have been impossible to do my experiments. Similar level of merits also goes to technician Ahmed, who designed the photo-reactor and Dr. Abd Elsakhi and Dr. Abd Elgafar for characterizing the catalysts.

This followed by warm thank to College of Water and Environmental Engineering, Sudan University of Science and Technology where all these experiments were carried at their laboratories. Countless thanks to Miss Sara Youssef.

Abstract

In this research work a feasible titanium dioxide photo-catalytic technology for removal of dyes from wastewater was explored in four stages; the synthesis and characterization of two catalysts, optimization of parameters influencing the photo-catalytic process, photo-decolortization process of four different dyes have been investigated to effect of each catalysts and kinetic studies of photo-decolorization of the dyes. The results showed that sol-gel method along with and using titanium tetrachloride as starting material is the best route to synthesize TiO_2 nanoparticles with optimum properties. From X-Ray Diffraction (XRD) data analysis it was found that both TiO_2 sol-gel which is prepared by sol-gel method and pure TiO_2 are antase phase with the particles size of pure TiO_2 (49.11070nm), TiO_2 sol-gel (22.0198nm), having high crystallinity and purity. From Fourier Transform Infra-Red Spectroscopy (FTIR) data, the spectra of both TiO_2 pure and TiO_2 sol-gel have the same vibrations frequency (400 – 800cm^{-1}) characteristic Ti—O, (1426-1696 cm^{-1}) characteristic of (O—Ti—O) bond and (Ti = O) bond). The specific surface areas of pure TiO_2 were (46.962 m^2/g), TiO_2 sol-gel (38.264 m^2/g.). The adsorption isotherm exhibits type IV pattern with hysteresis loop, when the adsorption and desorption isotherm was evaluated using Brunauer-Emmett-Teller (BET) method. TiO_2 sol-gel has optical absorption coefficient 0.99, extinction coefficient (1), the refractive index

16.3 and The energy band gap 3.23 eV, while TiO_2 pure has optical absorption coefficient (0.92), extinction coefficient (0.32). The refractive index 10.5 and an energy band gap (3.03 eV) determined by diffuse reflectance spectrum in which the Kubelka–Munk remission function replaces Beers-Lambert law. Potassium ferrioxalate actinometry fit for determination of photon flux during TiO_2 photo-catalytic process (λ_{max}= 385).

It was found that highly pure TiO_2 showed high Photo-decolorization percentage for Tubantin blue dye in basic solution (pH 9) under solar radiation. The Photo-decolorization percentage increased as a function of the amount of catalyst, amount 30% H_2O_2 and irradiation time while it decrease with increase of concentration of dye. The employment of efficient photo-catalyst and selection of optimal operational parameters might lead to complete decolorization. Photo-decolorization percentage of the four dyes under study differs according to type of catalyst and dye. The daily photon flux was nearly constant during the experiments, temperature solution differ depending on the catalyst type.

First-order and Langmuir Hinshelwood L-H models are fit to investigate the mechanism of the photo-decolorization for dyes at all initial dye concentrations. The initial dye concentration and dye type have a measurable effect on reaction rate constant. The effect of initial concentration on the reaction rate constant was following order the $C_{70} > C_{50} > C_{30}$ .The effect of

dye type on the reaction rate constant, is following order methylene blue > tubantin red > tubantin blue > yellow reactive at each photo-catalysts.

ملخص

قي هذا البحث اخضعت تقنيه الحفز الضوئي لثاني أكسيد التيتانيوم القابل للتطبيق لإزالة لون الأصباغ في اربع خطوات.اولا تحضير المحفز و التحقق من عامل الحفز. ثانيا تهيئه العوامل المؤثرة في عمليه الحفز الضوئي. وثالثا تم التحقق من تأثير كل من عاملي الحفز في عمليه الاازاله الضوئيه لاالوان اربع انواع مختلفة من الاصباغ. رابعا دراسة حركيه الإزالة الضوئية لألوان الأصباغ. واضحت النتائج أن طريقه السائل و الهلام من خلال استخدام رابع كلوريد التيتانيوم كماده خام هي الأفضل لتحضير ثاني أكسيد التيتانيوم بجسيمات نانونميترية بأفضل خواص. وجد من تحليل بيانات حيود الأشعة السينية كل من ثاني أكسيد التيتانيوم النقي وثاني أكسيد التيتانيوم السائل- الهلام المحضر بطريقة السائل الهلامي اطور اناتيس عالي التبلور والنقي, حجم الجسيمات ثاني أكسيد التيتانيوم النقي (49,11070 نانومتر) و ثاني أكسيد التيتانيوم (22,0198 نانومتر), من تحليل طيف الأشعة تحت الحمراء كل من ثاني أكسيد التيتانيوم النقي وثاني أكسيد التيتانيوم السائل-الهلام لها نفس التردد الاهتزازي تتصف الرابطة (Ti—O) بتردد (400-800سم$^{-1}$) تتصف الرابطة (O—Ti—O) و الرابطة (Ti=O) بتردد (1426-1696سم$^{-1}$) , تم حساب مساحة سطح ثاني وكسيد التيتانيوم النقي النوعية (46,692 م^2/جم), ثاني اوكسيد التيتانيوم سول- جل النوعية (38,264 م^2/جم) باستخدام الامتزاز والادمصاص الحراري بطريقه برانور-ايميت-تيلر ويعرض الامتزاز الحراري من النوع رباعي النمط مع حلقه التباطؤ وتم تقدير الخوص الضوئي لثاني أكسيد التيتانيوم سول- جل معامل الامتصاص الضوئي (0,99) ,ومعامل الخبوء (1) ,معامل الانكسار (16,3) و فجوة نطاق الطاقة (3,23 إلكترون فولت) في حين ثاني أكسيد التيتانيوم النقي معامل الامتصاص الضوئي (0,92) ,ومعامل الانقراض (0,32) ,معامل الانكسار (10,5) و فجوة نطاق الطاقة (3,03 إلكترون فولت) باستخدام منتشر طيف الانعكاس بحيث حلت دالة كوبيكا-مونك للانبعاث محل قانون بير-لامبرت لامتصاص. أيضا وجد أن بوتاسيوم أكسلات الحديد 3 اكتونيميتري مناسب لتقدير تدفق الفوتون أثناء الحفز الضوئي لثاني أكسيد التيتانيوم (الطول الموجي = 385نانومتر).

وجد أن أعلي نسبه مئوية للإزالة الضوئية للون صبغة التوبيتان تمت في وسط قاعدي (الأس الهيدروجيني 9) تحت أشعة الشمس, النسبة المئوية لأزاله الضوئية للون الصبغة تزداد كداله لكميه المحفز, حجم فوق أكسيد الهيدروجين ذو تركيز30% و زمن التشعيع, تنقص بزيادة تركيز الصبغة. باستعمال المحفز الضوئي الفعال واختيار عوامل التشغيل المثالية قد يؤدي لأزاله كاملة للون . وأيضا الإزالة الضوئية للون الأصباغ الأربعة تحت الدراسة تختلف اعتمادا علي نوع المحفز الضوئي ونوع الصبغة. وتدفق الفوتون اليومي ثابت أثناء إجراء كل التجارب, درجه حرارة الحلول تختلف أعتمادا علي نوع المحفز.

كان تفاعل الرتبة الأولي ولانقيمير-هينوشلود يمثلان نموذجا مناسبا لتتبع ميكانيكية الإزالة الضوئية للون للأصباغ عند كل التراكيز الابتدائية . التركيز الإبتدائي يؤثر علي ثابت معدل تفاعل , تأثير التركيز الابتدائي علي قيمة ثابت معدل التفاعل يتبع الترتيب تركيز70 جزء من المليون اكبر من 50 جزء من المليون اكبر من 30 جزء من المليون, تأثير نوع الصبغة علي قيمة ثابت معدل التفاعل يتبع الترتيب المثالين الأزرق من التوبيتان الأحمر اكبر من التوبيتان الأزرق اكبر من الصفراء النشطة لكل المحفزات الضوئية.

Table of Contents

List of Tables

List of Figures

List of Abbreviations

$\mathbf{A_{ads}}$	Electron acceptor
AOPs	Advance oxidation processes
AR 14	Acid Red 14 dye
$\boldsymbol{\alpha}$	absorption coefficient
ASTM	American Society of Test Material
BET	Brunauer-Emmett-Teller
BG	Bromocresol green dye
C.I.	Colour index
CPC	Compound Parabolic collector
CVD	Chemical vapour deposition
$\mathbf{C_e}$	concentration in the liquid phase at equilibrium. gl^{-1}
$\mathbf{C_0}$	Initial concentration. ppm
$\mathbf{C_{30}}$	Concentration ≥ 30. ppm
$\mathbf{C_{50}}$	Concentration ≥ 50. ppm
$\mathbf{C_{70}}$	Concentration ≥ 70. ppm
$\mathbf{D_{ads}}$	Electron donor
$\mathbf{e^-_{CB}}$	Electron conduction bond
$\mathbf{e^-_{TR}}$	The surface trapped valence band electron
$\mathbf{e^-/h^+}$	electron–hole pairs
ε	Molar decadic. $dm^3mol^{-1}cm^{-1}$
$\mathbf{E_g}$	Energy band gap. eV
FTIR	Fourier transform infrared
FWHM	Fullwidth at half maximum
$\mathbf{h^+_{VB}}$	Hole valence bond
$\mathbf{h^+_{TR}}$	The surface trapped conduction band hole

k	extinction coefficient
k_1	First-order rate constant. $Min^{-1}s^{-1}$
k_2	Second-order rate constant. $Mole^{-1}L^{-1}min^{-1}$
K_{ad}	adsorption constant. $mg^{-1}L$
K_{app}	apparent first order rate constant. Min^{-1}
k_L	Langmuir Hinshelwood rate constant. mg L^{-1} min^{-1}
K_{LH}	Langmuir Hinshelwood adsorption constant. L mg^{-1}
L-H	Langmuir Hinshelwood.
LMCT	Ligand to metal charge transfer
λ_{max}	Maximum wavelength for absorbance. nm
n	refractive index
PVD	Physical vapour deposition
PTCs	Parabolic-trough concentrators
Pzc	point of zero charge
Q_e	Amount of compound per unit weight catalyst. mg g^{-1}
Q_{max}	Maximum amount of adsorbed compound per unit. mg g^{-1}
Φ(λ)	quantum yield
$q_{n,p}$	The photon flux amount . Einstein s^{-1}
R	diffuse reflectance
R^2	regression coefficient
θ	Surface fraction covered by the substrate
SPD	Spray pyrolysis deposition
T	Transmittance
TiO_2 sol-gel	Titanium dioxide was prepared by sol-gel method
XRD	X-ray powder diffraction

Chapter one

Introduction, Objectives and Literature Review

1.1. Introduction

Synthetic dyes are organic compounds with complex aromatic structures (Kar *et al*., 2009), that give color to materials and are used extensively in various industries such as textiles, cosmetics, paper and plastic industries (Seyyedi and Jahromi, 2014; Kerkez-Kuyumcu *et al*., 2015). Despite the wide application of dyes, their disposal into the environment and contamination of water is a major problem that has aroused concern due to their adverse effects on human health, to fauna and to flora (Mohan et al., 2008). Biological, physical, chemical and physico-chemical methods were used for removal of dyes. Dyes are usually very difficult to be biodegraded, and are too hard to eliminate them under natural aquatic environment (Sarioglu and Atay, 2006); many dyes and their by-products break down into products which are toxic for living organisms (Yang *et al*., 2011). Advanced oxidation processes AOPs have been suggested as potential alternative method for decolorizing dyes (Neamtu *et al*., 2004; Domínguez *et al*., 2005; Hsing *et al*., 2007; Guimaraes *et al*., 2012). The principles of these AOPs are based on the generation of highly reactive transitory species (H_2O_2, $OH^{\bullet}$, O_2^- and O^{-2}) for mineralization of refractor organic compounds and pollutants, pathogens and disinfection by-products (Esplugas *et al*., 2002; Para-Tius *et al*., 2004). Among AOPs heterogeneous photo-catalyst employed semiconductors which has confirmed its efficiency in decolorization of dyes. Mane semiconductors have been tested although only TiO_2 in anatase form seems to have the most interesting required attributes such as high stability, good performance and low cost (Fujishima and Zhang, 2006). Various investigations have established that TiO_2 is much more effective as a

photo-catalyst in the form of nanoparticles than in bulk powder (Han *et al*., 2009). During the past two decades, several synthetics methods have been used to prepare TiO_2 nanoparticles (Su *et al*., 2006). Generally the methods of preparing nano-TiO_2 are gas methods and liquid methods, Properties of nano-TiO_2 particles are dependent on the method of synthesis. Among these methods sol-gel method is regarded as good method for synthesis of ultra-fine metallic oxide and has been widely employed for preparing titanium dioxide nanoparticles (Su *et al*., 2006). Many authors investigated efficiency of decolorization of dyes by using TiO_2 photo-catalyst under UV-radiation or using solar radiation (Neppolian *et al*., 2002; Suarez *et al*., 2003; Akpan & Hameed2009; Rauf & Salman, 2009).

Dyes decolorization depend on many parameters and it possible completely decolorization is obtained when applied optimum parameters. (Habibi, *et al*., 2005; Konstantinou and Albanis, 2004; Akpan and Hameed, 2009). Several approaches for modeling heterogeneous photo-catalysis reactions have been developed (Alfano and Cassano, 2008; Puma and Brucato, 2007; Marugan *et al*., 2013) Some models are complex, such as the radiation-absorption scattering models (Marugan et al., 2008), and others are simplified such as first order models (Ollis, 2005a; Daneshvar *et al*., 2003, Saquib *et al*., 2008), second order (Kumar *et al*., 2007) and the Langmuir-Hinshelwood (L-H). Generally first-order kinetics are appropriate for the entire concentration range up to few ppm, the Langmuir Hinshelwood L–H model was established to describe the dependence of the observed reaction rate on the initial solute concentrations. It is likely that adsorption of the dye is an important parameter in determining photo-catalytic degradation rates.

This thesis is divided in the following chapters:

Chapter one section three summarizes the literature survey relevant to the area of research.

Chapter two describes the experimental methods and materials used in this study analytical equipment as well as the experiment of procedures are also reported in detail.

Chapter three included three parts: part I reported results and discussions concerning the experimental preparation of TiO_2 catalyst by using sol-gel method and characterization of it and other catalyst pure TiO_2. Also preparation of chemical actinometer [potassium tris (oxalato) ferrate (III) trihydrate] commonly called ferrioxalate actinometer, and its UV-vis. Spectrum. Part II reported results and discussions concerning the experimental studying of optimum parameter of photo-decolorization of tubantin blue dye by using pure TiO_2 under solar radiation by compound parabolic collector CPC. Also reported results and discussion of applied optimum parameters to photo-decolorization of four crommical dyes by two types of catalyst pure TiO_2 and TiO_2 sol-gel. Part III reported results and discussion of the kinetic models considered for four dyes and two types photo-catalysts. The models are validated with experimental data, and its confidence intervals and coefficients are reported. In these kinetic models the experimental obtained adsorption constants are determined.

Chapter four reported the main conclusions and recommendations for future work.

1.2. Objectives

1.2.1. Main objective

This PhD thesis seeks to gain understanding application photo-catalytic process for removal dyes from titanium dioxide suspension under solar radiation. Final goal of this research is to investigate the appropriate kinetic model that photo-decolorization of each dye.

1.2.2. specific objective

- ❖ To apply sol-gel method for preparing titanium dioxide nanoparticles and characterized it and other catalyst pure titanium dioxide.
- ❖ To prepare chemical actinometer for determining the photon flux during experiments.
- ❖ To study the influence of different parameters (pH, dye concentration, amount of catalyst and oxidant concentration) on photo-decolorization of dye using photo-catalyst under solar radiation.
- ❖ To applied optimum parameters for photo-decolorization of different dyes using TiO_2 sol-gel and pure TiO_2 under solar radiation.
- ❖ To study kinetics of titanium dioxide photo-catalytic for removal dye.

1.3. Literature Review

1.3. 1. Wastewater

1.3.1.1. Definition

Wastewater may be defined as a combination of liquid or water carried waste removed from residences institution and commercial and industrial establishments together with ground water surface water and storm water. It generally contains a high load of oxygen demanding, water pathogenic or disease causing agents, organic materials nutrients that stimulate plant growth, inorganic chemical and minerals and sediments. It also contains toxic compounds [(136)].

1.3.1.2. Classification of wastewater

Waste water can be classified into four categories:

a. Domestic: wastewater discharged from residences and commercial institutions and similar facilities.
b. Industrial: wastewater in which industrial waste predominates.
c. Infiltration /Inflow: extraneous water that enters the sewer system through indirect and direct means such as through leaking joints, cracks or porous walls. Inflow is storm water that enters the sewer system from storm drain, connection, roof, headers, foundation and basement drain or through man bole covers.
d. Storm water : run off resulting from flooding due to rainfall (Sonune *et al*., 2004)

1.3.1.3. Industrial wastewater

It is the aqueous discard that results from the use of water in an industrial manufacturing process or the cleaning activities that take place along with that process. It may contain suspended, colloidal and dissolved (mineral and organic) solids. They may be organic or toxic material and possible pathogenic bacteria. These waste may be discharged into the sewer system provided, they have no desirable effect on treatment efficiency or undesirable effects on the

sewer system. They are varying widely in composition, strength, flow and volume depending on the specific industry or manufacturing establishment in the common-unity. (Wang *et al*., 2004)

1.3.1.4. Dyes for textile industries

Wastewater generated by the dye production industry and many other industries (textile, rubber, paper, leather, plastics, cosmetic, printing etc...(Mohan *et al*., 2008; Chatterjee *et al*., 2009; Yang *et al*., 2011) which were used dyes and pigments are high in both color and organic content (Gomez *et al*., 2007). About 10,000 different commercial dyes and pigments exist, and over 7 $X10^5$ tons are produced annually world-wide. It has been estimated that about 10–15% of these dyes are released as effluents during the dyeing processes (Gomez *et al*., 2007; Sen *et al*., 2011; Yao *et al*., 2009; Rafatullah *et al*., 2009). The type of dyes used in the textile industry are found to differ depending on the fabrics manufactured, cellulose fibers are dyed using reactive dyes, direct dyes, naphtha dyes and indigo dyes, Protein fibers are dyed using acid dyes and lanaset dyes, synthetic fibers are dyed using dispersed dyes, basic dyes and direct dyes (Ghaly *et al*., 2014). Dyes are having the complex aromatic structure, which make them more stable and more difficult to biodegrade (Mohan *et al*., 2008; Kar *et al*., 2009; Yang *et al*., 2011; Patel *et al*., 2012); their disposal into the environment and contamination of water is a major problem for several reasons (Alvarenga *et al*., 2015); Firstly, several classes of dyes are considered as possible carcinogens or mutagens by European and American authorities. Secondly, the high coloring power of dyes gives rise to esthetic damage. (Metivier *et al*., 2007). Thirdly some of the dyes present in wastewater even decompose into carcinogenic aromatic amines under anaerobic conditions and cause serious health problems to human beings as well as other animals (Chen *et al*., 2003). Fourthly inhibit amount of sunlight penetration, causing a reduction in the rate of photosynthesis and oxygen concentration in water so inhibit growth at different trophic levels, including bacteria, protozoans, algae,

plants and animals (Bakshi *et al*. 2003; Moawad *et al*., 2003; Bafana *et al*., 2009; Prigione *et al*., 2008). Biological , physical, chemical and physico-chemical methods such as coagulation and flocculation (Aleboyeh *et al*., 2008, Harrelkas *et al*., 2009, Zonoozi *et al*., 2009), membrane separation (Sachdeva and Kumar, 2009, Amini *et al*., 2011) sonochemical degradation (Abbasi and Asl, 2008), electrochemical (Gupta *et al*., 2007, Fan *et al*., 2008), activated carbon adsorption (Xu *et al*., 2008; Tan *et al*., 2008; Foo and Hameed, 2010), adsorption (Crini *et al*., 2005; Crini and Badot, 2008) were used for removal of dyes. However, these methods have their drawbacks, amongst which, the generation of hazardous waste or secondary intermediates, slow degradation rates and high costs are limitations that stand out.

Advanced oxidation processes have been suggested as potential alternative method for decolorizing dyes (Neamtu *et al*., 2004; Domínguez *et al*., 2005; Hsing *et al*., 2007; Guimaraes *et al*., 2012)

1.3.2. Advanced oxidation processes

Advanced oxidation processes (AOPs) is the common name of several chemical oxidation methods used to remediate substances that are highly resistant the biological degradation. The complete oxidation leads to mineralization and yields CO_2, H_2O and inorganic ions. AOPs can remediate differ all types of organic pollutants in liquid, gaseous or solid media.

1.3.2.1. Fundamental of advanced oxidation

Although different advanced oxidation processes use several different reaction systems, all of them have the same chemical characteristic: i.e., the production and use of hydroxyl radicals ($OH^{\bullet}$) (Eckenfelder *et al*., 2000; Metcalf & Eddy, 2003). Hydroxyl radicals are highly reactive species that are able to attack and destroy even the most persistent organic molecules that are not oxidized by the oxidants as oxygen, ozone or chlorine (Eckenfelder *et al*., 2000). Table (1) shows oxidation potential of the hydroxyl radical and compares it with others common oxidants used in chemical oxidation (Fox and Dulay, 1993).

Table (1): Oxidation potential of most common oxidizing agents

Oxidizing agent	**Oxidation potential, eV**
Fluorine	3.06
Hydroxyl radical	2.80
Atomic oxygen	2.42
Ozone	2.08
Hydrogen peroxide	1.78
Hypochlorite	1.49
Chlorine	1.36
Chlorine dioxide	1.27
Molecular oxygen	1.23

Hydroxyl radical is able to initiate several oxidation reactions leading to complete mineralization of the original organic substances and their subsequent degradation products. Hydroxyl radical reacts with all classes of organics mainly by hydrogen abstraction:

$$OH^{\bullet} + RH \rightarrow R^{\bullet} + H_2O \quad (1)$$

Hydrogen abstraction produces organic radicals are able to react with molecular oxygen and originating peroxyl radicals.

$$R^{\bullet} + O_2 \rightarrow R\,O_2^{\bullet} \rightarrow \quad (2)$$

Electrophilic additions may also occur.

$$OH^{\bullet} + PhX \rightarrow HOPhX^{\bullet} \quad (3)$$

Electron transfer reactions,

$$OH^{\bullet} + RX \rightarrow RX^{\bullet +} + OH^{-} \quad (4)$$

And reactions between hydroxyl radicals,

$$2OH^{\bullet} \rightarrow H_2O_2 \quad (5)$$

Hydroxyl radical is characterized by a non-selective attack, other relevant and important characteristics are the existence of several possible pathways for hydroxyl radical production and the fact that all reactions occur at normal temperature and pressure. Advanced oxidation processes enclose several different treatments options: as ozone, hydrogen peroxide, ultraviolet radiation,

ultrasound, homogeneous and heterogeneous photo-catalysis, photo-catalytic disinfection and also their combination (Hoffmann *et al*., 1995).

1.3.2.2. Heterogeneous photo-catalysis

The subject of photo-catalysis became extremely important since Fujishima and Honda demonstrated in 1972 the possibility of water splitting on an illuminated TiO_2 semiconductor surface (Fujishima and Honda, 1972). Photo-catalysis is the segment of catalysis, which cover the range of the reactions proceeding under the action of the light absorption by a catalyst or a substrate. The photo-catalysts are semiconductor materials, which include metal oxides (ZnO, ZrO_2, V_2O_5, Fe_2O_3, SnO_2, CdO and TiO_2) and metal sulphides (CdS and ZnS) (Herrmann *et al*., 1999; Karunakaran *et al*., 2004; Chong *et al*., 2010). Titanium dioxide is an important semiconductor material due to its properties such as cheap, nontoxic, photochemical and chemical stability, high refractive index; wide band gap and its holes are strongly oxidizing and redox selective (Alfano and Cassano, 2000; wang *et al*., 2010), so it was applied in environmental protection, paint, toothpaste, UV protection, photo-catalysis, photo-voltaic's, electrochromics, gas sensing, dye-sensitized solar cells, photo-induced hyrophilicity and so on (Liu *et al*., 2007; Chen *et al*., 2006; Zhang *et al*., 2001; Hayle *et al*., 2014; Chen *et al*., 2012; Wang *et al*., 2010; Ohenoja *et al*., 2013). The general mechanism of photo-catalysis is shown in Fig. (1) When the impinging light has energy equal to, or greater than the semiconductor band gap, radiation is absorbed and electrons are moved from valence band to the conduction band giving rise to the formation of electron–hole pairs. (Alfano and Cassano *et al*., 2000). These separated charges walk randomly to the surface of the catalyst, they can combine, get trapped in a stable surface state or participate in successive reaction. The holes react directly with an electron donor (D_{ads}) or with water to produce $OH^{\bullet}$ radicals. The electron reduces the adsorbed oxygen or reacts with hydrogen an electron acceptor (A_{ads}) to generate active species included

superoxide ($O_2^{\bullet-}$), hydroxyl radical ($OH^{\bullet}$) peroxide (H_2O_2) and singlet oxygen ($^1O_2^{\bullet}$)

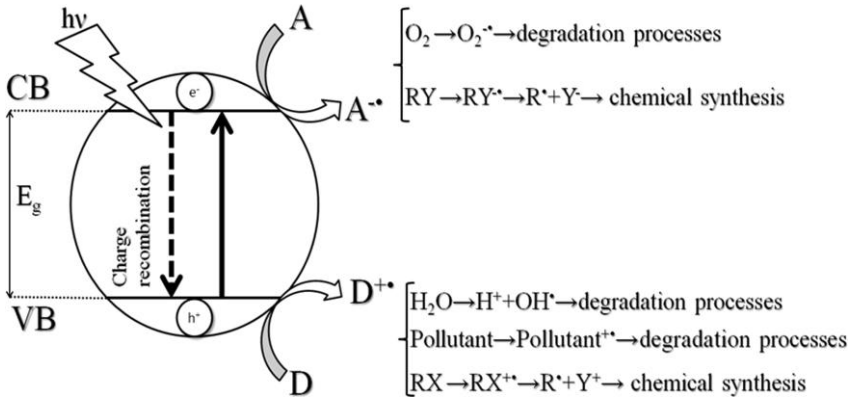

Fig (1): Photo-catalytic generation active species at the surface of a semiconductor Material. (Alfano and Cassano et al., 2000)

The energy required for the electron excitation depends on the particular characteristics of the semiconductors. The minimum wavelength necessary for the photo-excitation (λ_{Eg}) depends on the band gap of the photo-catalyst Table (2) gives band gap energies for some popular semiconductors.

Table (2): Band gap of various photo-catalysts (Bhatkhande 2002)

Photo-catalyst	**Energy band gap eV**	**λ_{Eg} nm**
Si	1.1	1127
WSe_2	1.2	1033
Fe_2O_3	2.2	564
CdS	2.4	517
WO_3	2.7	429
TiO_2 (rutile)	3.0	413
α-Fe_2O_3	3.1	400
ZnO	3.2	388
TiO_2 (anatase)	3.2	388
$SrTiO_3$	3.4	365
SnO_2	3.5	354
ZnS	3.7	335

1.3.2.2.1. Titanium dioxide TiO_2

Titanium dioxide (TiO_2) belongs to the family of transition metal oxide. TiO_2 crystallized in four natural phases: brookite (othorhomic), anatase (tetragonal), rutile (tetraganol) and TiO_2 (B) (monoclinic). Fig. (2) shows the three crystal structures of TiO_2. Besides these polymorphs two additional high pressure

forms have been synthesized from rutile; first form is TiO_2 (II) with a PdO_2 structure (Simons *et al*., 1967) and the second form is TiO_2 (H) with a hollandite structure (Latrocheet *et al*., 1989). Table (3) summarized the properties of three phases of TiO_2

Table (3): Properties of the rutile, anatase and brookite(Cromer *et al*., 1955; Baur *et al*.,1961; Mo and Ching, 1995)

Properties	**Anatase**	**rutile**	**Brookite**
Crystal structure	Tetragonal	Tetragonal	Orthorhombic
Lattice constant (Å)	a = 4.5936 c =2.9587	a = 3.784 c = 9.515	a = 9.184 b = 5.447 c = 5.154
Space group	P42/mnm	I41/amd	Pbca
Molecule (cell)	2	2	4
Volume/ molecule (Å^3)	31.2160	34.061	32.172
Density (g cm^{-3})	4.13	3.79	3.99
Ti–O bond length (Å)	1.949 (4) 1.980 (2)	1.937(4) 1.965(2)	1.87–2.04
O–Ti–O bond angle	81.2° - 90.0°	77.7° - 92.6°	77.0°–105°

Rutile TiO_2 has a tetragonal structure and contains 6 atoms per unit cell Fig. (2b). The TiO_6 octahedron is slightly distorted (Chen *et al*., 2007; Thompson *et al*., 2006; Diebold *et al*., 2003). The rutile phase is stable at most temperatures and pressures up to 60 K bar. (Zhang and Guo, 2000) found that anatase and brookite structures transformed to the rutile phase. The activity of the rutile phase as a photo-catalyst is generally very poor. Anatase TiO_2 also has a tetragonal structure but the distortion of the TiO_6 octahedron is slightly larger for the anatase phase (Mo and Ching, 1995) Fig. (2a). (Muscat *et al*., 2002) found that the anatase phase is more stable than the rutile at 0 K, but the energy difference between these two phases is small (~2 to 10 kJ/mol). The anatase structure is preferred over other polymorphs for solar cell applications because of its higher electron mobility, low dielectric constant and lower density (Carp *et al*, 2004). The increased photo-reactivity is because of the slightly higher Fermi level, lower capacity to absorb oxygen and higher degree of hydroxylation in the anatase phase (Tanaka *et al*., 1991)

Brookite TiO_2 belongs to the orthorhombic crystal system. Its unit cell is composed of 8 formula units of TiO_2 and is formed by edge-sharing TiO_6 octahedra Fig (2c). It is more complicated, has a larger cell volume. (Thompson *et al*., 2006)

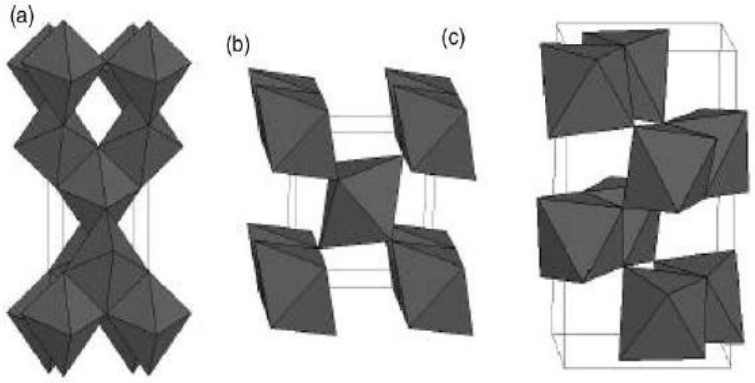

Fig (2): Crystal structures of TiO_2 anatase (a), rutile (b), brookite (c)

TiO_2 can be prepared in the form of powder, crystals or thin film. Both powder and thin film can be built up from crystallites ranging from a few nanometers to several micrometers.

1.3.2.2.2. TiO_2 nano-particles

Titanium dioxide nano-materials have been widely studied in the last two decades (Burda *et al*., 2005). Various investigations have established that TiO_2 is much more effective as a photo-catalyst in the form of nanoparticles than in bulk powder (Han and Bai, 2009). Recently, TiO_2 has been prepared in special morphologies including nanotubes, nanorods, platelets, nanowires, nanowalls, and nanoribbons (Carp *et al*, 2004). During the past two decades, several synthetics methods have been used to prepare TiO_2 nanoparticles (Su *et al*., 2006). Carp *et al*, 2004 reviewed generally the methods of preparing nano-TiO_2 liquid methods and gas methods.

A- Liquid methods are used for some application especially the synthesis of thin film. It has the advantage of control over the stoichiometry, producing homogeneous materials, allowing formation of complex shapes and preparation of composite materials. However there are several

disadvantages among which can be expensive precursors, long processing time and the presence of carbon as an impurity. It includes

i. Precipitation (co-) methods: these involve precipitation of hydroxides by the addition of basic solution (NaOH, NH_4OH and urea) to raw material (titanium chloride or sulfate) followed by calcinations to crystallize the oxide. The disadvantage is the tedious control of particle size and size distribution, as fast precipitation often causes formation of large particles

ii. Solvothermal method: these methods employ chemical reaction in aqueous (hydrothermal method) or organic media (solvothermal method) under self-produced pressure at low temperatures < 250°C; in general these are required to crystallize the final material. They are useful to control grain size, particle morphology, crystalline phase and surface chemistry by regulating the solution composition, reaction temperature, pressure, solvent properties, additives and ageing time.

iii. Sol-gel methods: these are used for the synthesis of thin film, powder and membranes. Two types are known: the non-alkoxide (uses inorganic salt such as nitrates, chlorides, acetates carbonates, acetylacetonates etc.) and alkoxide (metal alkoxides) route. It has many advantages such as purity, homogeneity, felicity, stoichiometry control, ease of processing, control over composition and flexibility in introducing dopants in large concentration. Usually sol-gel procedure includes three steps hydrolysis, drying and calcinations.

iv. Micro-emulsion methods: water in oil micro-emulsion has been successfully utilized for synthesis nanoparticles. This method may be defined as thermodynamically stable, optically isotopic solution of two immiscible liquids consisting of micro-domains of one or both stabilize by interfacial film of surfactant. The surfactant molecule has a polar (hydrophilic) head and a long chain aliphatic (hydrophobic) tail. In particular hydrolysis of titanium alkoxide in micro-emulsion based on

sol-gel methods has yielded uncontrolled aggregation and flocculation except at very low concentration. Recently an improved methods using carbon dioxide instead of oil.

v. Combustion synthesis: these (hyperbolic) leads to highly crystalline fine large area particles. They involves a rapid heating of a solution, compound containing redox mixture, redox groups during combustion, the temperature reaches about 650°C for short period of time (1-2min) making the material crystalline.

vi. Electrochemical synthesis: these may be used to prepare advanced thin film such as epitaxial, super lattice, quantum dot and nanoporous ones. Also varying electrolysis parameters like potential, current density, temperature and pH can easily control the characteristic states of the film.

B- Gas phase methods: for thin film most synthesis routes are performed the gas methods which can be of chemical or physical nature. Most of these techniques can also synthesize powder. The main techniques are:

a. Chemical vapor deposition (CVD): CVD is a widely used as versatile technique to coat large surface area in a short span of time. In industry this is employed in continuous process to produce ceramic and semiconductor films. CVD is extensive and split out according to differences in activation method, pressure and precursors. Compounds are formed from chemical reaction in the gas phase.

b. Physical vapor deposition (PVD): PVD is another class of thin film deposition technique. Films are formed from the gas phase but without chemical transition. Only possible with substances that are stable in the gas phase and can be directed towards the substrate. The most commonly employed PVD technique is thermal evaporation. They have superior characteristic over CVD grown films where smoothness, conductivity, presence of contaminations and crystallinity are concerns but production is slower and more laborious.

c. Spray pyrolysis deposition (SPD): SPD is an aerosol deposition technique for thin films and powder related to CVD. The main differences are that in spray; an aerosol is formed from precursor solution instead of a vapor in CVD, the aerosol is directly focused onto the sample whereas diffusion is dominant process in CVD and the heated substrates are at ambient pressure. It has been used for preparation of mixed oxides powder film and uses metal–organic compounds or metal salt as precursors. Compared to other deposition methods it has merits such as simplicity, low cost, reproducibility and possibility of deposition of large areas in short time while film exhibit good electrical and optical properties but is cases a problem as is the smoothness of the films.

C- There are several other thin film techniques based on vapor-phase deposition. Sputtering is used quite frequently to produce TiO_2 films. The technique uses the plasma consisting of argon and oxygen. Molecular beam epitaxial is technique uses pulsed laser to ablate parts of TiO_2 ceramic target. This lead to high quality films with control over the orientation. Ion implantation is used to synthesize TiO_2 and based on the transformation of precursor plasma to TiO_2 which only becomes crystalline after an annealing step. Dynamic ion beam mixing which uses high energy O_2^+ and or O^+ beams and Ti vapor to deposit TiO_2 $f_i$lm with high speed and control over the composition.

1.3.2.2.3. Fundamentals and Mechanism of TiO_2 Photo-catalysis

The fundamentals of photo-physics and photochemistry underlying the heterogeneous photo-catalysis employing the semiconductor TiO_2 catalyst have been reported (Gaya and Abdullah, 2008). TiO_2 is a large band semiconductor, with band gaps of 3.2, 3.02, and 2.96 eV for the anatase, rutile and brookite phases, respectively (Wunderlich, 2004). The valence band of TiO_2 is composed

of the 2p orbital of oxygen hybridized with the 3d orbital of titanium, while the conduction band is only the 3d orbital of titanium (Paxton et al., 1998). When TiO_2 is exposed to near-UV light, electrons in the valence band are excited to the conduction band leaving behind holes (h^+), as shown in Fig. (3)

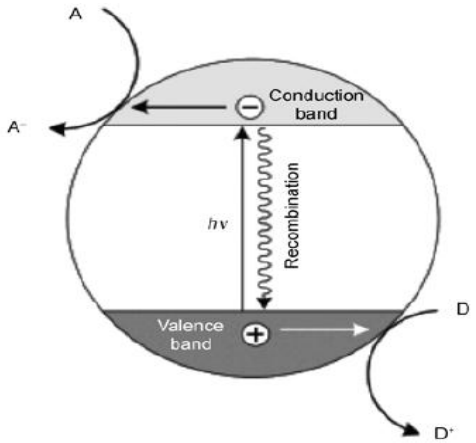

Fig (3): Mechanism of light absorption by TiO_2 (Szaciłowski *et al*, 2005).

The semiconductor TiO_2 has been widely utilized for inducing a series of reductive and oxidative reactions on its surface. The series of chain oxidative – reductive reactions.

Photo-excitation: $TiO_2 + h\nu \longrightarrow e^- + h^+$ (6)

Charge carrier trapping of e^-: $e^-_{CB} \longrightarrow e^-_{TR}$ (7)

Charge carrier trapping of h^+: $h^+_{VB} \longrightarrow h^+_{TR}$ (8)

Electron – hole recombination: $e^-_{TR} + h^+_{TR} \longrightarrow e^-_{CB}$ + heat (9)

Photo-excited e^- scavenging: $(O_2)_{ads} + e^- \longrightarrow O_2^{\bullet-}$ (10)

Oxidation of hydroxyls: $OH^- + h^+ \longrightarrow OH^\bullet$ (11)

Photo-gradation by $OH^\bullet$: $R\text{-}H + OH^\bullet \longrightarrow R^\bullet + H_2O$ (12)

Direct photo-hole: $R + h^+ \longrightarrow$ intermediate / final degradation product (13)

Protonation of superoxide: $O_2^{\bullet-} + OH^\bullet \longrightarrow HOO^\bullet$ (14)

Co-scavenging of e^-: $HOO^\bullet + e^- \longrightarrow HO_2^-$ (15)

Formation of H_2O_2: $HOO^- + H^+ \longrightarrow H_2O_2$ (16)

The e^-_{TR} and h^+_{TR} in equation (4) represent the surface trapped valence band electron and conduction band hole respectively. It was reported that these trapped carriers are usually TiO_2 surface bound and do not recombine

immediately after excitation. In the absence of electron scavengers the photo-excited electron recombines with the valence band hole in nanoseconds with simultaneous dissipation of heat energy. Thus the presence of electron scavengers is vital to prolong the recombination and successful functioning of photo-catalysis. So it should be noted that all these occurrences in photo-catalysis were attributed to the presence of both dissolved oxygen and water molecules. The oxidative pathway leads in many cases to complete mineralization of organic substrate to CO_2, HO_2 and in some cases an inorganic acid. This also leads to the generation of intermediate species before complete mineralization is achieved.

1.3.2.2.4. Decolorization of dye by titanium dioxide photo- catalytic

(Neppolian et al., 2002) found that aqueous solutions of reactive blue 4 textile dye are totally mineralized (the dye molecules were completely degraded to CO_2, SO_2^{-4}, NO^{-3}, NH_4^{+1} and H_2O) when irradiated with TiO_2 photo-catalyst by solar radiation. (Han *et al*., 2009) reviewed novel achievements in the modification of TiO_2 photo-catalytic systems aimed at enhanced TiO_2 photo-catalytic efficiency; complete mineralization of organic dyes; efficient utilization of visible and/or solar light; stability and reproducibility of the modified TiO_2; recycle and reuse in real wastewater treatment. (Suarez *et al*., 2003) concluded that visible light-induced degradation of blue azo dyes has been carried out onTiO_2/CdO-ZnO nanoporous coupled films. (Konstantinou and Albanis, 2004; Rauf & Salman, 2009; Akpan & Hameed2009) reviewed that photo-catalytic degradation of azo dyes containing different functionalities by using TiO_2 as photo-catalyst in aqueous solution under solar and UV irradiation, The degradation of dyes depend on several parameters such as pH, catalyst concentration, substrate concentration and the presence of electron acceptors such as hydrogen peroxide and ammonium persulphate besides molecular oxygen. (Qamar *et al*., 2005) agree with them. The mechanism of the photo-degradation depends on the radiation used. Kinetic analyses indicate that

the photo-degradation rates of azo dyes can be approximated as pseudo-first-order kinetics according to the Langmuir–Hinshelwood model. (Habibi *et al*., 2005) found that the photo-catalytic degradation of three commercial textile diazo dyes in water on TiO_2 photo-catalyst under 400W high-pressure mercury lamp irradiation are very different and depend on the concentration of dye, oxygen flux, solution temperature, amount of photo-catalyst, UV-irradiation time, pH of solution and inorganic ions concentration. (Mahmoodi and Arami, 2006) found that photo-catalytic degradation of Acid Red 14 (AR 14) by using immobilized titanium(IV) oxide nanoparticles effect by operational parameters such as H_2O_2, dye concentration, anions (NO^-_3, Cl^-, SO_4^{2-}, HCO_3^- and CO_3^{2-}) and pH, it was first-order reaction. (Saquib *et al*., 2008) investigated the photo-catalytic degradation of a dye derivative under different conditions such as different types of TiO_2, reaction pH, catalyst and substrate concentration containing hydrogen peroxide (H_2O_2), besides molecular oxygen in the presence of TiO_2. (Chaleshtori et al., 2013) synthesized non porous and porous titanium–niobium oxides derived from $KTiNbO_5$, investigated photo-catalytic degradation of bromocresol green dye (BG) in aqueous solution using sun light and their catalytic activities was most efficient in acidic solutions. The new porous oxides have large porous and high surface areas and high catalytic activity. (Seyyedi and Jahromi, 2014) was investigated 90% decolorization of C.I. Direct Black 38 by photo-catalytic using titanium dioxide (Degussa P25) TiO_2 was obtained for initial dye concentration of 50 ppm, hydrogen peroxide dosage of 26.56 mM, TiO_2 dosage of 0.75 g/l and pH 5. TiO_2. (Zangeneh *et al*., 2015) applied (Ce-TiO_2, Fe-TiO_2 and Gd-TiO_2) to provide high photo-activity under visible light. It was found that different dopants do not have the same effect on the interaction with electrons and/or holes, due to the different position of the dopants in the host lattice. (Touati *et al*., 2015) investigated 1% Ce-TiO_2 significantly inhibits the electron-hole pairs recombination and reduces the energy gap values of the materials. (Khan, and Fulekar, 2016) studied the

using of Bacillus amyloliquefaciens for the biosynthesis of titanium dioxide nanoparticles and also investigates the role of bacterial enzymes in the biosynthesis of titanium dioxide nanoparticles .they concluded The microbial mediated synthesis of TiO_2 nanoparticles exhibits greater advantage over other conventional techniques, as it produces uniform spherical shaped nanoparticles for photo-catalytic Reactive Red 31 dye degradation.

1.3.3. Kinetic models of photo-catalytic decolorization of dyes

Several approaches for modeling heterogeneous photo-catalysis reactions have been developed (Alfano and Cassano, 2008; Puma and Brucato, 2007; Marugan *et al*., 2013). Some models are complex, such as the radiation-absorption scattering models (Marugan *et al*., 2008), and others are simplified such as first order models (Ollis, 2005; Daneshvar *et al*., 2003, Saquib *et al*., 2008), second order (Kumar *et al*., 2007) and the Langmuir-Hinshelwood (L-H). The simplified models have been shown to successfully describe the photo-catalytic degradation of various contaminants (Chen *et al*., 2007; Khataee *et al*., 2010; Ollis, 2005; Jawad *et al*., 2015; Alvarez-Corena *et al*., 2016). Generally first-order kinetics is appropriate for the entire concentration range up to few ppm. The L–H model was established to describe the dependence of the observed reaction rate on the initial solute concentrations. The expression for the rate of photo-mineralization of organic substrates such dyes with irradiated TiO_2 follows the Langmuir–Hinshelwood (L–H) law for the four possible situations; (a) the reaction takes place between two adsorbed substances, (b) the reaction occurs between a radical in solution and an adsorbed substrate molecule, (c) the reaction takes place between a radical linked to the surface and a substrate molecule in solution, and (d) the reaction occurs with the both of species being in solution. (Prieto et al., 2005). Pseudo-first-order kinetics has also been widely reported by several researchers for heterogeneous catalytic dye degradation systems (Alvarez-Corena *et al*., 2016). It is likely that adsorption of the dye is

an important parameter in determining photo-catalytic degradation rates. The adsorbed dye on the surface of the semiconductor particles acts as an electron donor, injecting electrons from its excited state to the conduction bond of the semiconductor under UV irradiation. Adsorption tests in dark conditions must be carried out in order to evaluate the equilibrium constants of the adsorption of dye on the TiO_2 surface (Sauer *et al*., 2002)

1.3.3.1. First order kinetic model

$$r = -\frac{dC}{dt} = k_1 C \quad (1)$$

Where r is the rate of dye degradation, min^{-1} mg/dm^3; C is the concentration at any time, mg/L; k_1 is the first-order rate constant, min^{-1}. Integrating Eq (1) with respect to the limits $C = C_0$ at time $t = 0$ and $C = C_t$ at any time t, the non-linearized form of first-order expression can be obtained as:

$$C = C_0 e^{-kt} \quad (2)$$

With rearrangement:

$$\ln \frac{C_0}{(C_0 - C_t)} = k_1 t \quad (3)$$

1.3.3.2. Second-order kinetic model

$$r = -\frac{dC}{dt} = k_2 C^2 \quad (4)$$

Where r is the rate of dye degradation, min^{-1} mg/dm^3; C is the concentration at any time, mg/L; k_2 is the second-order rate constant, min^{-1}. Integrating Eq (4) with respect to the limits $C = C_0$ at time $t = 0$ and $C = C_t$ at any time t, the non-linearized form of second-order expression can be obtained as:

$$C_t = \frac{C_0}{k_2 C_0 t + 1} \quad (5)$$

With rearrangement:

$$\frac{1}{(C_0 - C_t)} = k_2 t + \frac{1}{C_0} \quad (6)$$

1.3.3.3. Langmuir-Hinshelwood kinetic model

This model considers that the reaction rate is proportional to the photo-catalyst surface fraction covered by the substrate (θ).

$$r = -\frac{dC}{dt} = k\,\theta \quad (7)$$

with

$$\theta = \frac{K\,C}{(1+KC)} \quad (8)$$

where k is the reaction kinetic constant and K is the constant of the reactant adsorption on the particles of TiO_2.

Substituting Eq. (8) in Eq. (7) it became:

$$r = -\frac{dC}{dt} = k\,\frac{KC}{(1+KC)} \quad (9)$$

Langmuir-Hinshelwood equation (L-H) models a reaction mechanism involving adsorption equilibrium and a slow surface reaction. This equation can be linearized to fit the experimental data and find the kinetic constants, using the substrate concentration curves, C, versus time, t, to calculate the actual reaction rate, r.

$$\frac{1}{r} = \frac{1}{k} + \frac{1}{kKC} \quad (10)$$

From the L-H kinetic expression, Eq. (10), the values of the rate constant, k, and the adsorption constant, K are calculated.

1.3.3.4. Conventional Langmuir isotherm

The classical model of Langmuir isotherm gives a good description of dyes on TiO_2 at equilibrium (Houas et al., 2001; Kuo & Ho, 2006; Hu *et al*., 2013). The well-known expression of the Langmuir model is given by the following equation:

$$Q_e = \frac{Q_{max} K_{ad} C_e}{(1+ K_{ad} C_e)} \quad (11)$$

Where Q_e (mg g^{-1}) and C_e (mgl^{-1}) are the amount of compound per unit weight and the concentration in the liquid phase at equilibrium, respectively. Q_{max} (mg g^{-1}) is the maximum of compound adsorbed that forms a monolayer on the TiO_2 powder and K_{ad} ($mg^{-1}l$) is adsorption constant. In order to find K_{ad} and Q_{max} from experimental data, the expression shown in eq (11) need rearrangement. On linearization the equation it becomes:

$$\frac{1}{Q_e} = \frac{1}{Q_{max}} + \frac{1}{Q_{max}K_{ad}C_e} \quad (12)$$

From the slope and intercept of eq. (12). K_{ad} and Q_{max} can be calculated

1.3.4. Solar photo-catalytic

1.3.4.1. Solar resources

(Rodrıguez *et al*., 2004) reported that the earth receives about $1.7x10^{14}$ kW of solar radiation, meaning $1.5x10^{18}$ kWh per year. Extraterrestrial radiation has an intensity of 1367 W m^{-2} and a wavelength of between 0.2 μm and 50 μm, which is reduced to between 0.28 μm and 4.0 μm when reaching the planet's surface due to the absorption of the rest by different atmospheric components (mainly ozone, oxygen, carbon dioxide, aerosols, steam, and clouds). The solar radiation that reaches the ground without being absorbed or scattered is called direct beam radiation; radiation that reaches the ground but has been dispersed before is called diffuse radiation, and the sum of both is called global radiation .

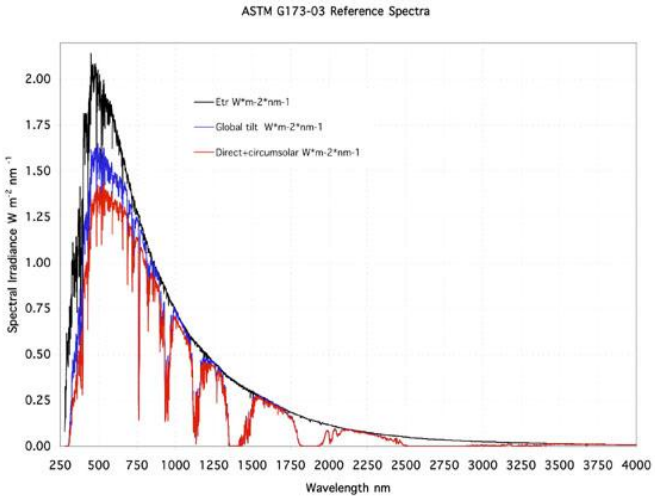

Fig (4): ASTM global irradiance standard solar spectrum (AM 1.5) up to wavelength of 4000nm[137]

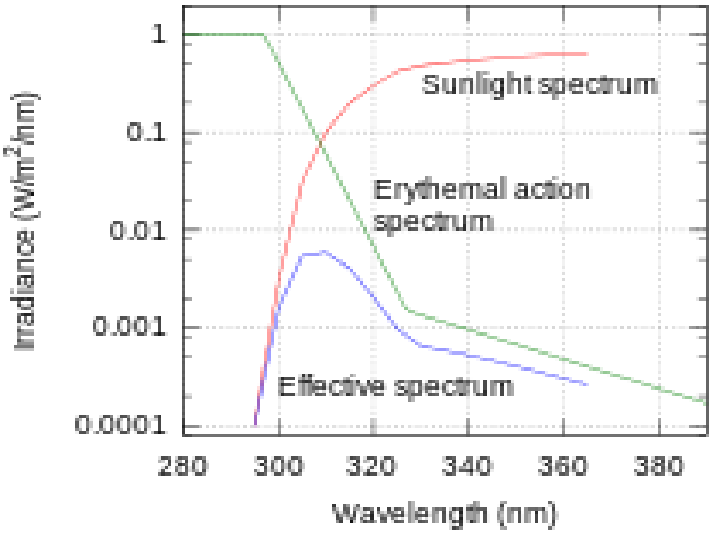

Fig (5): UV irradiance in solar spectrum [138]

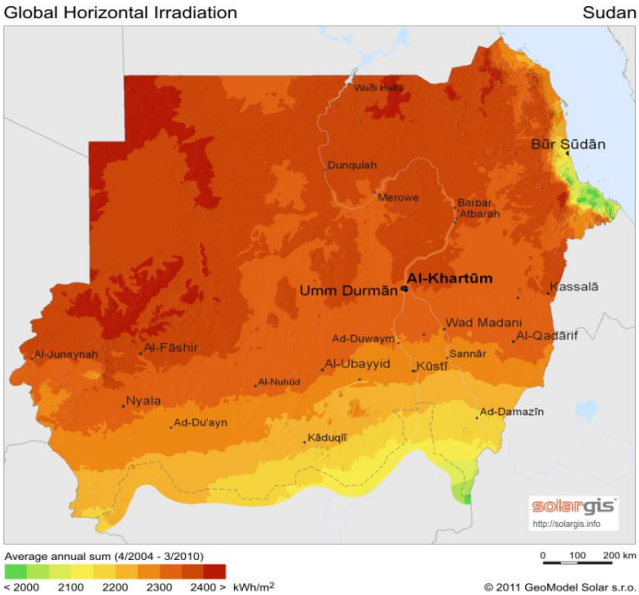

Fig (6): Sudan solar radiation map [139]

1.3.4.2. Solar photo-catalytic technology

Solar photo-catalytic technology may be defined as that which efficiently collects solar photons and enters them in a suitable reactor to promote specific catalytic reactions. The equipment that does this is called a solar collector. Traditionally, solar collector systems have been classified in three broad groups depending on the degree of concentration reached in them, which is directly related to the temperature attainable by the system

These three groups are:

(i) non-concentrating, low concentration or low temperature, systems (up to 150°C)

(ii) medium-concentrating, or medium temperature, systems (from 150 to 400°C);

(iii) high-concentrating, or high temperature, systems (over 400°C

1.3.4.3. Solar collectors for photochemical applications

1.3.4.3.1. Concentrating collectors

The first solar photo-reactor designs for photochemical applications were based on line focus parabolic-trough concentrators (PTCs). In this type of concentrators an absorber tube is placed in the focus of a parabolic reflector. The reflector redirects radiation parallel to the axis of the parable towards the absorber tube in the focus. Consequently, this type of concentrator has to track the sun and can use only parallel direct beam radiation (I_B). One-axis and two-axis tracking systems can be used for this purpose. PTCs concentrators represent a nature engineering concept due to their former similar development for solar thermal applications. They can be easily set-up and scaled-up due to the simple engineering concepts involved (tubular plug-flow photo-reactor with turbulent flow conditions). Turbulent flow ensures good mass-transfer and maintains TiO_2 particles in suspension in case of TiO_2 slurry photo-catalysis. Another advantage is that the photo-reactors are closed systems. Therefore, no

vaporization of volatile compounds takes place. A disadvantage of PTCs is, that due to their geometry they can use only direct beam radiation, which makes them practically useless, when the sky is clouded. They also are rather expensive systems due to the necessary sun tracking system. This applies to the investment as well as to the maintenance costs, because moving parts are prone to require enhanced maintenance effort. Another aspect that has to be taken into account is the possibility of overheating water in large-scale installations with residence times in the concentrating collectors in the range of several minutes (Minero *et al*., 1993)

1.3.4.3.2. Non-concentrating collectors

The elevated prices of PTCs have encouraged the search for cheaper reactor concepts with non-concentrating geometry. Some different types of non-concentrating solar reactors reported are:

• Free-falling film: In the process fluid falls slowly over a tilted plate with a catalyst attached to the surface, which faces the sun and is open to the atmosphere (Wyness *et al*., 1994a; Gernjak *et al*., 2003).

• Pressurized flat plate: consists of two plates between which the fluid circulates using a separating wall (Van Well *et al*., 1997).

• Solar ponds: Small, shallow, on-site pond reactors (Wyness *et al*., 1994b).

As stated, non-concentrating or one-sun collectors are, in principle, cheaper than PTCs as they have no moving parts or solar-tracking devices. They do not concentrate radiation so that efficiency is not reduced by factors associated with concentration and solar tracking. A major advantage is that they harvest not only direct beam but also diffuse radiation. Consequently, they can as well be operated under cloudy sky conditions, although of course with reduced efficiency compared to sunny conditions. Depending on the type of collector vaporization of contaminants can occur. One problem common to non-concentrating collectors is mass transfer problems caused by laminar flow in non-concentrating systems. So, although non-concentrating collectors

potentially present several important advantages their scale-up can be difficult due to reasons such as high pressure drop, inhomogeneous flow conditions.

1.3.4.3.3. Compound Parabolic Collectors (CPC)

CPCs are an interesting cross between PTCs and non-concentrating collectors without their respective disadvantages. CPCs are static collectors with a reflective surface formed by two connected parabolic mirrors with an absorber tube in the focus and have been found to provide the most efficient light-harvesting optics for low concentrating systems (Muschaweck *et al*., 2000). They have no tracking system and the design permits the solar rays to be reflected onto the absorber tube attaining a low concentration factor. The concentration factor is defined as the ratio of the collector aperture to the absorber tube perimeter and is usually between 1 and 1.5 depending on the type of application. Thanks to the reflector design, almost all the radiation (not only direct, but also diffuse) incident at the CPC aperture area can be collected and is available for the process in the reactor. The light reflected by the CPC is distributed around the back of the tubular photo-reactor see Fig (7). The absorber tubes are closed system photo-reactors, in which the waste water can be circulated under turbulent flow conditions. They can be easily up-scaled due to the simple engineering concepts involved. All these factors contribute to excellent performance of CPC collectors in solar photochemical and photo-catalytic applications (Ajona and Vidal, 2000).

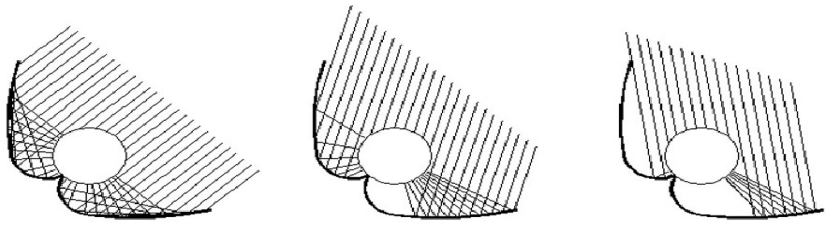

Fig (7): Geometric principle of Compound Parabolic Collector (CPC)

Reactor material must be inert to chemicals and resistant to high or low pH. The choice of materials that are both transparent to UV light and resistant to its destructive effects is limited to quartz glass, fluoropolymers and borosilicate glass. Low-iron-content borosilicate glass has good Tran's missive properties in the solar range to about 285 nm, is cheaper than the others and therefore, seems to be the most adequate (Blanco *et al*., 2000). The ideal reflective surface for solar photochemical applications must be highly UV-reflective, weather-resistant to guarantee long lifetime and reasonably priced. The materials currently available that best fit these requirements are electro-polished anodised aluminum and organic plastic films with an aluminum coating (Blanco *et al*., 2000).

1.3.5. Photo-catalytic reactor

The development and design of water and air treatment systems based on heterogeneous photo-catalysis is an area of great technical importance (De Lasa *et al*., 2005). The design of a highly efficient photo-catalytic system is vital interest and one of the most desirable. An important obstacle in the development of an efficient reactor is the establishment of effect reactor design for intermediate and large scale use as demanded by industrial and commercial use. To achieve a successful implementation several reactor design parameters must be optimized such as photo-reactor geometry, the type of photo-catalyst and its concentration, utilization radiated energy, operating condition.

1.3.5.1. Photo-reactor configuration

Photo-catalytic reactor for water treatment can be classified according to their design characteristics; the majority of them fall under the following categories (De Lasa *et al*., 2005; Mukherjee and Ray, 1999)

a. State of TiO_2 catalyst: slurry reactor or reactor in immobilized photo-catalyst.

b. Type of radiation: photo-reactor can be irradiated using artificial UV light, UV polychromatic lamps or solar radiation.
c. Position of the irradiation source: immersed light source, external light source and distributed light source such as reflectors or optical fibers.

Slurry reactor present larger photo-catalytic activity (De Lasa *et al*., 2005) immobilized of catalyst generally reduce the overall performance of the reactor due to the mass transfer limitations and less irradiated area (Mukherjee and Ray, 1999). Table (4) summarizes the advantages and disadvantages of slurry and immobilized photocatalytic reactor reported by (De Lasa *et al*., 2005; Mukherjee and Ray, 1999).

Table (4): The advantages and disadvantages of slurry and immobilized photo-catalytic reactor

Slurry reactors	**Immobilized reactors**
Advantages • Fairly uniform catalyst distribution • High photo-catalytic surface area to reactor volume ratio • Limited mass transfer • Minimum catalyst fouling effect due to the possible continuous removal and catalyst replacement • Well mix particles suspension • Low pressure drop through reactor **Disadvantages** • Requires post-process filtration • Difficult to assess light scattering and absorption in the particles suspended medium	**Advantages** • Continuous operation • Improved removal of organic Materials from water phase while using a support with adsorption properties • No need for addition catalyst separation operation **Disadvantages** • Low light utilization efficiencies due to light scattering by immobilized photo-catalyst • Restricted processing capacities due to possible mass transfer limitations • Possible catalyst deactivation and catalyst wash out

In the case of photo-catalytic reactor with solar radiation most of the reactor's designs are slurry. (De Lasa *et al*., 2005). The implementation of solar photo-catalytic reactor needs special attention in the design of solar thermal collector, given the important characteristics shared by these units; however specific constrains for the design of solar photo-catalytic reactor; for instance the need of expensive UV transparent materials. Solar photo-catalytic reactor can operate in continuous and discontinuous model. (Rodriguez *et al*., 1996) studied the

degradation of several real waste water samples at the plataforma solar de Almeria (Spain) applying a solar photo-catalytic reactor. They proved the feasibility of solar photo-catalytic detoxification with add oxidants for the treatment of industrial effluents with organic loads of hundreds of ppm. They studied a solar slurry photo-reactor with TiO_2 as catalyst in two different configuration; compound parabolic reactor concentrating reactor and parabolic trough system. Their results showed that the degradation of industrial wastewater can be treated with heterogeneous photo-catalytic within the range of medium or low concentration on total organic carbon load.

1.3.5.2. Operating condition in photo-catalysis

The decolorization of dyes in TiO_2 photo-catalysis is dependent on a number of the operation parameters:

1.3.5.2.1. Effect initial concentration

It was observed that the photo-decolorization decreases with an increase in the initial concentration of dyes. The presumed reason when the initial concentration of dye is increased, more and more dye molecules are adsorbed on the surface of TiO_2, the large amount of adsorbed dye is thought to have an inhibitive effect on the reaction of dye molecules with photo-generated holes or hydroxyl radicals, because of the lack of any direct contact between them. Once the concentration of dye is increased, it also causes the dye molecules to adsorb light and the photons never reach the photo-catalyst surface, thus the photo-decolorization efficiency decreases. (Neppolian *et al*., 2002; Daneshvar *et al*., 2003; Konstantinou and Albanis, 2004; Rauf and Ashraf. 2009; Qamar *et al*., 2005; Saquib *et al*., 2008)

1.3.5.2.2. Effect of pH

Electrostatic interaction between semiconductor surface, solvent molecules, substrate, and charged radicals formed during photo-catalytic oxidation is

strongly dependent on the pH of the solution (Akpan & Hameed, 2009). According to the authorities (Seyyedi and Jahromi, 2014; Sun *et al*., 2008; Huang *et al*., 2008) the interpretation of pH effects on the efficiency of dye photo-catalytic process is a very difficult task because of its multiple roles. First, it is related to the ionization state of the surface according to the following reactions

$$TiOH + H^{+} \Leftrightarrow TiOH_2^{+} \quad (17)$$

$$TiOH + OH^{-} \Leftrightarrow TiO^{-} + H_2O \quad (18)$$

as well as to that of reactant dyes and products such as acids and amines. The pH changes can thus influence the adsorption of dye molecules onto the TiO_2 surfaces, an important step for the photo-catalytic oxidation to take place. The point of zero charge (pzc) of the TiO_2 anatase is at pH = 6.8. Thus, the TiO_2 surface is positively charged in acidic media (pH < 6.8), whereas it is negatively charged under alkaline conditions (pH > 6.8). Second, hydroxyl radicals can be formed by the reaction between hydroxide ions and positive holes. The positive holes are considered as the major oxidation species at low pH whereas hydroxyl radicals are considered as the predominant species at neutral or high pH levels. It was stated that in alkaline solution $OH^{\bullet}$ are easier to be generated by oxidizing more hydroxide ions available on TiO_2 surface, thus the efficiency of the process is logically enhanced between hydroxide ions and positive holes. It was stated that in alkaline solution $OH^{\bullet}$ are easier to be generated by oxidizing more hydroxide ions available on TiO_2 surface, thus the efficiency of the process is logically enhanced. Similar results are reported in the photo-catalyst decolorization of acidic azo dyes and triazine containing azo dyes although it should be noted that in alkaline solution there is a Coulombic repulsion between the negative charged surface of photo-catalyst and the hydroxide anions. This fact could prevent the formation of $OH^{\bullet}$ and thus decrease the photo-oxidation. Very high pH has been found favorable even when anionic azo dyes should hamper adsorption on the negatively charged

surface. At low pH, reduction by electrons in conduction band may play a very important role in the degradation of dyes due to the reductive cleavage of azo bonds. Third, the TiO_2 particles tend to agglomerate under acidic condition and the surface area available for dye adsorption and photon absorption would be reduced. Hence, pH plays an important role in the reaction mechanisms that can contribute to dye degradation, namely, hydroxyl radical attack, direct oxidation by the positive hole and direct reduction by the electron in the conducting band. An additional explanation for the pH effects can be related with changes in the specification of the dye. That is, protonation or de-protonation of the dye can change its adsorption characteristics and redox activity

1.3.5.2.3. Effect of Concentration of catalyst

Concentration of TiO_2 as a photo-catalyst has an important role in the efficiency of the photo-catalytic process (Seyyedi and Jahromi, 2014). (Akpan & Hameed, 2009; Huang *et al.*, 2008) generally advanced for this the increase in the amount of catalyst increases the number of active sites on the photo-catalyst surface, which in turn increase the number of hydroxyl and superoxide radicals. (Sun *et al.*, 2008) In high concentration of catalyst TiO_2 particles form a dense mass and so the active sites of catalyst surface are reduced. The decolorization rate decreases due to the interception of the light by the suspension. (Sun *et al* 2008; Huang *et al*., 2008; Habibi *et al*., 2005) Agglomeration and sedimentation of the TiO_2 particles increased turbidity of the solution and reduces the light transmission through the solution. While concentration of TiO_2 was decreased, it is assumed that the catalyst surface and absorption of light by the catalyst are limiting, thus the quantity of photo-decolorizing $OH^{\bullet}$ radicals are insufficient. The optimum amount of TiO_2 has to be added in order to avoid unnecessary excess catalyst and also to ensure total absorption of light photons for efficient photo-decolorization. (Neppolian *et al*., 2002; Daneshvar *et al*., 2003). This optimum loading of photo-catalyst is found to be dependent on the initial solute

concentration, type of photo-reactor and irradiation methods used (Habibi *et al*., 2005; Zhang et al., 2002).

1.3.5.2.4. Effect of Oxidants

According to (Akpan & Hameed, 2009; Konstantinou, and Albanis. 2004; Saquib *et al*., 2008) oxidizing agents (hydrogen peroxide (H_2O_2), ammonium persulphate ($(NH_4)_2S_2O_8$) and potassium bromate ($KBrO_3$) oxygen (O_2) have a great deal of influence on the photo-catalytic decolorization of dyes. The decolorization rate was found to increase with increase in H_2O_2 concentration. The reactive radical intermediates ($OH^{\bullet}$) formed from hydrogen peroxide (H_2O_2) by reactions with the photo-decolorization electrons can exert a dual function: as strong oxidant themselves and as electron scavengers, thus inhibiting the electron–hole recombination at the semiconductor surface according to the following equations:

$$H_2O_2 + O2^{-\bullet} \rightarrow OH^{\bullet} + OH^- + O_2 \quad (18)$$

$$H_2O_2 + h\nu \rightarrow 2OH^{\bullet} \quad (19)$$

$$H_2O_2 + e_{CB}^- \rightarrow OH^{\bullet} + OH^- \quad (20)$$

Hydrogen peroxide may also be split photo-catalytically to produce hydroxyl radical directly, as cited in the studies of homogeneous photo-oxidation using UV/H_2O_2 Eq. (21)

$$H_2O_2 + h\nu \rightarrow 2OH^{\bullet} \quad (21)$$

At higher dosage of H_2O_2 beyond the optimum, the rate of degradation decreased, because the very reactive $OH^{\bullet}$ radicals and valence band holes could be consumed by H_2O_2 itself as given in Eqs. (22) – (24). At the same time, radical–radical recombination as a competitive reaction must be taken into account, as described in Eq. (25) (Daneshvar *et al*., 2003).

$$OH^{\bullet} + H_2O_2 \rightarrow HO_2^{\bullet} + H_2O \quad (22)$$

$$OH^{\bullet} + HO_2^{\bullet} \rightarrow O_2 + H_2O \quad (23)$$

$$TiO_2(h_{VB}^+) + H_2O_2 \rightarrow TiO2 + O_2 + 2H^+ \quad (24)$$

$$HO^{\bullet} + HO^{\bullet} \rightarrow H_2O_2 \quad (25)$$

Since $HO_2^{\bullet}$ is less reactive than $OH^{\bullet}$ and H_2O_2 can be adsorbed onto TiO_2 particles to modify their surfaces and subsequently decrease its catalytic activity .(Touati *et al*., 2015; Daneshvar *et al*., 2003; Qamar *et al*., 2005; Neppolian *et al*., 2002; Seyyedi, and Jahromi, 2014)

1.3.5.2.5. Effect of temperature

It is well known that the photo-catalytically oxidation rate is not much affected by minor changes in temperature. This weak dependence of the degradation rate on temperature is reflected by the low activation energy (a few kJ/mol) compared to ordinary thermal reactions. Due to the low thermal energy, thus no contribution to the activation energy of the wide band gap TiO_2. The best temperature range for the photo-degradation is 20-80^{o} C (Carp et al., 2004), from the catalyst surface and the exothermic adsorption of pollutant on the catalyst surface, respectively. In general, an increase in temperature increases the recombination of charge carriers and also the desorption process of adsorbed reactant species, so decreases photo-catalytic activity. This is in accordance with the Arrhenius equation, for which the apparent first order rate constant K_{app} should increase linearly with $\exp^{-1/T}$ (Rauf, and Ashraf. 2009). Temperature can also affect adsorption/desorption processes of dyes molecules on the TiO_2 photo-catalyst surface. Since the band gap energy of TiO_2 is so high (3 eV); therefore, thermal excitations do not have an important role. Hence, bulk and surface phenomena can be strongly influenced with temperature variation.(Habibi *et al*., 2005)

1.3.5.2.6. Photon flux

Solar light irradiance changes daily and even on the same day (Tianyong *et al*., 2002). The rate of initiation for photo-catalysis and electron–hole formation in the photochemical reaction is strongly dependent on the light intensity. Higher light intensity will enhance excitation of photo-catalyst particles to generate electron–hole pairs (e^-/h^+), Because at low light intensity reactions involving electron–hole (e^-/h^+) formation are predominant and electron–hole

recombination is negligible. However, at increased light intensity electron–hole pair (e^-/h^+) separation competes with recombination, thereby causing lower effect on the reaction rate. It is evident that the percentage of decolorization and photo-degradation increases with increase in irradiation time. (Konstantinou, and Albanis., 2004).

Chemical actinometer:

According to the Glossary of terms used in photochemistry, an actinometer is a chemical system or physical device by which the number of photon in abeam absorbed into the defined space of a chemical reactor. Photon flux can be estimated by chemical actinometer which is a chemical system (fluid, gas, solid or micro-heterogeneous environment) that undergoes a light-induced reaction (at a certain wavelength λ) for which the quantum yield Φ (λ) is accurately known. In chemical actinometer photochemistry conversion is directly related to the number of photons absorbed because the chemical action of light means reversible or irreversible change. Chemical actinometer has been employed for about 70 years in photochemistry as a relatively simple and accurate method for radiation measurement. In particular, iron (III) potassium oxalate trihydrate $K_3[Fe(C_2O_4)_3].H_2O$ which is commonly called ferrioxalate actinometer is the most popular actinometer, because it has high and constant quantum yields over the UV-vis. region (250-500 nm) (Kuhn et al., 2004). Ferrioxalate actinometry is based on the photo-generation of Fe^{2+} ions through the photo-induced (ligand-to-metal charge transfer) (LMCT) eq. (26) and the subsequent reductive reaction via CO_2 radical anions, $CO_2^{\cdot-}$ eq. (28). The concentration of Fe^{2+} ions has been commonly determined after complexation with 1-10-phenanthroline and the subsequent absorbance measurement (λ_{max}) 510 nm) (Demas *et al*., Lee *et al*., 2007).

$$[Fe\ (C_2O_4)^3]^{3-} + h\nu \longrightarrow Fe^{2+} + C2O4^{\cdot-} + 2(C_2O_4)^{2-} \quad (26)$$

$$C_2O_4^{\cdot-} \longrightarrow CO_2 + CO_2^{\cdot-} \quad (27)$$

$$[Fe\ (C_2O_4)^3]^{3-} + CO_2^{\cdot-} \longrightarrow Fe^{2+} + 3(C_2O_4)^{2-} + CO_2 \quad (28)$$

Chapter two

Materials and Methods

2.1. Materials

2.1.1Chemicals

- A.R. Pure Titanium dioxide from Aldrich.
- Tubantin blue BRR-HC, Tubantin red, Methylene blue and Reactive and Yellow 145 from Bezema Fig. (8) is shown their chemical structure.
- A.R. Titanium tetrachloride ($TiCl_4$)(MW 189.87gmol-1, 99.9%),
- A.R. absolute ethanol.
- A.R. Ammonium hydroxide (MW, 17.03gmol-1, 25%)
- Distilled water.
- A.R. silver nitrate (MW 169.87 gmol-1, 98.4%).
- A.R. Ferric trichloride ($FeCl_3$)
- A.R. potassium oxalate.
- A.R. conc sulfuric acid.
- A.R. sodium hydroxide 1%
- A.R. 1-10phenanthroline
- A.R. Sodium acetate.

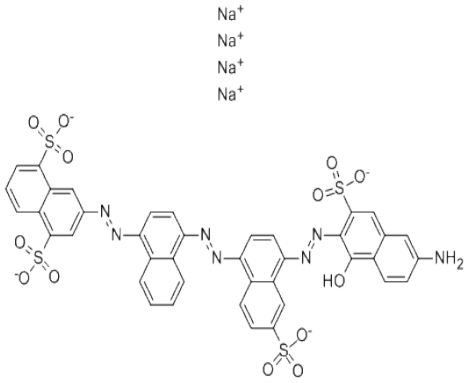

Tubantin blue BRR HC

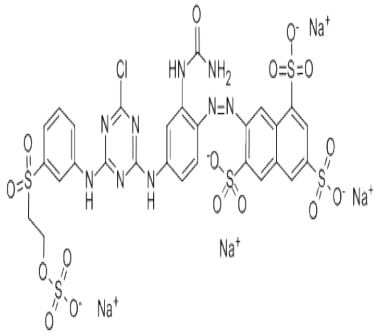

Tubantin red 6BLL C

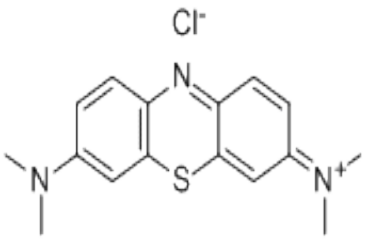

Methylene blue

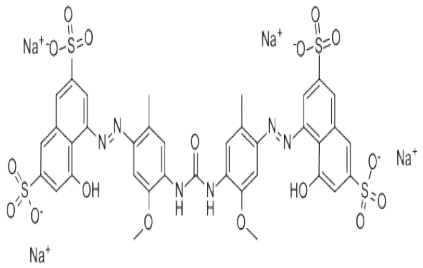

Reactive Yellow 145

Fig (8): chemical structure of dyes under study [140]

2.1.2 Instruments

- PANalytical's X-ray diffractometer (Cu X-ray λ = 1.540598Å) over range 10 – 60 °2θ
- Micrometric gas adsorption analyzer using the nitrogen pressures at a constant temperature (typically liquid N_2, 77K).
- Fourier transform infrared (FTIR) spectroscopy using FTIR-8400S.
- Ocean optio USB2000 Spectrometer connects to desktop PC via USB port or serial port, Ocean Optics OOIBase32 software application installed and configured for use with the USB2000 OOIBase32 can use to perform spectroscopic measurements (such as absorbance, reflectance, and emission).
- pH meter.

- UV-visible spectrophotometer (Aqunova spectrophotometer (Jenway).
- Sensitive balance.
- Centrifuge.
- Magnetic stirrer.
- Stop watch.
- Parabolic compound collector (CPC) solar collector was built by Dr. Saleh Hamdo at Solar Energy Equipment Co) and Photo-reactor : borosilicate tube (length 50 cm, d 5cm) (built by technician Ahmed at physics Department – faculty of science – University of Khartoum) with slot on end to outlet the product

2.2. Methods

2.2.1. Preparation of actinometer

1.5M ferric trichloride solution was prepared (60.9375g in 250 cm^3). 1.5M Potassium oxalate solution was prepared (62.25g in 250 cm^3). Then 3 vol. of $K_2C_2O_4$ solution were mixed with 1 vol. of $FeCl_3$ with vigorous stirring for 30 min. The precipitate was recrystallized three times from warm water and the crystals were dried in air at 45°C. The composition corresponds to potassium tris (oxalato ferrate III) trihydrate $K_3[Fe(C_2O_4)^3].3H_2O$. The absorption spectrum was taken for the complex.(Kuhn et al., 2004)

2.2.2. Preparation of TiO_2 sol-gel catalyst

Sample of titanium dioxide was prepared by using Sol-gel method , 30 cm^3 of titanium tetrachloride was added to 500cm^3 distilled water in ice bath in fume hood followed by addition 350 cm^3 of ethanol with vigorous stirring for 30 min at room temperature , drops of ammonia solution 25% were added wisely to mixture until pH 8 and precipitate was obtained. After stirring vigorously for 30 min the solution was made to settle for 24 hours. Then the precipitate was centrifuged and washed with distilled water to remove chloride ions using silver

nitrate to detect that, then the precipitate was centrifuged and dried at 200 °C for two hours and amorphous TiO_2 was obtained. The amorphous TiO_2 was calcinated at 600 for four hours. Finally the powder of titanium dioxide nanoparticles was obtained. (Hayle and Gonfa, 2014).

2.2.3. Characterization of TiO_2 catalysts

2.2.3.1. X-ray powder diffraction (XRD)

X-ray powder diffraction (XRD) was performed using PANalytical's X-ray diffractometer (Cu X-ray λ = 1.540598Å) over range 10 – 60 °2θ The powdered sample was packed on the sample holder by back pressure technique and mounted on the sample stage of the machine. This was and used to characterize both (pure TiO_2 & TiO_2 sol-gel) samples and determine particles structure and crystal size from the XRD pattern. The crystallite sizes of the TiO_2 nano-materials were estimated using Schere equation (13) (Han 2012, Hayle and Gonfa , 2014)

$$d = \frac{\lambda K}{\beta \cos \theta} \qquad (13)$$

where d is crystallite size in nanometer, K is shape factor constant, which is 0.89, β is the fullwidth at half maximum (FWHM) in radian, λ is the wavelength of the X-ray which is 0.1540598 nm for Cu target Kα radiation and θ is the Bragg angle.

2.2.3.2. The specific surface area and porosity of the TiO_2 catalyst

The specific surface area and porosity of the pure TiO_2 and TiO_2 sol-gel were evaluated by using Micrometric gas adsorption analyzer, in which the nitrogen pressures were at a constant temperature (typically liquid N_2, 77 K). The sample loaded (0.1036 g of sample 1, 0.6098 g of sample 2)(Analysis Time is 281.6 min for sample 1571.2 min for sample 2) then nitrogen adsorption isotherm of both samples were analyzed for the specific surface area using the BET equation (15) which required a linear plot of $1/[W(P/P_0)-1]$ against P/P_0

$$slope = \frac{C-1}{W_m\,C}\ ,Intercept = \frac{1}{W_m\,C} \quad (14)$$

$$\frac{1}{W\left((P_0\ /P)-1\right)} = \frac{1}{W_m\,C} + \frac{C-1}{W_m\,C}\left(\frac{P}{P_0}\right) \quad (15)$$

W= weight of gas adsorbed, P/P_0 =relative pressure, W_m = weight of adsorbed as monolayer, C = BET constant

2.2.3.3. Fourier transform infrared (FTIR) spectrum of TiO_2 catalysts

Fourier transform infrared (FTIR) spectrum was recorded by using FTIR-8400S Fourier transform infrared spectroscopy samples were grind down with KBr and press to make disk and insert into the sample holder then take the FTIR spectra in range (400 – 3000cm^{-1}).

2.2.3.4. Optical properties of TiO2 catalysts

Optical properties (absorption coefficient, extinction coefficient, the refractive index and the energy band gap) were determined by using Ocean optio USB2000 Spectrometer connects to desktop PC via USB port or serial port, Ocean Optics OOIBase32 software application installed and configured for use with the USB2000 OOIBase32. It can be used to perform spectroscopic measurements (such as absorbance, reflectance, and emission). First stored reference and dark measurements then the light from the light source transmits through an optical fiber to the sample so the light interacts with the sample. There is another optical fiber collects and transmits the result of the interaction to the spectrometer, The spectrometer passes the sample information to OOIBase32 then OOIBase32 compares the sample to the reference measurement and displays processed spectral information. In reflectance spectroscopy, the Kubelka–Munk remission function $F(R)$ replaces the Lambert-Beer law (Sikorska *et al*., 2003).

$$F(R) = \frac{(1-R)^2}{2R} = \frac{K}{S} \quad (16)$$

Where *R* represents the observed diffuse reflectance from the surface of the sample, *K* and *S* are absorption and scattering coefficients, respectively. It should be noted that the values of *F*(*R*) are proportional to *K*, which is proportional to the absorber concentration. However, for quantitative simulation of an absorption spectrum of a sample in a scattering environment, the use of Kubelka–Munk function is essential (Sikorska et al., 2003)

The optical absorption coefficient, *α*, which is the relative rate of decrease in light intensity along its path of propagation, was calculated using equation (17) from the transmittance and reflectance data in the wavelength range 300 - 800 nm. The nature of the optically induced transitions was determined from these data (Baydoğan *et al*., 2013)

$$\alpha(h\nu) = \frac{1}{d} ln\left[\frac{(100-R)^2}{T}\right] \quad (17)$$

Where *T* is the transmittance, *R* is the reflectance, and *d* is the sample thickness.

The extinction coefficient was calculated using equation (18) (Baydoğan *et al*., 2013).

$$k = \frac{\alpha\lambda}{4\pi} \quad (18)$$

Where k is extinction coefficient, α is absorption coefficient and λ is wavelength.

The energy band gap of these materials is determined using the reflection spectra. According to the Taucc relation, the absorption coefficient, for direct band gap material is given by Sharma equation (19) .

$$\alpha(h\nu) = \left(B - E_g\right)^n \quad (19)$$

Where E_g the energy gap, B constant is different for different transitions, (hν) is energy of photon and n is an index which assumes the values 1/2, 3/2, 2 and 3 depending on the nature of the electronic transition responsible for the reflection. The exponent *r* = 1/2, 3/2 for indirect transition is allowed or

forbidden in the quantum mechanical sense, and r = 2, 3 for allowed and forbidden direct transition, respectively. (Baydoğan *et al*., 2013)

The refractive index determined using transmittance and reflectance measurements which are given by the following relation:

$$n = \left(\frac{1+R}{1-R}\right) + \sqrt{\left(\frac{4R}{(1-R)^2} - k^2\right)} \quad (20)$$

Where n is the refractive index, R is the reflectance and k is extinction coefficient. (Yakuphanogle *et al*., 2004)

2.2.4. TiO_2 photo-catalytic for removal dyes under solar radiation

2.2.4.1. Photo-reactor setup

All experiments were performed under the air and natural solar radiation using the solar CPC which was constituted of one CPC unit (0.2m^2) and tilted 15° N local latitude. The cylindrical photochemical reactor which was made-up of borosilicate glass (length 50cm, d 5cm) its capacity is800 cm^3. The slot was opened during experimentation Fig. (9).

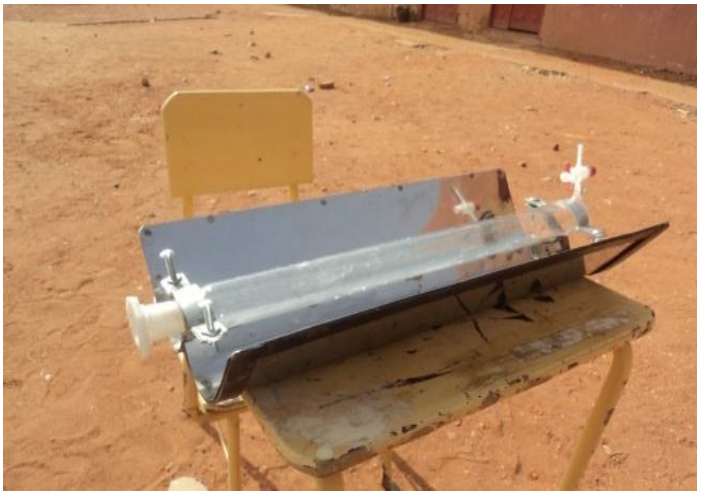

Fig (9): Photo-reactor for photo-decolorization of dye

2.2.4.2. Determination of photon flux

2.947g of ferrioxalate actinometry (0.006M) solution was prepared in 100 cm^3 of H_2SO_4 (0.5 M) and diluted with distilled water to 1 dm^3. 450 cm^3 (V_1) of solution irradiated under solar light using photo-reactor in Fig. (9) for 30 min. 10 cm^3 (V_2) of irradiated solution was transferred into 50 cm^3 volumetric flask

(V_3) containing a mixture of 5 cm^3 of 0.1% 1.10-phenanthroline solution and 2.5 cm^3 buffer pH 5 and diluted to the mark with distilled water. A reference is prepared in the same way except that it has not been irradiated. Both solutions were kept in the dark for (about 30 min) until full color development is achieved, and the absorbance difference between the two samples were measured at 510 nm [optical path length l=2.5cm, ε (510nm) = 11100 $dm^3mol^{-1}cm^{-1}$, Φ (510 nm) = 1.26 (0.006M)]. The photon flux amount $q_{n,p}$ Einstein s^{-1} was calculated by (Kuhn *et al*., 2004)

$$q_{n,p} = \frac{\Delta A V_1 V_3}{\Phi(\lambda)\, \varepsilon(510nm)\, V_2 l t} \qquad (21)$$

2.2.4.3. Influence of operating conditions on photo-decolorization of dye

500 cm^3 of dye solution was taken for all experiments, desired initial concentration for the different experiment (12.5, 25, 50, 100 and 200 ppm) were prepared from a stock solution of 1000 ppm. The pH was adjusted in (1.7, 3.3, 7.4, 9.4 and 10.6) using 1% H_2SO_4 or 1% NH_4OH. Desired amount of catalyst (0.1, 0.125, 0.25, 1, 2 and 3 g). The experiments were repeated using H_2O_2 (30%) in different volumes (12.5, 20, 25, 37.5, 50 cm^3). In all experiments the reactor was washed with distilled water. Then the mixture was stirred for 30 min. and exposed to solar radiation for two hours. The effect of irradiation time (1-6 hours) under optimum parameters was monitored. Then the absorbance was taken at 436,525 and 620nm and the average were calculated (Alinsafi *et al*., 2007). The percentage removal color was determined using equation (22):

$$decolorizatin\,\% = \frac{A_i}{A_f} \times 100 \quad \text{- (22)}$$

Where A_i is initial absorbance and A_f is final absorbance (Selcuk, 2005; Alinsafi *et al*., 2007; Khlifia *et.al*., 2010), then the decolorization percentage versus irradiation time was plotted .

2.2.4.4. Photo-decolorization of different dyes

In all experiments the reactor was washed with distilled water. 50 ppm of dyes (Tubantin blue BRR-HC, Tubantin red, Methylene blue and reactive Yellow

145) solution was taken. The pH 9 was adjusted using 1% H_2SO_4 or 1% NH_4OH. 1g/dm^3 of catalyst (pure TiO_2 and TiO_2 sol-gel) was added then the mixture was stirred for 30min and was put in the photo-reactor containing 20 cm^3 of H_2O_2 (30%) and exposed to solar radiation for five hours. The sample was taken each hour and separated by centrifuge then absorbance was taken at 436, 525 and 620 nm and the average was calculate and the percentage of color removal was determination by equation (22):

2.2.5. Kinetic study of photo-decolorization of dyes

2.2.5.1. Determination of (λ_{max}) of dyes

It was prepared 10 ppm of dye solution and was recorded its absorbance at wavelength in range (400-800 nm), then was plotted the absorbance versus the wavelength.

2.2.5.2. Calibration curve for dyes

It was prepared different concentration (10-50 ppm) of (Tubantin blue BRR-HC, Tubantin red, Methylene blue and Reactive and Yellow 145) dyes solution, then was recorded the absorbance of each concentration at 610 nm for methylene blue, 593 nm for tubantin blue, 510 nm for tubantin red and 417 nm for yellow reactive, then was plotted the absorbance versus concentration.

2.2.5.3. Determination of change of dye concentration during photo-catalytic reaction

In all experiments the reactor was washed with distilled water. 50 ppm of dyes (Tubantin blue BRR-HC, Tubantin red, Methylene blue and reactive Yellow 145) solution was taken. The pH 9 was adjusted using 1% H_2SO_4 or 1% NH_4OH. 1g/dm^3 of catalyst (pure TiO_2 and TiO_2 sol-gel) was added then the mixture was stirred for 30 min and was put in the photo-reactor containing 20 cm^3 of (30%) H_2O_2 and was exposed to solar radiation for five hours. Samples were taken each hour and separated by centrifuge then absorbance was read at 610 nm for methylene blue, 593 nm for tubantin blue, 510 nm for tubantin red

and 417 nm for yellow reactive, then dye concentration was calculated independent on their absorbance from calibration curve.

Chapter three

Results and Discussion

Part I: preparation of actinometry and Titanium dioxide and characterization

3.1.1. Preparation of potassium ferrioxalate actinometry

When mixing 3vol of $K_3C_2O_4$ solution with 1 vol. of $FeCl_3$ with vigorous stirring green crystal of potassium (tris (oxalato) ferrate III) trihydrate is formed, see Fig.(10). Table (5) and Fig. (11) are shown the result of scan for potassium (tris(oxalato)ferrate III) trihydrate by using UV-visible spectrophotometer and λ_{max} 385 nm.

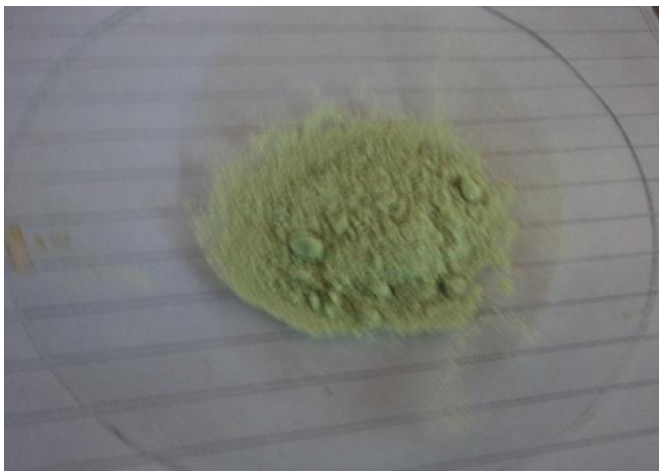

Fig (10): Potassium ferrioxalate actinometry

Table (5): Total absorption spectrum to Potassium ferrioxalate

Wavelength λ nm	**Absorbance A**
380	0.200
385	0.210
390	0.181

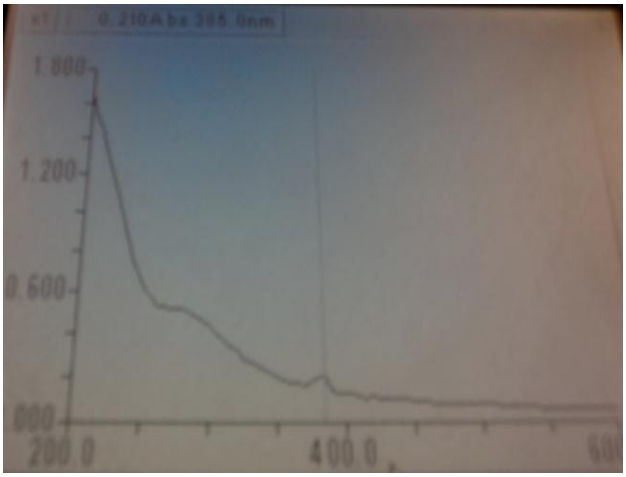

Fig (11): Total absorption spectrum to Potassium ferrioxalate

3.1.2. Preparation of Sol-gel TiO2 catalyst

When added $TiCl_4$ solution to distilled water under fume hood, an exothermic reaction were observed. Then, a white precipitate was obtained after adding a drop of ammonium hydroxide (NH_4OH) wisely; and the yellow gel rose. The gel being yellow indicates the formation of Ti $(OH)_4$. After stirring the solution using magnetic stirrer for 30 min and settling overnight, the precipitate was centrifuged. Then, the obtained precipitate was placed in an oven at 200^oC for 2 hours in order to dry, which leads to the formation of white amorphous TiO_2; after cooling at room temperature, the amorphous white TiO_2 was obtained. The obtained amorphous white TiO_2 was placed in furnace at 600°C for 4 hours to calcinate. This calcination leads to the formation of white powder TiO_2. After cooling at room temperature, the product was ground using agate mortar. Finally, the ground TiO_2 powder was obtained. The Weight of precipitate before calcination is 19.2005 g. The weight of precipitate after calcinations is 14.4458 g.

Fig (12): Titanium dioxide by Sol-gel

3.1.3. Characterization of the catalysts

3.1.3.1. X-Ray Diffraction

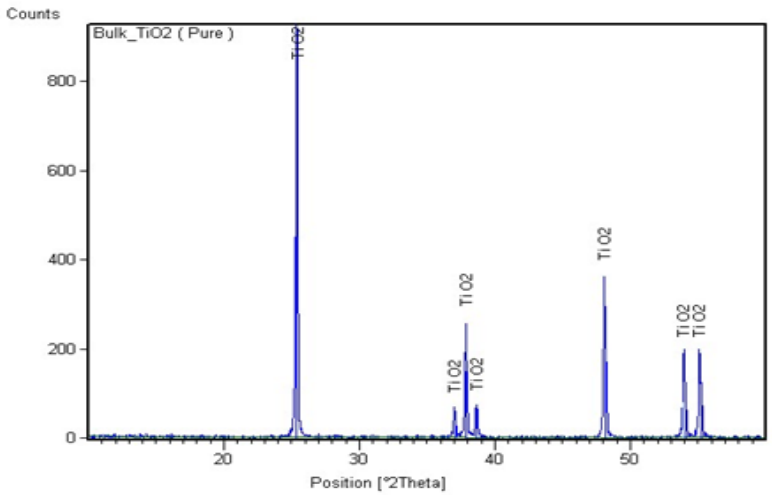

Fig (13): The XRD pattern of pure TiO_2

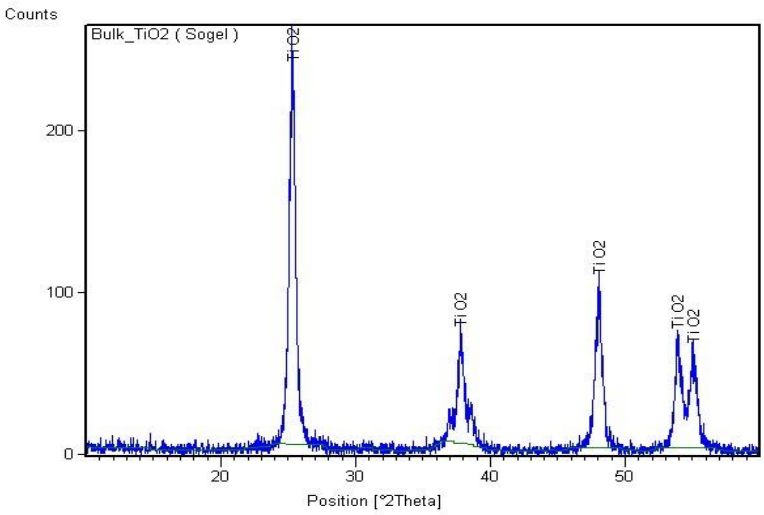

Fig (14): : The XRD pattern of TiO_2 sol-gel

As can be observed from Fig (13and 14) , the XRD peaks were in the angle range of 20°< 2θ° < 60° for pure TiO_2 are 25.4039°, 36.9877°, 37.8628°, 38.6280°,48.0839°,53.9365° and 55.1030° and for TiO_2 sol-gel are 25.3275°, 37.8174°,48.0607°, 53.8852° and 55.0714°. Among the XRD peaks, the width of 25.4039° for pure TiO_2 and 25.3275° for TiO_2 (sol-gel) are useful peaks since they have high intensity which in turn are used to determine crystals size using equation (13) the estimated crystalline size is given in the Table (6). The peaks value corresponds to the tetragonal anatase phase.

Table (6): Crystallite size (d) of pureTiO_2 & sol-gel TiO_2 nano-materials equation (13)

Sample	**2θ°**	**FWHM radians**	**Crystalline size Nm**
TiO_2 (pure)	25.4039	0.0030908	49.11070
TiO_2(sol-gel)	25.0819	0.0068696	22.08194

3.1.3.2. Micrometric gas adsorption analyzer

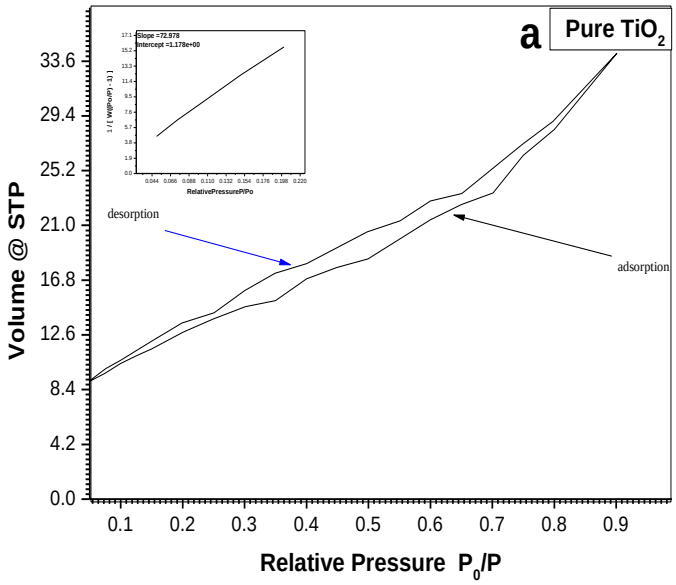

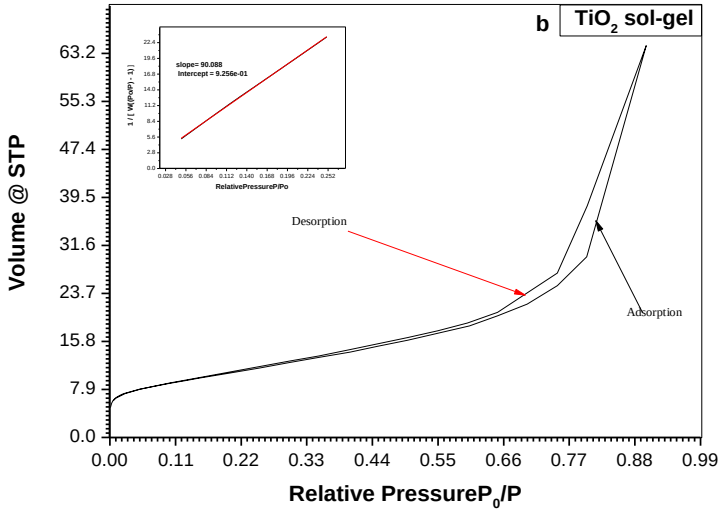

Fig (15): a. Nitrogen Adsorption-Desorption isotherm of pure TiO_2 b. Nitrogen Adsorption-Desorption isotherm of TiO_2 sol-gel

Fig. (15a, b) are shown the nitrogen adsorption and desorption isotherm. The isotherm exhibits type IV pattern with hysteresis loop characteristic of mesoporous material according to the classification of IUPAC. A sharp increase in adsorption volume of N_2 was observed and located in the P/Po range of (0.067 – 0.88), (0.36 – 0.89) for pure TiO_2 and TiO_2 sol-gel respectively. The specific surface area of the pure TiO2 is 46.962m²/g and the specific surface area of the TiO_2 sol-gel is 38.264m²/g. (Govindaraj *et al*., 2015)

3.1.3.3. Fourier transform infrared (FTIR) spectroscopy

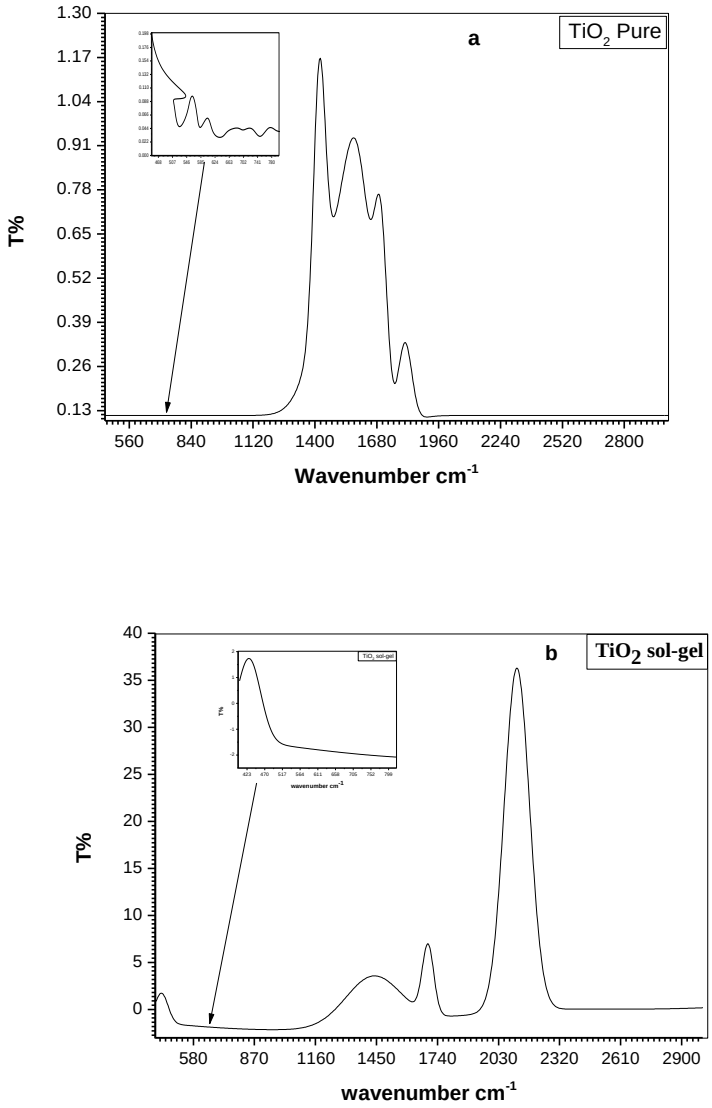

Fig (16): a. The FTIR spectra of pure TiO_2 b. The FTIR spectra of TiO_2sol-gel

In these spectrums different peaks formed at different wave number (400 – 3000cm^{-1}). It is observed in both spectrums that pure TiO_2, TiO_2 sol-gel various frequency vibrations which are shown by different peaks formed. The peak in range (400 – 800cm^{-1}) is characteristic Ti—O. The peak in range 1426-1696 cm-1 were characteristic of O—Ti—O bond and Ti = O bending region. In the Fig. (16b) there is a peak in range (2000- 3000cm^{-1}) characteristic O—H **(** Grujić-Brojčin *et al*., 2006**)**

3.1.3.4. Optical properties using USB2000 spectrometer

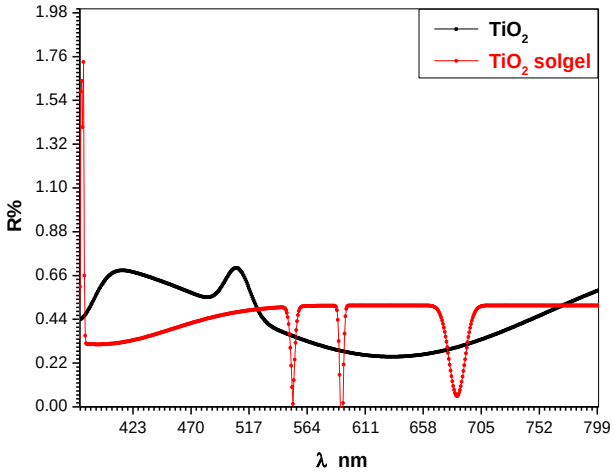

Fig (17): The reflectance spectra of pure TiO_2 and TiO_2 sol-gel

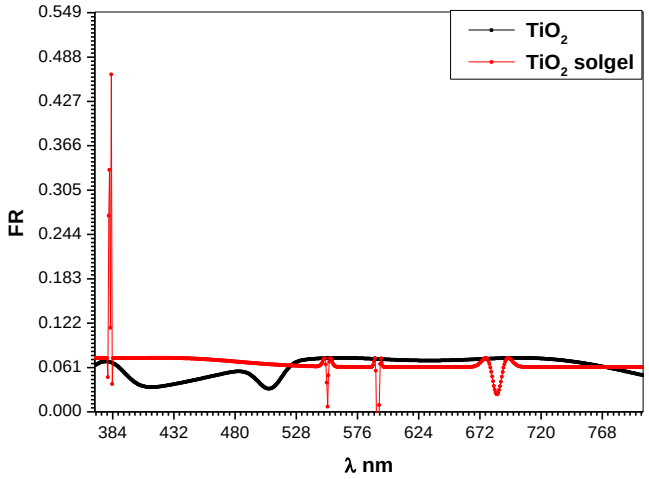

Fig (18): Diffuse reflectance spectrum of pure TiO_2 and TiO_2 sol-gel with Kubelka-Monk conversion

Fig. (17and 18) shows that the reflectance spectra and Diffuse reflectance spectrum of pure TiO_2 and TiO_2 sol-gel. From reflectance spectra noticed that maximum value at region (371 – 408 nm), (483- 506 nm) and above 650 nm decreased in region (410 - 629) for pure TiO_2, while TiO2 sol-gel it has a maximum value at region (373 – 694 nm) the curves reach saturation above 669nm, decreased in region (520 -540 nm),(576 - 584) and (657 -690 nm) .

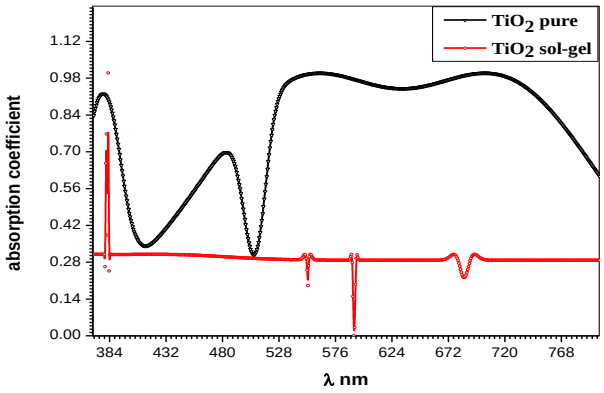

Fig (19): The optical absorption coefficient of pure TiO_2 and TiO_2 sol-gel

The optical absorption coefficient, α, which is the relative rate of decrease in light intensity along its path of propagation, was calculated using equation (17) from the transmittance and reflectance data in the wavelength range 300 - 800 nm. (Baydoğan *et al*., 2013). The optical absorption coefficient was found to be exponentially dependent on the photon energy. The exponential dependence of the optical absorption coefficient may arise from the electronic transitions between the localized states, which have tailed off in the band gap. However when the particle size decrease the optical absorption coefficient will increase. Fig. (19) shows that TiO_2 sol-gel has high value 0.99 at 384nm and pure TiO_2 has 0.92 at 379nm.

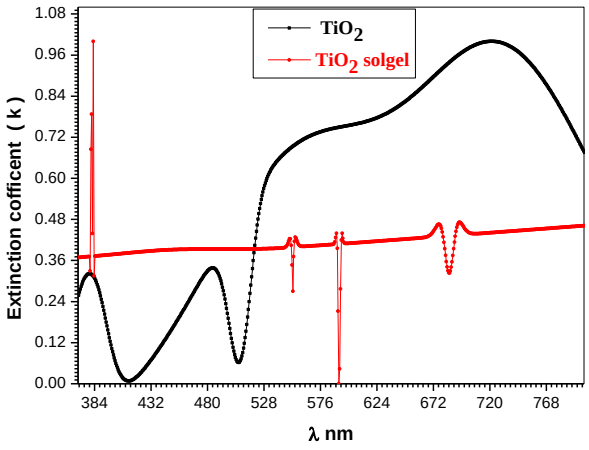

Fig (20): The extinction coefficient pure TiO_2 and TiO_2 sol-gel

The extinction coefficient shown in the Fig. (20) which was calculated using equation (18). The difference in values of extinction coefficient for the two sample pure TiO_2 (0.32), TiO_2 sol-gel due to the fact that TiO_2 sol-gel calcined at 600°C and has small particle size.

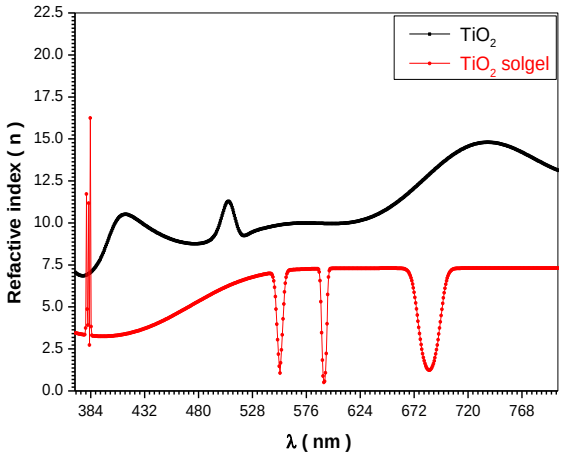

Fig(21)The refractive index as a function of wavelength of pure TiO_2 and TiO_2 sol-gel

In Fig. (21) it is noticed that refractive index determined using transmittance and reflectance measurements from Fig. (21) is noticed the fact that the refractive index has a maximum value of 10.5 at wavelength 415 nm for TiO_2 pure and 16.3 at wavelength 384 nm for TiO_2 sol-gel which is due to interactions taking place between photons and electrons. The refractive index changes with the variation of the wavelength of the incident light beam were due to these interactions, i.e. the optical loss caused by absorption and scattering (Baydoğan *et al*., 2013).

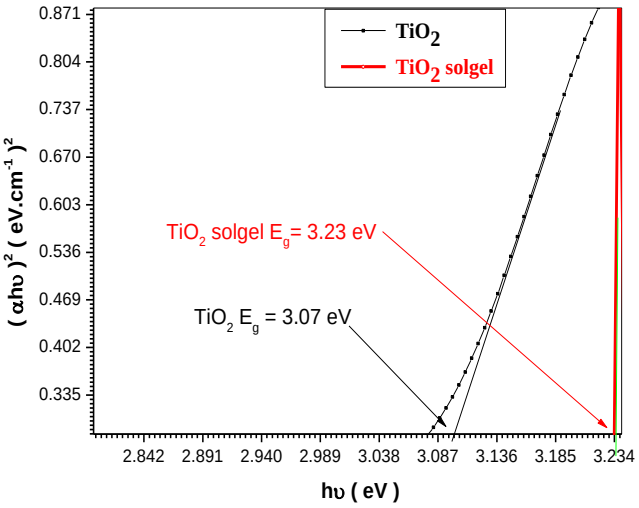

Fig (22): The optical energy gab spectrum for pure TiO_2 and TiO_2 sol-gel

The energy band gap of these materials is determined using the reflection spectra. According to the Taucc relation, the absorption coefficient, for direct band gap material is given by Sharma equation (19). From fig (22) the difference in the energy band gap is 3.07 eV for pure TiO_2 and 3.23eV for TiO_2 sol-gel was due to their particle size (Baydoğan *et al*., 2013)

Part II: parameters optimization for decolorization of Tubantin blue and decolorization of different kinds of dyes

3.2.1. parameters optimization

3.2.1.1. Effect of pH

Table (7): Change of dye absorbance photo-decolorization of Tubantin blue dye dependent on pH of solution

pH		Absorbance at 436nm	Absorbance at 525 nm	Absorbance at 620 nm	Average	De-colorization %
1.7	**before**	0.911	2.183	2.331	1.808	**16.03**
	after	1.501	1.946	1.090	1.518	
3.3	**before**	0.563	1.486	1.812	1.193	**10.34**
	after	1.174	1.308	0.846	1.451	
7.4	**before**	0.662	1.823	2.264	1.583	**16.80**
	after	0.984	1.649	1.889	1.512	
9.4	**before**	0.550	1.564	2.086	1.400	**36.90**
	after	0.775	1.046	0.829	0.883	
10.6	**before**	0.441	1.223	1.735	1.133	**10.94**
	after	0.999	1.168	1.131	1.009	

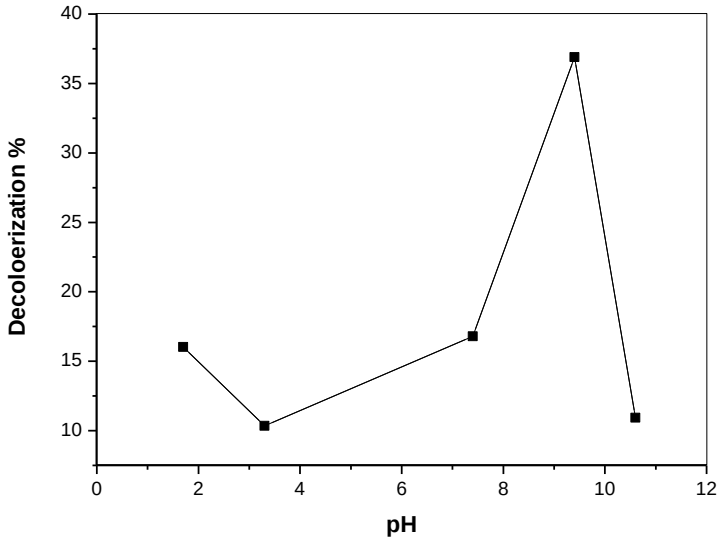

Fig(23) : Decolorization percentage of Tubantin blue dye dependent on pH

The pH of the solution is useful to achieve maximum removal. The pH control of solution is very effective, so that changes in pH of solution have a significant impact on the decolorization process. Table (7) presented the effect of solution pH was studied in the range of (1.7, 3.3, 7.4, 9.4 and 10.6) using 1% NaOH and

1%H_2SO_4, Fig. (23) demonstrates the photo-catalytic decolorization of Tubantin blue, The best results for of Tubantin blue BRR-HC was obtained in alkaline pH (9.4), due to the dye molecular weight and its structure, very high pH have been found favorable even when anionic azo dyes should hamper adsorption on the negatively charged surface. Also they were stated that in alkaline solution $OH^{\bullet}$ are easier to be generated by oxidizing more hydroxide ions available on TiO_2 surface, thus the efficiency of the process is logically enhanced (Mohammad *et al*., 2005; Konstantinou, and Albanis., 2004; Akpan, 2009; Saquib *et al*., 2008).

3.2.1.2. Effect of Amount of Catalyst

Table (8): Change of absorbance of dye on photo-decolorization of Tubantin blue dye at dependent on amount of catalyst

Amount of catalyst g/dm^3		**Absorbance at 436nm**	**Absorbance at 525nm**	**Absorbance at 620nm**	**Average**	**Decoloration %**
0.1	**before**	0.662	1.823	2.264	1.583	**4.466**
	after	0.928	1.720	1.889	1.512	
0.125	**before**	0.675	1.798	2.242	1.572	**0.191**
	after	0.996	1.786	1.924	1.569	
0.25	**before**	1.046	2.480	2.500	2.009	**1.082**
	after	1.304	2.041	2.249	1.747	
1	**before**	0.662	1.823	2.264	1.583	**16.80**
	after	0.984	1.649	1.318	1.317	
2	**before**	0.521	1.552	2.120	1.418	**1.880**
	after	1.341	1.693	1.342	1.391	
3	**before**	0.521	1.552	2.120	1.418	**11.80**
	after	1.104	1.421	1.224	1.250	

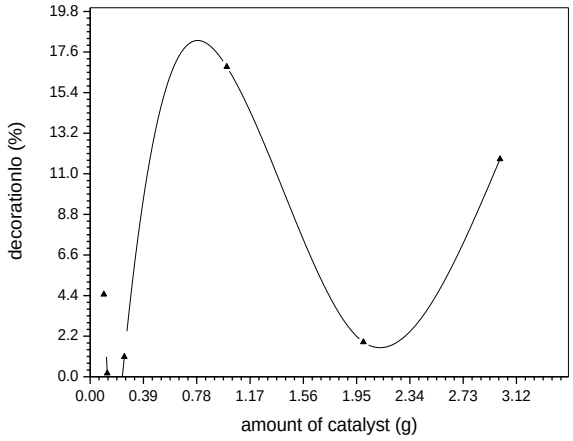

Fig(24) : Decolorization percentage of Tubantin blue dye dependent on amount of catalyst

Table (8) demonstrates the effect of TiO_2 amount on the photo-catalytic on decolorization of Tubantin blue BRR-HC which was studied in the range of (0.1, 0.125, 0.25, 1, 2, 3g). In Fig. (24) it was observed decolorization was increased by increasing the photo-catalyst amount (Akpan, 2009). The reason generally due to the increase in the amount of catalyst increases the number of active sites on the photo-catalyst surface, which in turn increase the number of hydroxyl and superoxide radicals which leads to an increase in the percentage of decolorization. Otherwise it was decreased the catalyst surface and absorption of light by the catalyst are limiting (Neppolian *et al*., 2002; Daneshvar *et al*., 2003).

3.2.1.3. Effect of Initial Concentration of Dyes

Table (9): Change of absorbance of dye on photo-decolorization of Tubantin blue dye dependent on concentration of dye

Concentration of dye ppm		**Absorbance at 436 nm**	**Absorbance at 525 nm**	**Absorbance at 620 nm**	**Average**	**Decolorization %**
12.5	**before**	0.176	0.425	0.635	0.4120	**53.46**
	after	0.222	0.180	0.170	0.1910	
25	**before**	0.343	0.825	1.226	0.8070	**42.54**
	after	0.505	0.510	0.376	0.4633	
50	**before**	0.662	1.823	2.264	1.5830	**16.8**
	after	0.984	1.649	1.318	1.3170	
100	**before**	1.070	2.406	2.485	1.9870	**1.857**
	after	1.352	2.031	2.190	1.8577	
200	**before**	1.046	2.480	2.500	2.0090	**1.8747**
	after	1.304	2.041	2.249	1.8747	

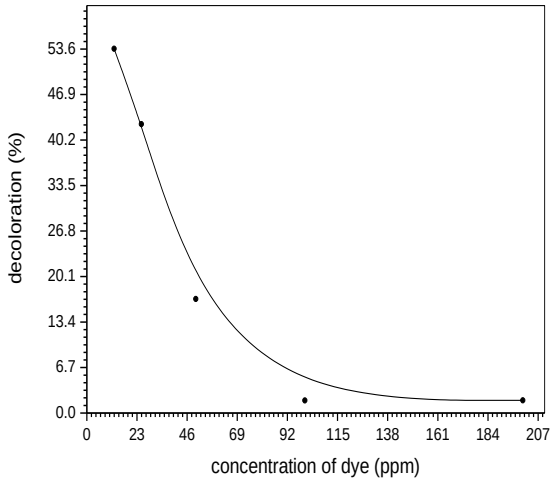

Fig. (25) : Decolorization percentage of Tubantin blue dye dependent on concentration of dye

The effect of initial concentration of dye on the rate of degradation was performed by varying the initial dye concentration (12.5, 25, 50, 50,100 and 200ppm). It can be seen from Table (8) and Fig (25) percentage decolorization decreases as the initial concentration of the dye increases. According to (Daneshvar *et al.*, 2003; Konstantinou, and Albanis., 2004) the rate of decolorization relates to the probability of $OH^{\bullet}$ radicals formation on the catalyst surface and to the probability of $OH^{\bullet}$ radicals reacting with dye molecules so

when the initial concentration of dye is increased more and more dye molecules are adsorbed on the surface of TiO_2 whereas less number of photons are available to reach the catalyst surface and therefore less $OH^{\bullet}$ are formed.

3.2.1.4. Effect of Time of Irradiation

Table (10): Change of absorbance of dye on photo-decolorization of Tubantin blue dye dependent on radiation time

Time of irradiation hour	Absorbance at 436 nm	Absorbance at 525 nm	Absorbance at 620 nm	Average	Decolorization %
0	0.515	1.394	1.929	1.2793	**0**
1	0.730	1.148	1.124	1.0007	**21.8**
2	0.675	0.790	0.647	0.7040	**45.0**
3	0.679	0.567	0.402	0.5493	**54.7**
4	0.386	0.299	0.177	0.2873	**77.5**
5	0.272	0.179	0.116	0.1504	**88.2**
6	0.132	0.125	0.048	0.1017	**92.01**

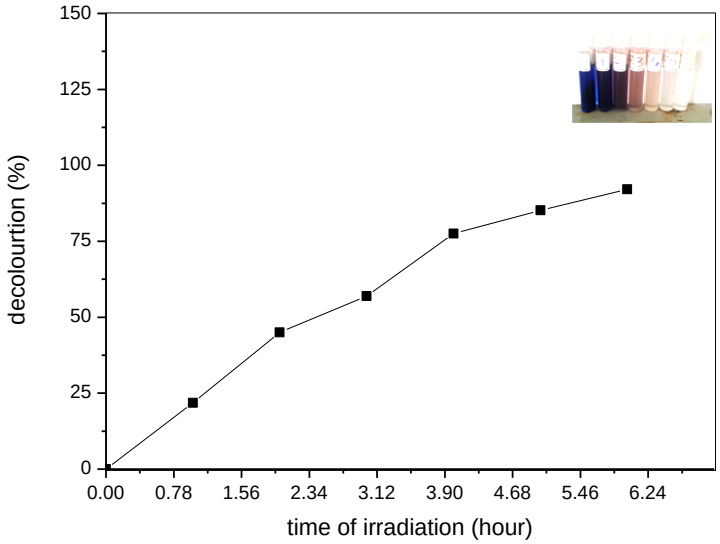

Fig. (26): Decolorization percentage of Tubantin blue dye dependent on radiation time

It can be seen from Table (10) and Fig (26) percentage decolorization increased as function of irradiation time, due to the fact hydroxyl radical ($OH^{\bullet}$) has short half life time.

3.2.1.5. Effect of Temperature

Table (11): The variation of temperature against the irradiation time during decolorization of Tubantin blue dye

Irradiation time hour	Temperature ˚C
1	27
2	42
3	44
4	44
5	44

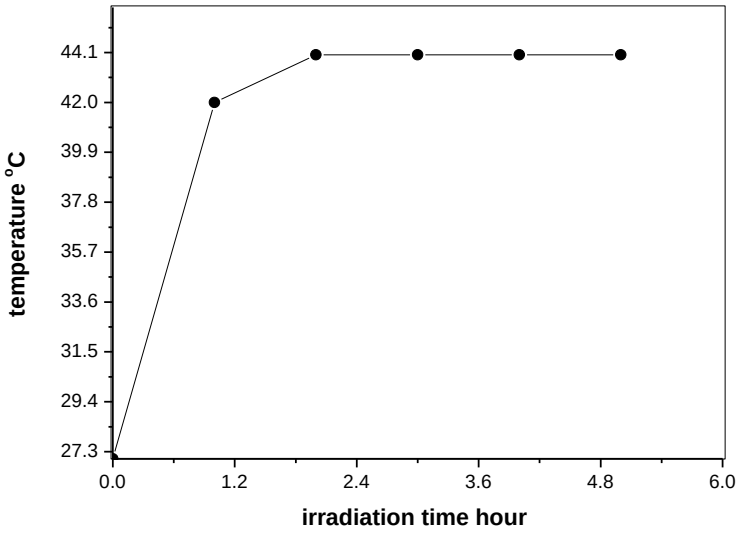

Fig (27): The variation of temperature against the irradiation time during decolorization of Tubantin blue dye

Table (11) and Fig (27) showed the temperature during the decolorization of tubantin blue. It was noted that temperature was increased during experiment, due to the use CPC collector, and also it is related to daily period. Although temperature is increased the decolorization uninfluenced. The best temperature range for the photo-degradation is 20-80˚C according to (Carp *et al.*, 2004).

3.2.1.6. Effect of Photon Flux

Table (12): The variation of photon flux during decolorization of Tubantin blue

Irradiation time hour	Photon flux Enstien / second
First	$7.6156X10^{-5}$
Second	$5.2126X10^{-5}$
Third	$3.6439X10^{-5}$
Fourth	$2.4940X10^{-5}$
Fifth	$3.6716X10^{-5}$

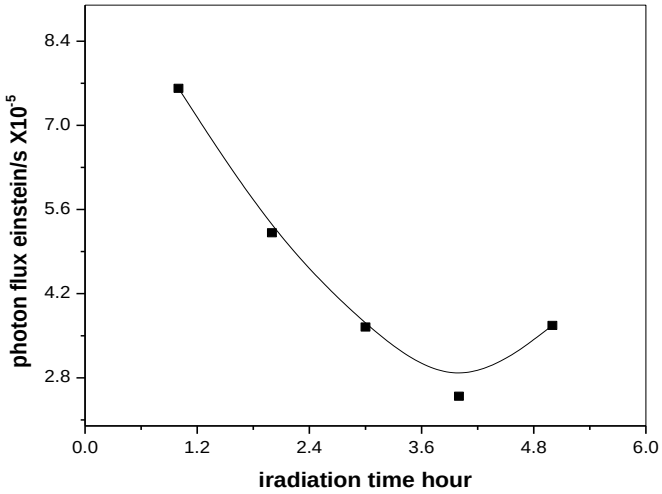

Fig (28): The various of photon flux during decolorization of Tubantin blue dye

According to (Tianyong *et al*., 2002), solar light irradiance changes daily, and even on the same day, this was confirmed by photon flux variation show in table (12) and Fig. (28) during the decolorization of tubantin blue as function of irradiation time in optimum conditions.

3.2.1.7. Effect of Hydrogen peroxide H_2O_2

Table (13): Change of dye absorbance photo-decolorization of Tubantin blue dye dependent on 30% H_2O_2 volume

Concentration of dye ppm		Absorbance at 436nm	Absorbance at 525nm	Absorbance at 620nm	Average	Decolorization %
12.5	**before**	0.560	1.992	2.008	1.520	**55.9211**
	after	0.528	0.809	0.673	0.673	
20	**before**	0.509	1.439	1.222	0.992	**34.5063**
	after	0.6210	0.935	0.845	0.800	
25	**before**	0.560	1.992	2.008	1.520	**84.4079**
	after	0.270	0.289	0.152	0.237	
37.5	**before**	0.727	1.238	1.302	1.089	**52.7090**
	after	0.662	0.505	0.378	0.515	
50	**before**	0.560	1.992	2.008	1.523	**91.3563**
	after	0.179	0.130	0.086	0.131	

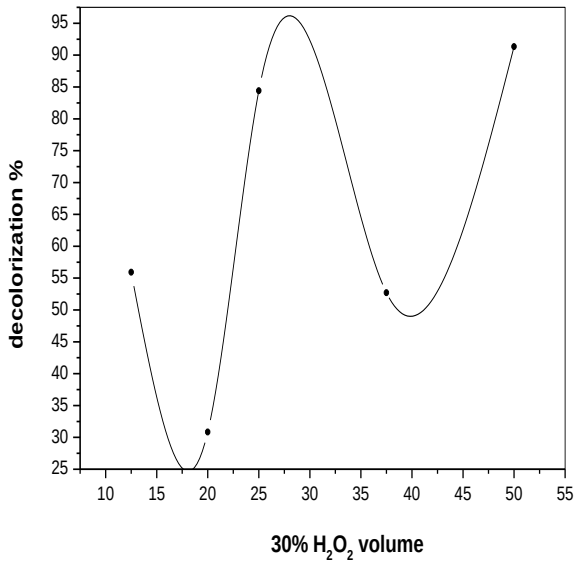

Fig (29): Decolorization percentage of Tubantin blue dye dependent on 30% H_2O_2 volume

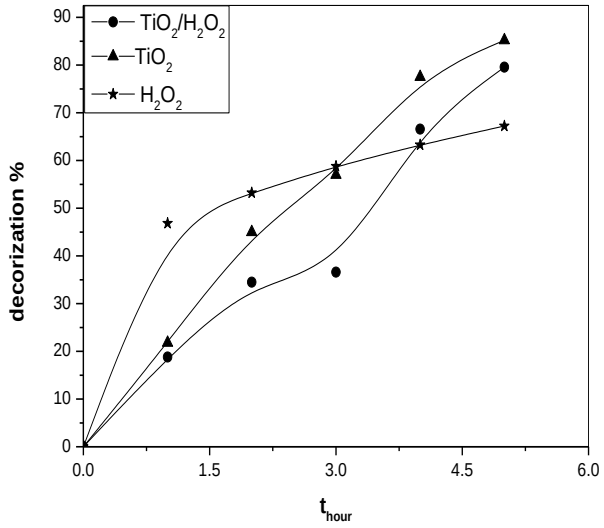

Fig (30): Decolorization % of Tubantin blue dye depending on H_2O_2/ TiO_2

According to (Akpan, 2009; Konstantinou, and Albanis, 2004; Saquib *et al*., 2008) oxidizing agents (hydrogen peroxide (H_2O_2), ammonium persulphate ($(NH_4)_2S_2O_8$) and potassium bromate ($KBrO_3$) oxygen) have a great deal of influence on the photo-catalytic degradation of dyes. The effect of volume of 30% H_2O_2 on the rate of decolorization of tubantin blue BRR-HC was performed by varying the volume of 30% H_2O_2 (12.5, 20, 25, 37.5 and 50 cm^3). It can be seen from Table (13) and Fig. (29) Percentage decolorization increases as volume of 30% H_2O_2 increases. This increase is due to the effect of the additionally produced hydroxyl radicals. Fig. (30) shows that TiO_2/H_2O2 system gave high decolorization percentage.

3.2.2. photo- decolorization of different kinds of dyes

Table (14): Change of absorbance methylene blue during the photo-decolorization by using pure TiO_2

Time	Absorbance at 436nm	Absorbance at 525nm	Absorbance at 620nm	Average	Decolorization %
0	0.271	0.967	2.310	1.1827	**0**
1	0.144	0.480	2.212	0.9453	**20.07**
2	0.186	0.273	1.161	0.5400	**54.34**
3	0.100	0.111	0.324	0.1783	**84.91**
4	0.011	0.013	0.020	0.0147	**98.76**
5	0.001	0.017	0.009	0.0090	**99.24**

Table (15): Change of absorbance methylene blue during the photo-decolorization by using TiO_2 sol-gel

Time	Absorbance at 436nm	Absorbance at 525nm	Absorbance at 620nm	Average	Decolorization %
0	0.231	0.968	2.324	1.1743	**0**
1	0.197	0.166	0.832	0.3983	**66.08**
2	0.254	0.153	0.239	0.2153	**81.66**
3	0.162	0.118	0.124	0.1347	**88.53**
4	0.071	0.058	0.044	0.0577	**95.09**
5	0.002	-0.079	0.021	-0.0187	**101.59**

Table (16): Change of absorbance tubantin blue during the photo-decolorization by using pure TiO_2

Time hour	Absorbance in 436nm	Absorbance in 525nm	Absorbance in 620nm	Average	Decolorization %
0	0.509	1.439	1.718	1.222	**0**
1	0.612	1.143	1.222	0.992	**18.79**
2	0.621	0.935	0.845	0.800	**34.51**
3	0.651	0.892	0.781	0.775	**36.61**
4	0.406	0.473	0.346	0.408	**66.58**
5	0.263	0.303	0.183	0.250	**79.57**

Table (17): Change of absorbance tubantin blue during the photo-decolorization by using TiO_2 sol-gel

Time hour	Absorbance at 436nm	Absorbance at 525nm	Absorbance at 620nm	Average	Decolorization %
0	0.552	1.708	1.587	1.2823	**0**
1	0.424	0.913	0.813	0.7167	**44.112**
2	0.442	0.646	0.506	0.5313	**58.565**
3	0.08	0.054	0.033	0.0557	**95.659**
4	-0.014	-0.025	-0.034	-0.0243	**101.897**
5	-0.105	0.052	0.043	-0.0033	**100.260**

Table (18): Change of absorbance tubantin red during the photo-decolorization by using pure TiO_2

Time hour	Absorbance at 436nm	Absorbance at 525nm	Absorbance at 620nm	Average	Decolorization %
0	0.991	1.618	0.057	0.8887	**0**
1	0.815	1.199	0.028	0.6807	**23.4059**
2	0.679	0.847	0.062	0.5293	**40.4352**
3	0.700	0.694	0.237	0.5437	**38.8222**
4	0.426	0.339	0.149	0.3047	**65.7164**
5	0.367	0.301	0.189	0.2857	**67.8544**

Table (19): Change of absorbance tubantin red during the photo-decolorization by using TiO_2 sol-gel

Time hour	Absorbance at 436nm	Absorbance at 525nm	Absorbance at 620nm	Average	Decolorization %
0	0.475	0.582	0.407	0.4880	**0**
1	0.316	0.227	0.046	0.1963	**44.1123**
2	0.203	0.140	0.125	0.1560	**58.5651**
3	0.08	0.060	0.050	0.0633	**95.6590**
4	0.012	0.008	0.020	0.0133	**101.8973**
5	-0.008	0.020	0.036	0.0160	**100.2597**

Table (20): Change of absorbance reactive yellow during the photo-decolorization by using pure TiO_2

Time hour	Absorbance at 436nm	Absorbance at 525nm	Absorbance at 620nm	Average	Decolorization %
0	1.137	0.188	0.032	0.4523	**0**
1	0.934	0.132	0.016	0.3607	**20.2652**
2	0.459	0.142	0.051	0.2173	**55.7074**
3	0.210	0.063	0.031	0.1013	**77.5977**
4	0.062	0.020	-0.015	0.0223	**96.2417**
5	-0.008	-0.008	0.003	-0.0043	**101.9904**

Table (21): Change of absorbance reactive yellow during the photo-decolorization by using TiO_2 sol-gel

Time hour	Absorbance at 436nm	Absorbance at 525nm	Absorbance at 620nm	Average	Decolorization %
0	1.031	0.173	-0.019	0.395	**0**
1	0.561	0.009	-0.053	0.172	**56.371**
2	0.492	0.067	0.046	0.202	**48.945**
3	0.240	0.032	0.006	0.093	**76.540**
4	0.054	-0.028	-0.040	-0.005	**101.182**
5	-0.077	-0.068	-0.029	-0.058	**114.684**

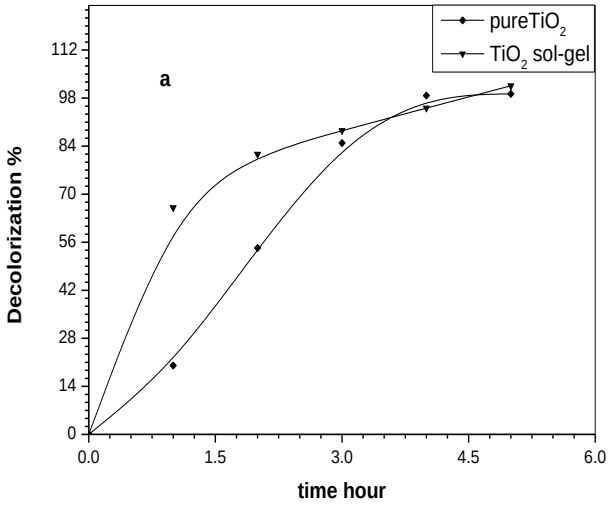
pureTiO2
TiO2 sol-gel
a
Decolorization %
time hour
0
14
28
42
56
70
84
98
112
0.0
1.5
3.0
4.5
6.0

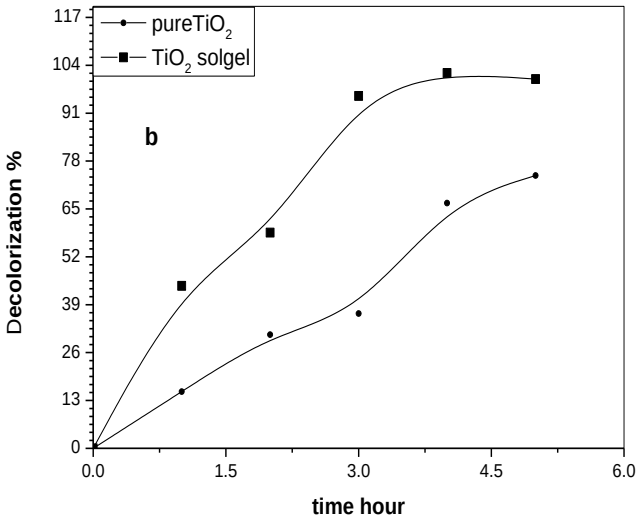
pureTiO2
TiO2 solgel
b
Decolorization %
time hour
0
13
26
39
52
65
78
91
104
117
0.0
1.5
3.0
4.5
6.0

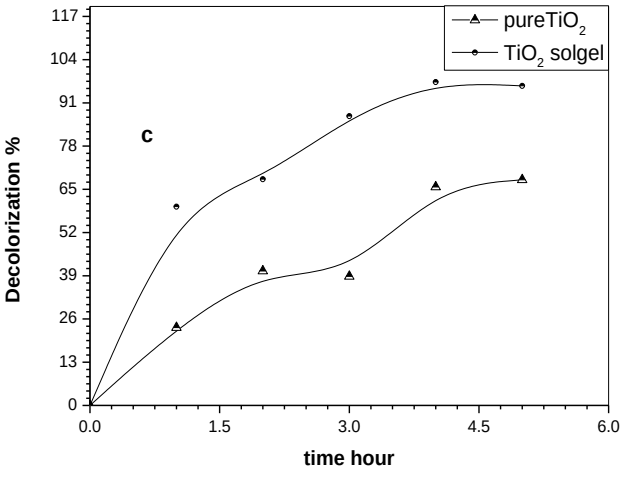
pureTiO2
TiO2 solgel
c
Decolorization %
time hour
0
13
26
39
52
65
78
91
104
117
0.0
1.5
3.0
4.5
6.0

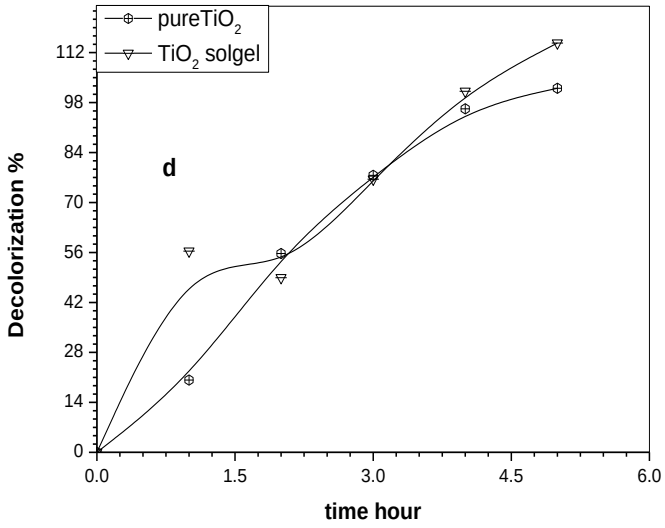

Fig (31): Decolorization percentage of (a) methylene blue (b) tubantin blue (c) tubantin red (d) yellow reactive by using pure TiO2 and TiO2 sol-gel

When applied at optimum condition of 1g/dm^3 catalyst (pure TiO_2 ,TiO_2 sol-gel), pH(9), 50 ppm dyes and 20 cm^3 30% H_2O_2 for decolorization of four dyes (methylene blue, tubantin blue BRR-HC, reactive yellow and tubantin red**).** Tables (14-21) and Figs (31) presented the experimental data of decolorization of (methylene blue, tubantin blue, tubantin red and reactive yellow) dyes by using pure TiO_2 and TiO_2 sol-gel.

3.2.2.1. Influence of different kinds of dyes

Table (22): The photo-decolorization of four kinds of dyes by using pure TiO_2 & TiO_2 sol-gel

Decolorization %		**Methylene blue**	**Tubantin red**	**Tubantin blue**	**Reactive yellow**
0 hour	**Pure TiO_2**	0	0	0	0
	TiO_2sol-gel	0	0	0	0
1 hour	**Pure TiO_2**	20.06770	23.40590	18.79460	20.26516
	TiO_2 sol-gel	66.08000	59.77000	44.11230	56.37130
2 hours	**Pure TiO_2**	54.34048	40.43520	34.50630	55.70741
	TiO_2sol-gel	81.66340	68.03000	58.56510	48.94510
3 hours	**Pure TiO_2**	84.91110	38.82220	36.60660	77.59770
	TiO_2 sol-gel	88.53240	87.02000	95.65900	77.59770
4 hours	**Pure TiO_2**	98.75890	65.71640	66.58490	96.24171
	TiO_2 sol-gel	95.08930	97.27000	100.2597	101.1823
5 hours	**Pure TiO_2**	99.23900	96.10656	79.56900	101.9904
	TiO2 sol-gel	101.5900	67.85440	101.8973	114.6835

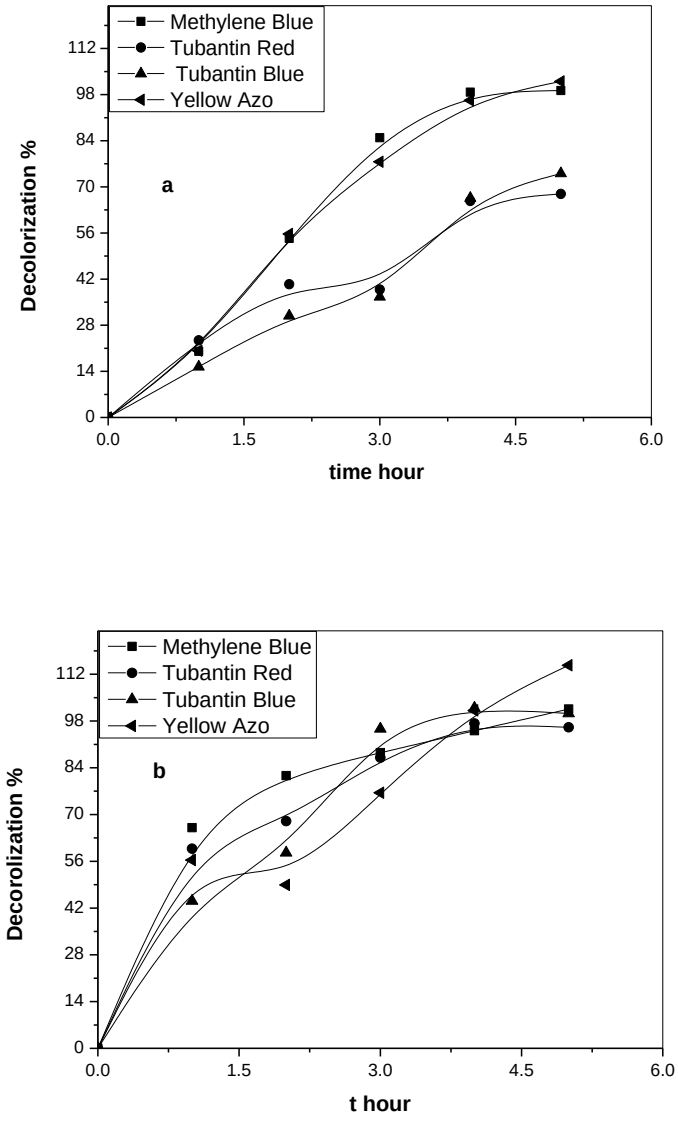

Fig (32): The photo-decolorization of four kinds of dyes by using (a) pure TiO_2 (b) TiO_2 sol-gel

Table (22) and Fig. (32) summarized the photo-decolorization methylene blue , tubantin blue , tubantin red and reactive yellow for each catalysts. Fig. (32) indicated that decolorization percentage of the four dyes were in the following order: reactive yellow > methylene blue > tubantin blue > tubantin red, due to differences their molecular structural; the functional groups (nitrite groups, alkyl side chain, chloro, carboxylic, sulfonic substituent, and hydroxyl groups) of the molecular structure of dye tends to decrease the solubility of molecules in water (Khataee and Kasiri, 2010) and effect on adsorption characteristics and

susceptibility to photo-degradation system (Zhang *et al*., 2011). Decolorization of reactive yellow dye is high because it has two hydroxyl substituent next to the azo bond, according to (Moon *et al*., 2003; Buitron *et al*., 2004) the electronic properties of a hydroxyl group are −I and +M effects, so hydroxyl groups in the dye molecule can intensify this resonance and consequently the decolorization of the dye. Tubantin red was low due to presence of chloro, ethyl side chain and five sulfonic substituent , according to (Khataee and Kasiri, 2010) chloro groups decreases the process, alkyl side chain decreases the solubility of molecule in water and more sulfonic substituents are less reactive in the photo-catalytic process.

3.2.2.2. Influence of photo-catalyst type

Table (23): properties for both pure titanium dioxide and titanium dioxide sol-gel

Photo-catalyst	**Surface area**	**Particles size**	**Energy gab**
Pure titanium dioxide	46.962 m^2/g	49.11070 nm	3.03eV
Titanium dioxide sol-gel	38.264 m^2/g	22.0198 nm	3.23eV

Returning to table (22) and Fig (32) we observed a high decolorization by using TiO_2 sol-gel due to smaller particle size, smaller surface area and wider energy gab than pure TiO_2 which was appeared in Table (23). Carp *et al*., 2004 reviewed that large surface area are usually associated with large amounts of crystalline defects, which favor the recombination of electrons and holes leading to a poor photo-activity, Particle size is an important parameter for photo-catalytic efficiency and increase in the band gap leads to a blue shift in the absorption edge.

3.2.3. Photon flux and temperature

Methylene blue:

Table (24): Photon flux and temperature during photo-decolorization of methylene blue pure TiO_2 & TiO_2 sol-gel

Time	T °C		Photon flux Einstein/s	
	Pure TiO_2	TiO_2 Sol-gel	Pure TiO_2	TiO_2 Sol-gel
1	40	36	$2.969E^{-5}$	$3.112E^{-5}$
2	46	40	$3.165E^{-5}$	$3.123E^{-5}$
3	45	42	$3.183E^{-5}$	$3.111E^{-5}$
4	50	44	$3.156E^{-5}$	$3.126E^{-5}$
5	50	44	$3.158E^{-5}$	$3.111E^{-5}$

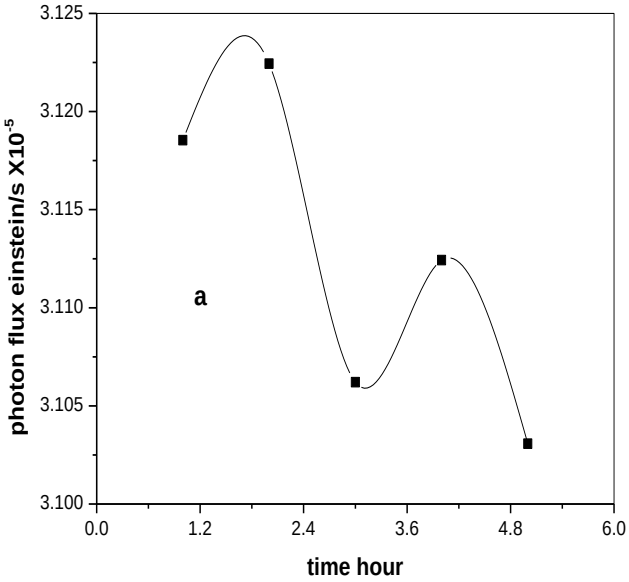

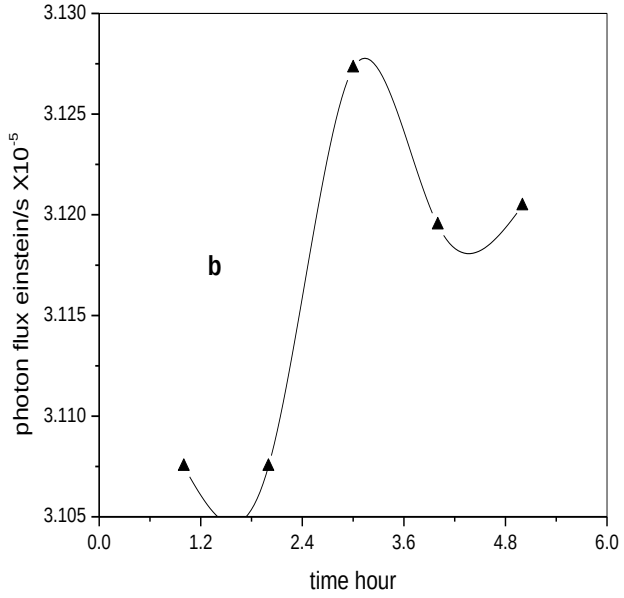
3.130
3.125
3.120
3.115
3.110
3.105
photon flux einstein/s X10-5
b
0.0
1.2
2.4
3.6
4.8
6.0
time hour

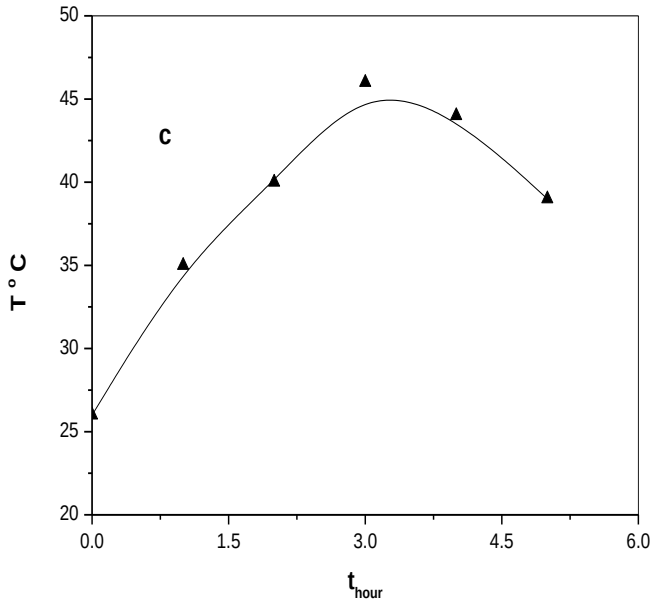
50
45
40
35
30
25
20
T ° C
c
0.0
1.5
3.0
4.5
6.0
thour

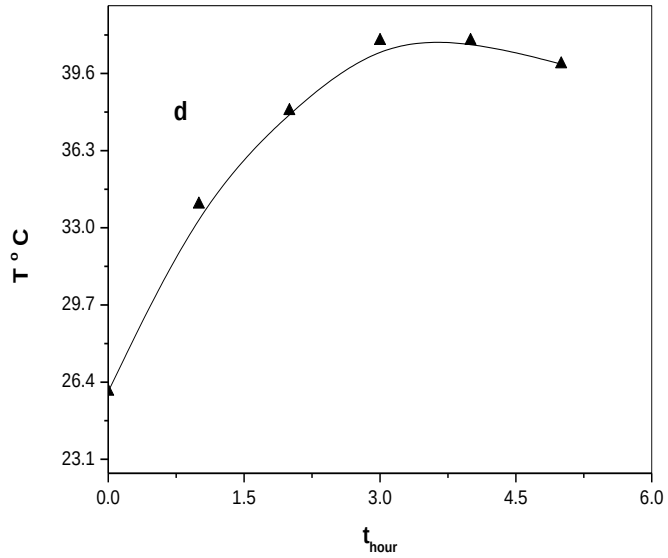

Fig (33): Photon flux and temperature during photo-decolorization of methylene blue using (a &c) pure TiO_2 (b&d) TiO_2 sol-gel

Tubantin blue:

Table (25): photon flux and temperature during photo-decolorization of tubantin blue pure TiO_2 & TiO_2 sol-gel

Time	T °C		Photon flux Einstein/s	
	Pure TiO_2	TiO_2 Sol-gel	Pure TiO_2	TiO_2 Sol-gel
1	35	34	$3.119E^{-5}$	$3.108E^{-5}$
2	40	38	$3.122E^{-5}$	$3.108E^{-5}$
3	46	41	$3.106E^{-5}$	$3.127E^{-5}$
4	44	41	$3.112E^{-5}$	$3.119E^{-5}$
5	39	40	$3.103E^{-5}$	$3.120E^{-5}$

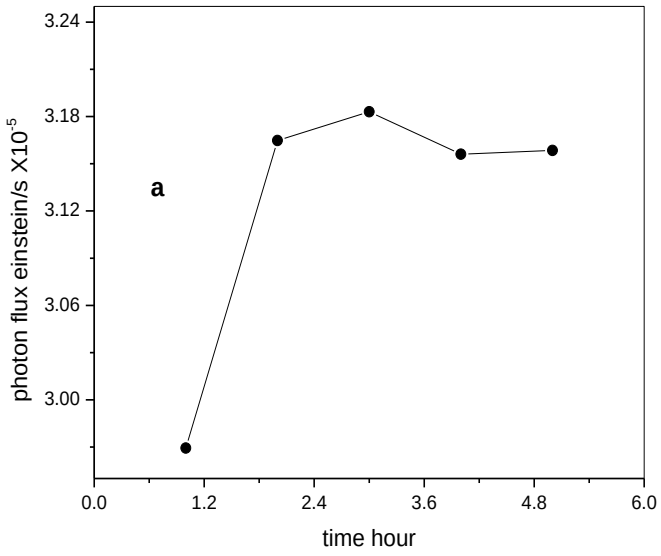
3.24
3.18
3.12
3.06
3.00
photon flux einstein/s X10-5
a
0.0
1.2
2.4
3.6
4.8
6.0
time hour

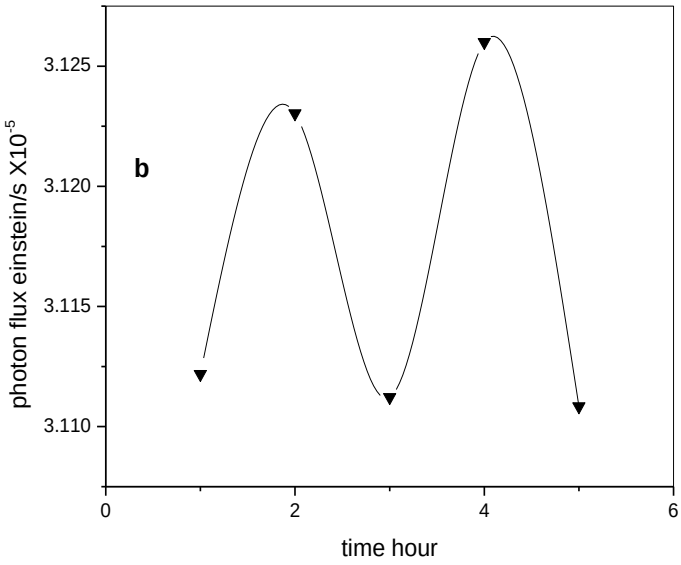
3.125
3.120
3.115
3.110
photon flux einstein/s X10-5
b
0
2
4
6
time hour

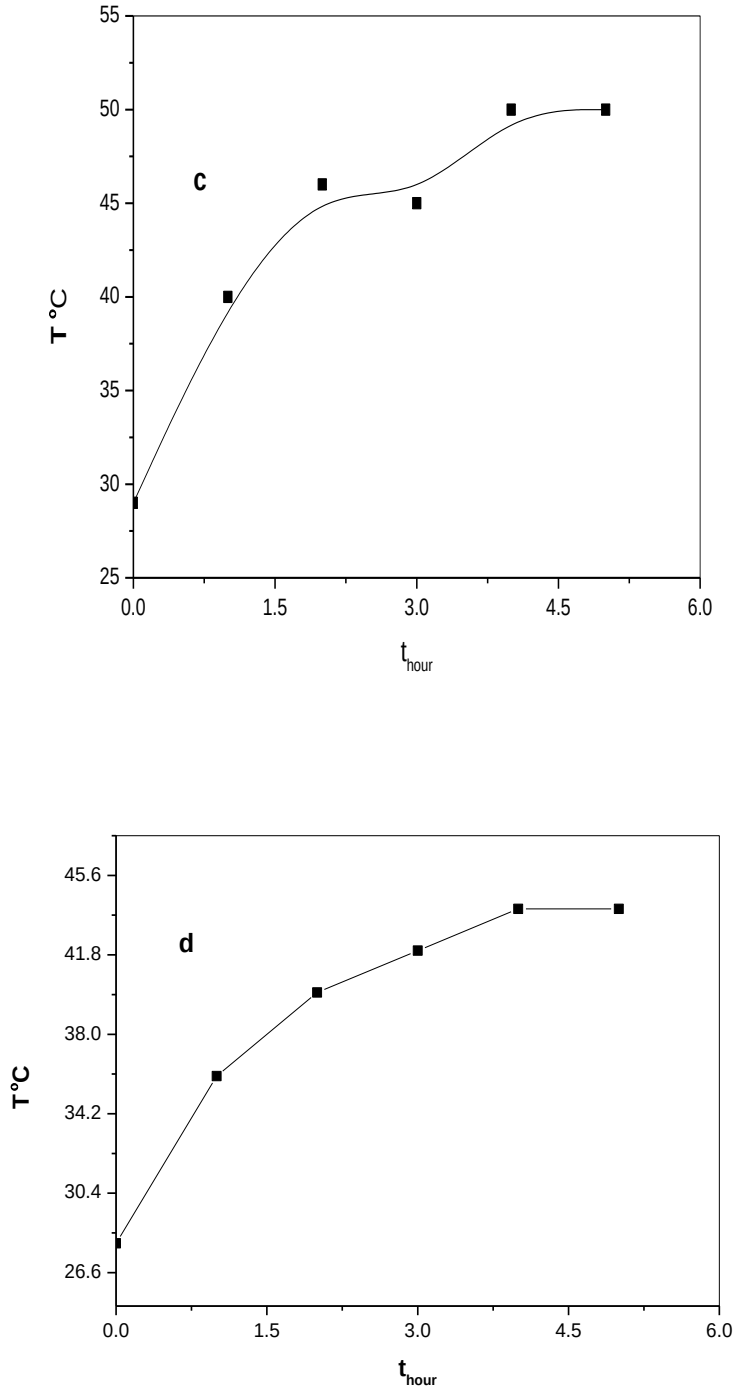

Fig (34): Photon flux and temperature during photo-decolorization of tubantin blue using (a &c) pure TiO_2 (b&d) TiO_2 sol-gel

Reactive Yellow:

Table (26): photon flux and temperature during photo-decolorization of reactive yellow blue pure TiO_2 &TiO_2 sol-gel

Time	T °C		Photon flux Einstein/s	
	Pure TiO_2	TiO_2 Sol-gel	Pure TiO_2	TiO_2 Sol-gel
1	37	35	$3.126E^{-5}$	$3.128E^{-5}$
2	44	39	$3.122E^{-5}$	$3.126E^{-5}$
3	44	41	$3.124E^{-5}$	$3.129E^{-5}$
4	41	42	$3.119E^{-5}$	$3.125E^{-5}$
5	38	40	$3.113E^{-5}$	$3.123E^{-5}$

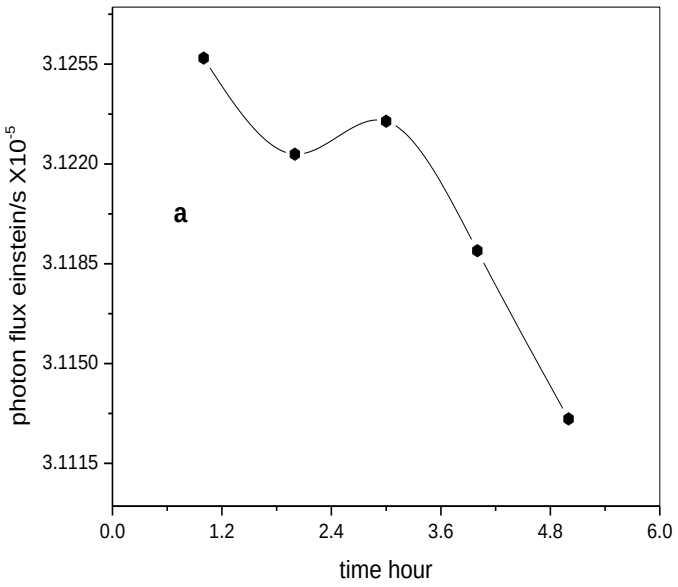

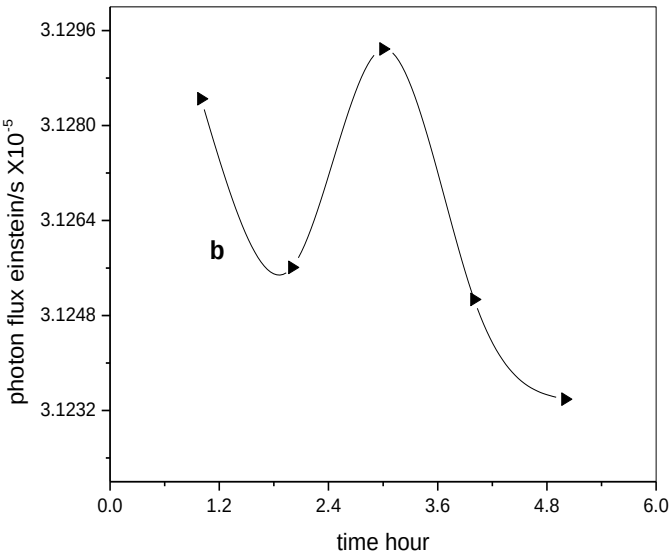
3.1296
3.1280
3.1264
3.1248
3.1232
photon flux einstein/s X10-5
b
0.0
1.2
2.4
3.6
4.8
6.0
time hour

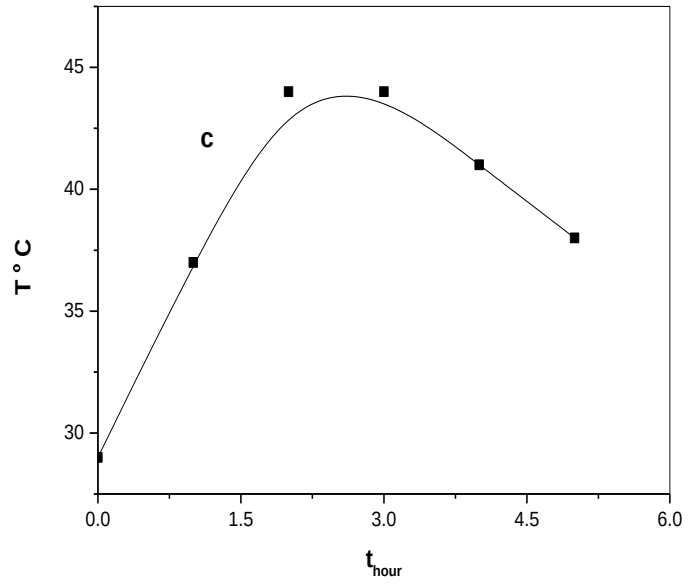
45
40
35
30
T ° C
c
0.0
1.5
3.0
4.5
6.0
thour

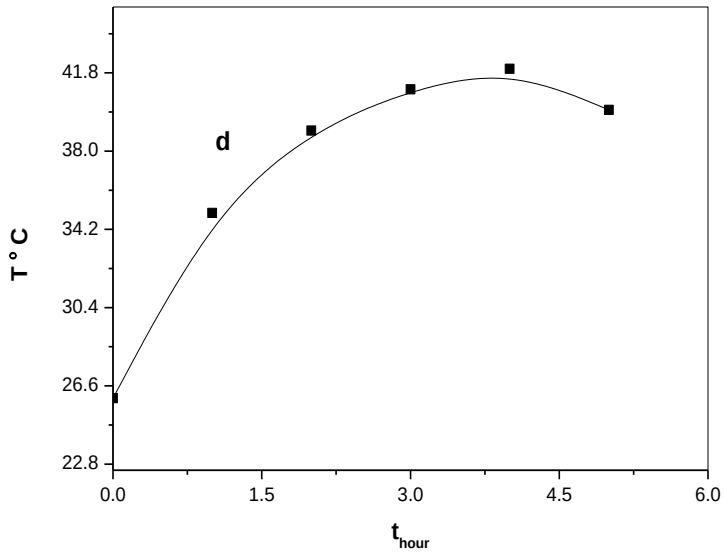

Fig (35): Photon flux and temperature during photo-decolorization of reactive yellow using (a &c) pure TiO_2 (b&d) TiO_2 sol-gel`

Tubantin red:

Table (27): photon flux and temperature during photo-decolorization of Tubantin red pure TiO_2 &TiO_2 sol-gel

Time	T °C		Photon flux Einstein/s	
	Pure TiO_2	TiO_2 Sol-gel	Pure TiO_2	TiO_2 Sol-gel
1	36	38	$3.115E^{-5}$	$3.111E^{-5}$
2	42	42	$3.124E^{-5}$	$3.112E^{-5}$
3	43	46	$3.122E^{-5}$	$3.107E^{-5}$
4	43	42	$3.111E^{-5}$	$3.112E^{-5}$
5	42	40	$3.115E^{-5}$	$3.106E^{-5}$

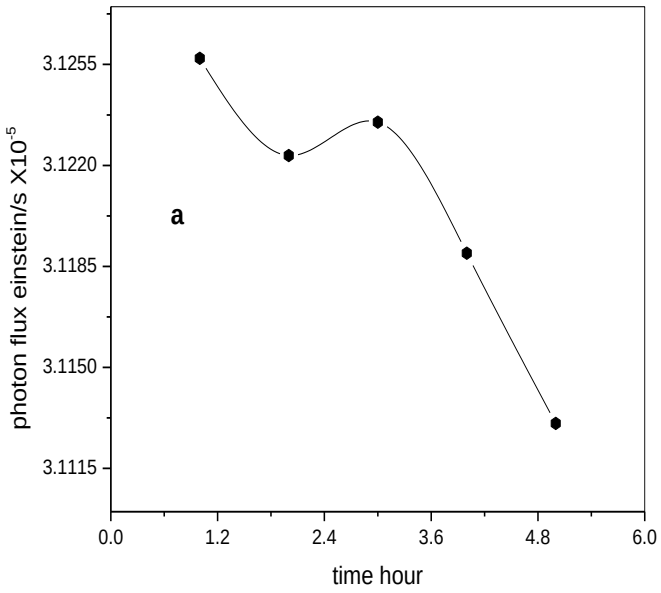
3.1255
3.1220
3.1185
3.1150
3.1115
photon flux einstein/s X10-5
a
0.0
1.2
2.4
3.6
4.8
6.0
time hour

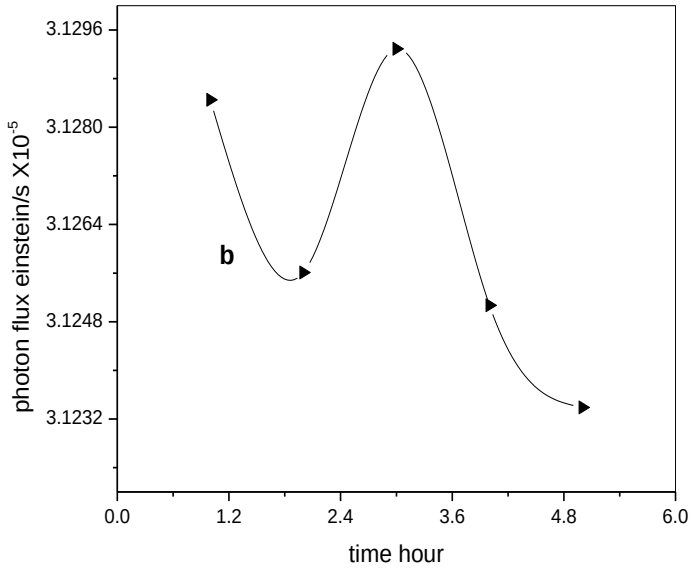
3.1296
3.1280
3.1264
3.1248
3.1232
photon flux einstein/s X10-5
b
0.0
1.2
2.4
3.6
4.8
6.0
time hour

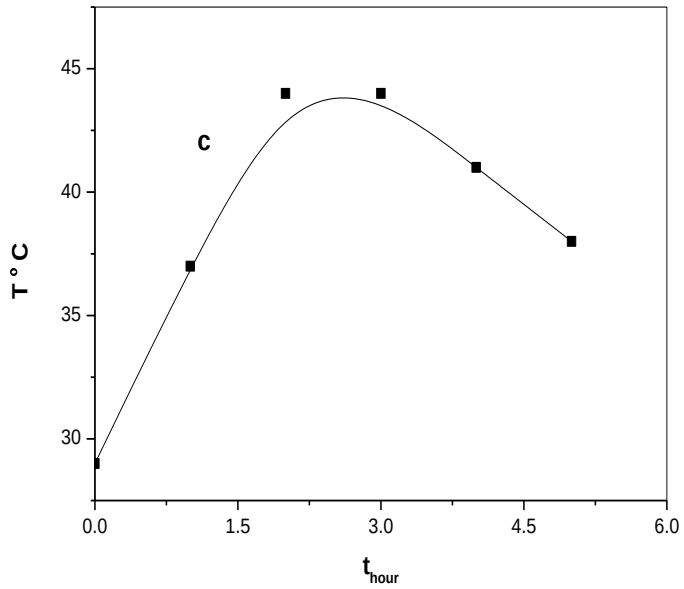
45
40
35
30
T ° C
c
0.0
1.5
3.0
4.5
6.0
thour

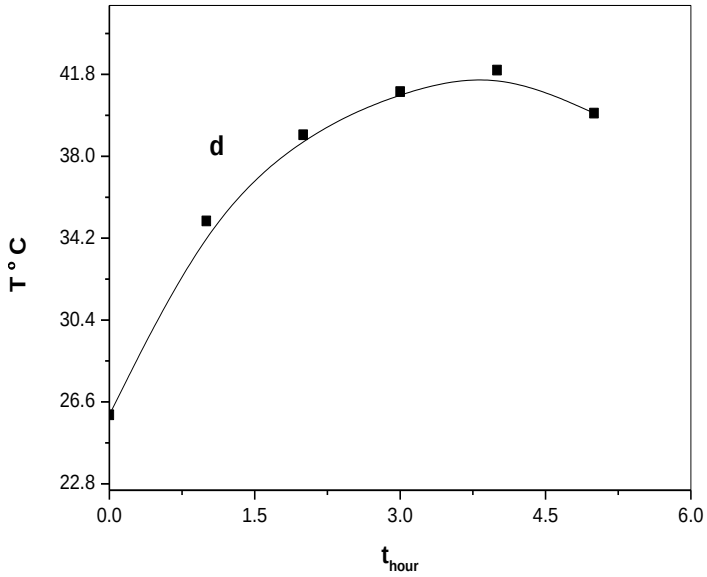

Fig (36): Photon flux and temperature during photo-decolorization of tubantin red using (a &c) pure TiO_2 (b&d) TiO_2 sol-gel

Decolorization experiments of four dyes were conducted at 10 pm – 3 am on $2^d/11$ – $29^{th}/11$ Solar light intensity (photon flux) was measured for every hour by using ferrioxalate actinometry Tables (24-27) and Fig. (33-36) presented the experimental data of values of photon flux and temperature during the decolorization of (methylene blue, tubantin blue, tubantin red and reactive yellow) dyes by using pure TiO_2 and TiO_2 sol-gel.

Table (28): solution temperature (average) and daily photon flux average during photo-decolorization of the four dyes

Dye	**Solution temperature (average) °C**		**Daily photon flux (average) Einstein/s**	
	Pure TiO_2	**TiO_2 sol-gel**	**Pure TiO_2**	**TiO_2 sol-gel**
Methylene blue	46.2	41.2	$3.126E^{-5}$	$3.117E^{-5}$
Tubantin blue	40.8	38.8	$3.113E^{-5}$	$3.116E^{-5}$
Tubantin red	41.2	41.6	$3.117E^{-5}$	$3.110E^{-5}$
Reactive yellow	40.8	39.4	$3.121E^{-5}$	$3.126E^{-5}$

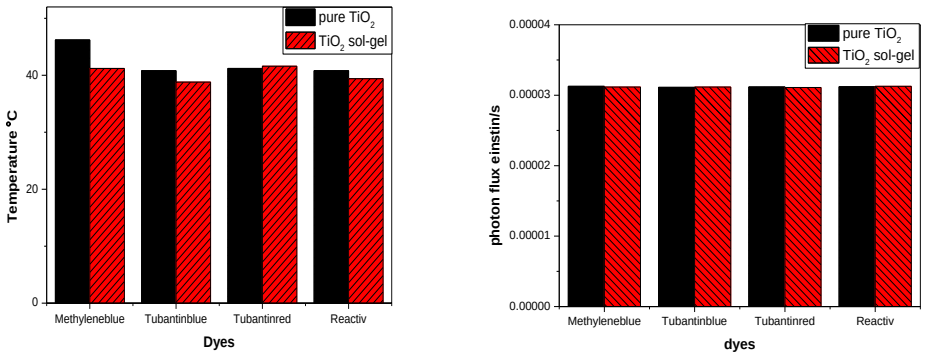

Fig (37): Average of solution temperature and average of daily photon flux during decolorization of four comerical dyes

Table (28) and Fig. (37) summarized the average photon flux and average solution temperature during decolorization of the four kinds of dyes under study by using two forms of photo-catalysts pure TiO_2 and TiO_2 sol-gel. Fig (37) indicated that the average of photon flux was nearly constant during the experiments and the average of solution temperature increased over the duration of each experiment. When using pure TiO_2 the increasing in solution temperature was higher than using TiO_2 sol-gel, due to the fact that pure TiO_2 has large surface area which associated with large amounts of crystalline defects leads to favor the recombination of electrons and holes and generated heat (Carp *et al*., 2004).

Part III: study of photo-catalytic kinetic of four dyes

3.3.1. Determination of λ_{max} for four dyes:

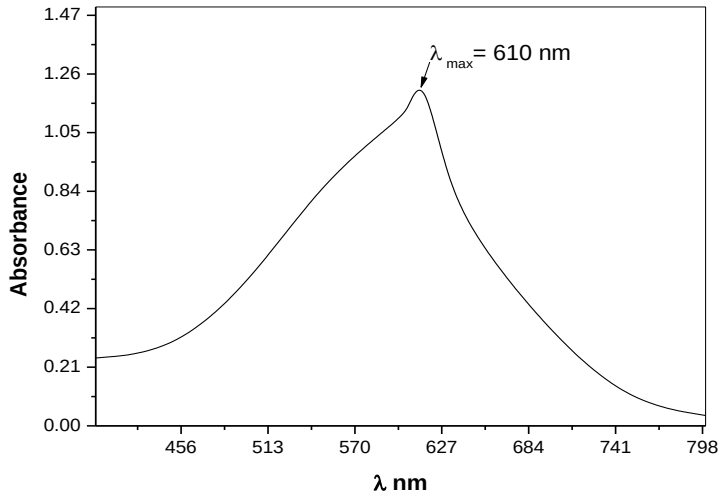

Fig (38): Total absorption spectrum of methylene blue

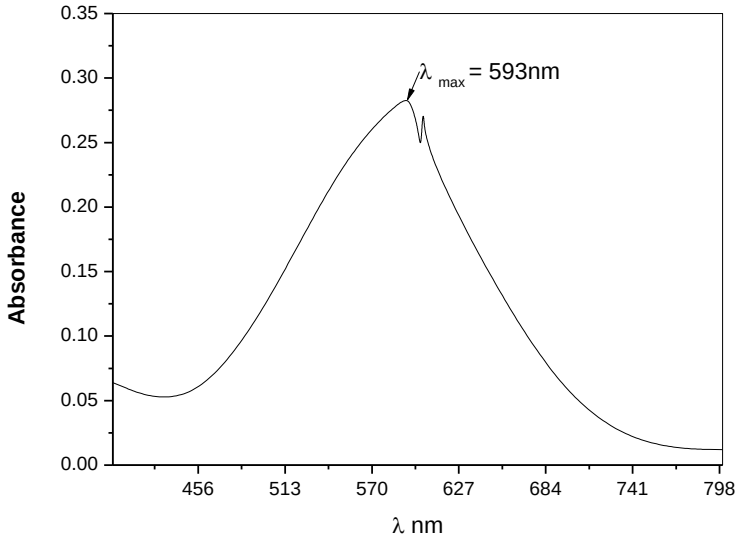

Fig (39): Total absorption spectrum of tubantin blue

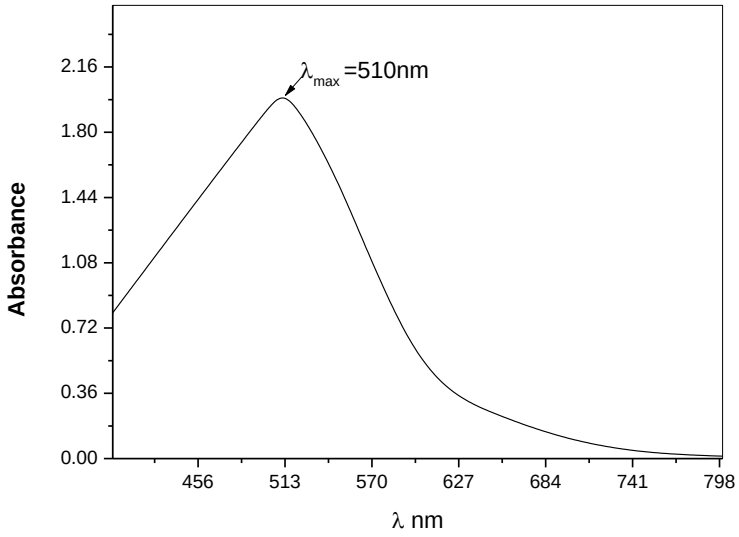

Fig (40)**:** Total absorption spectrum of tubantin red

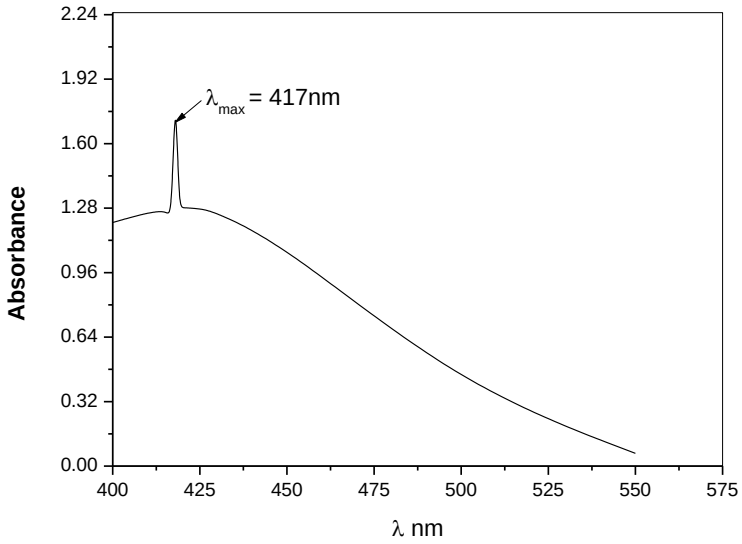

Fig (41): Total absorption spectrum of reactive yellow

Table (29): The maximum wavelength λ_{max} nm of four dyes

Dye	**The maximum wavelength λ_{max} nm**
Methlene blue	**610**
Tubantin blue	**593**
Tubantin red	**510**
Reactive yellow	**417**

Figs.(38-41) presented the total absorption spectrum of four crommmecial dyes (methalene blue, tubantin blue, tubantin red and reactive yellow) which

summmerized the values maximum wavelength (λ_{max} nm) for each dye that are important for determing the concentration change as function in absorbance in Table (29).

3.3.2. Callibration curve for four dyes

Table (30): Methylene blue dye verse absorbance at 610nm

Concentration ppm	Absorbance A
0	0
4.675	1.314
9.340	1.912
14.011	2.217
20.031	2.237
28.023	2.462

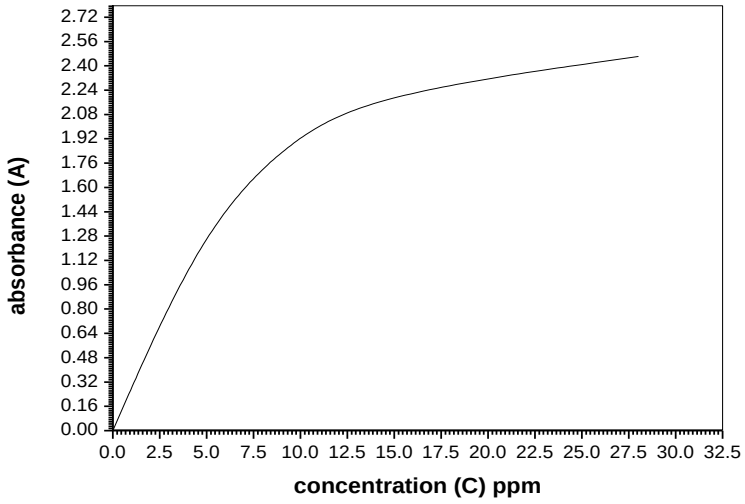

Fig (42):Calliberation curve for methylene blue

Table (31): Tubantin blue dye verse absorbance at 593nm

Concentration ppm	Absorbance A
0	0
6.2	0.301
12.4	0.735
18.6	1.041
24.8	1.303
51.0	2.270

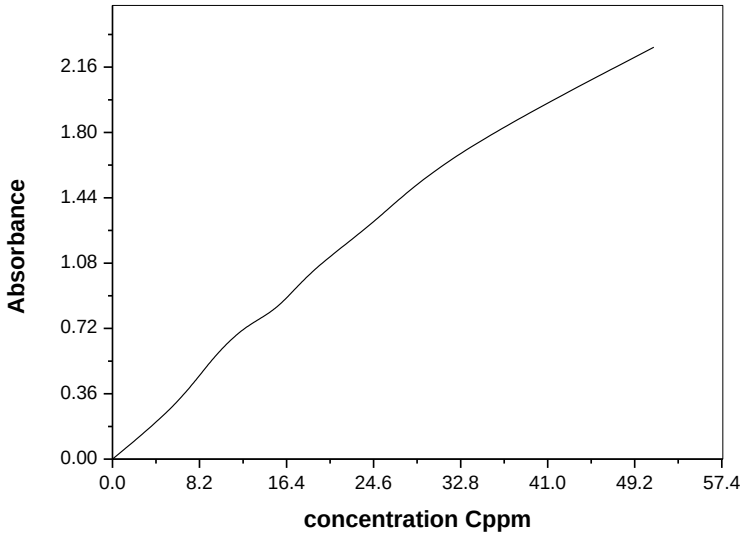

Fig (43):Calliberation curve for tubantin blue

Table (32): Tubantin red dye verse absorbance at 510nm

Concentration ppm	Absorbance A
0.000	0.000
5.430	0.214
10.86	0.444
16.29	0.637
27.15	1.015
32.58	1.277

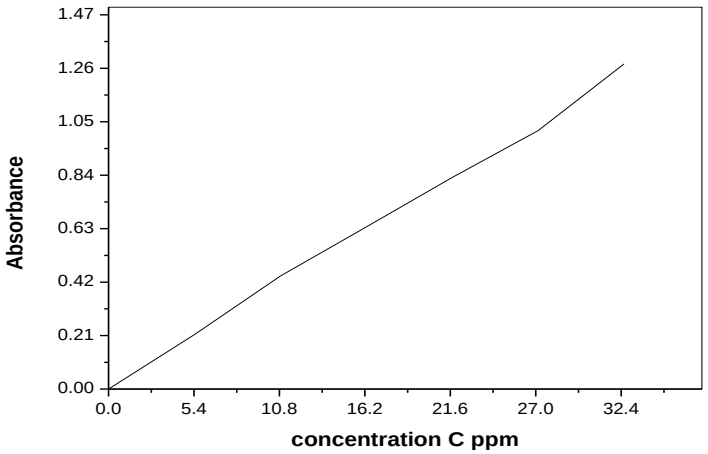

Fig (44): Calliberation curve for tubantin red

Table (33): Reactive yellow dye verse absorbance at 417nm

Concentration ppm	Absorbance A
0.000	0.000
4.740	0.320
9.480	0.463
14.22	0.710
16.59	0.857
23.70	1.132

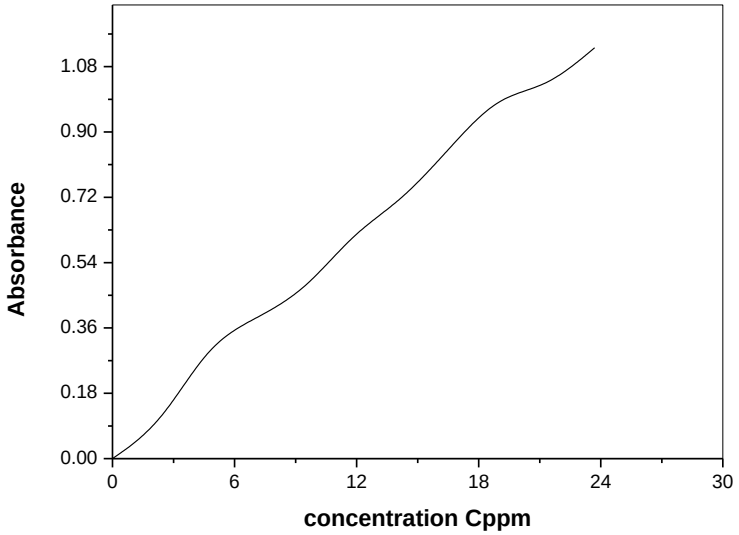

Fig. (45): Calliberation curve for reactive yellow

Tables (30-33) presented the experiments data that included the value of absorbance as function of initial concentration at its maxinun wavelength (λ_{max} is 610 nm for methylene blue, 593 nm for tubantin blue, 510 nm for tubantin red and 417 for reactive yellow) which used to plote the callibration curve for each dyes Fig. (42-45), it useful to determine the dye concentration change during experiements.

3.3.3. Change of dyes concentration during photo-catalytic reaction

Table (34): Concentration of four dyes in (C_{30}) during photo-decolorization using two types of photo-catalysts

Time hour	Concentration of dye ppm							
	Methylene blue		Tubantin blue		Tubantin red		Reactive yellow	
	Pure TiO_2	TiO_2 sol-gel	Pure TiO_2	TiO_2 sol-gel	Pure TiO_2	TiO_2 sol-gel	Pure TiO_2	TiO_2 sol-gel
0	$3.54E^{-2}$	$3.18E^{-2}$	$3.54E^{-2}$	$3.25E^{-2}$	$3.33E^{-2}$	$3.42E^{-2}$	$3.00E^{-2}$	$3.06E^{-2}$
1	$1.29E^{-2}$	$1.10E^{-2}$	$3.26E^{-3}$	$1.75E^{-3}$	$1.15E^{-2}$	$4.88E^{-3}$	$5.63E^{-3}$	$2.84E^{-3}$
2	$8.52E^{-3}$	$6.54E^{-3}$	$2.55E^{-3}$	$1.19E^{-3}$	$9.03E^{-3}$	$3.23E^{-3}$	$4.62E^{-3}$	$2.64E^{-3}$
3	$2.35E^{-3}$	$1.04E^{-5}$	$2.41E^{-3}$	$8.44E^{-4}$	$4.06E^{-3}$	$2.12E^{-3}$	$2.11E^{-3}$	$2.60E^{-3}$
4	$4.98E^{-5}$	$7.40E^{-6}$	$2.12E^{-3}$	$6.38E^{-4}$	$3.13E^{-3}$	$1.60E^{-3}$	$1.72E^{-3}$	$1.50E^{-3}$
5	$2.01E^{-5}$	$1.91E^{-6}$	$2.04E^{-3}$	$2.43E^{-4}$	$1.86E^{-3}$	$-2.26E^{-4}$	$1.02E^{-3}$	$1.27E^{-3}$

Table (35): Concentration of four dyes in (C_{50}) during photo-decolorization using two types of photo-catalysts

Time hour	Concentration of dye ppm							
	Methylene blue		Tubantin blue		Tubantin red		Reactive yellow	
	Pure TiO_2	TiO_2 sol-gel	Pure TiO_2	TiO_2 sol-gel	Pure TiO_2	TiO_2 sol-gel	Pure TiO_2	TiO_2 sol-gel
0	$5.00E^{-2}$	$5.00E^{-2}$	$5.08E^{-2}$	$4.32E^{-2}$	$5.00E^{-2}$	5.00E-2	$5.00E^{-2}$	$5.00E^{-2}$
1	$1.57E^{-2}$	$2.88E^{-3}$	$3.28E^{-2}$	$1.94E^{-2}$	$1.79E^{-2}$	$1.15E^{-2}$	$6.36E^{-3}$	$4.53E^{-2}$
2	$4.51E^{-3}$	$9.62E^{-4}$	$2.29E^{-2}$	$1.03E^{-2}$	$8.91E^{-3}$	$9.61E^{-3}$	$4.13E^{-3}$	$2.27E^{-3}$
3	$8.79E^{-4}$	$1.07E^{-5}$	$1.68E^{-2}$	$2.68E^{-4}$	$3.88E^{-3}$	$4.23E^{-3}$	$5.32E^{-4}$	$5.29E^{-4}$
4	$1.04E^{-4}$	$7.10E^{-6}$	$7.70E^{-3}$	$-9.58E^{-4}$	$1.44E^{4}$	$1.53E^{-4}$	$5.07E^{-4}$	$-1.40E^{-4}$
5	$7.40E^{-5}$	$-1.72E^{-4}$	$6.20E^{-3}$	$-8.80E^{-4}$	$1.79E^{-4}$	$-2.26E^{-4}$	$2.78E^{-4}$	$-7.12E^{-4}$

Table (36): Change concentration of four dyes in (C_{70}) during photo-decolorization using two types of photo-catalysts

Time hour	Concentration of dye ppm							
	Methylene blue		Tubantin blue		Tubantin red		Reactive yellow	
	Pure TiO_2	TiO_2 sol-gel	Pure TiO_2	TiO_2 sol-gel	Pure TiO_2	TiO_2 sol-gel	Pure TiO_2	TiO_2 sol-gel
0	$7.00E^{-2}$	$7.05E^{-2}$	$7.03E^{-2}$	$7.28E^{-2}$	$7.15E^{-2}$	$7.00E^{-1}$	$7.15E^{-2}$	$7.03E^{-2}$
1	$2.57E^{-2}$	$2.28E^{-2}$	$5.72E^{-2}$	$9.35E^{-3}$	$1.82E^{-2}$	$2.70E^{-1}$	$1.44E^{-2}$	$5.46E^{-3}$
2	$1.42E^{-2}$	$2.01E^{-2}$	$1.78E^{-3}$	$3.13E^{-3}$	$1.61E^{-2}$	$2.54E^{-1}$	$5.59E^{-}3$	$3.66E^{-3}$
3	$8.60E^{-3}$	$8.99E^{-3}$	$1.49E^{-3}$	$1.64E^{-3}$	$1.06E^{-2}$	$1.90E^{-1}$	$3.88E^{-3}$	$2.48E^{-3}$
4	$2.81E^{-3}$	$1.79E^{-3}$	$1.11E^{-3}$	$1.13E^{-3}$	$4.64E^{-3}$	$1.29E^{-1}$	$2.48E^{-3}$	$1.67E^{-3}$
5	$3.91E^{-5}$	$3.69E^{-4}$	$1.02E^{-3}$	$2.46E^{-4}$	$3.33E^{-4}$	$1.08E^{-2}$	$9.65E^{-4}$	$1.59E^{-3}$

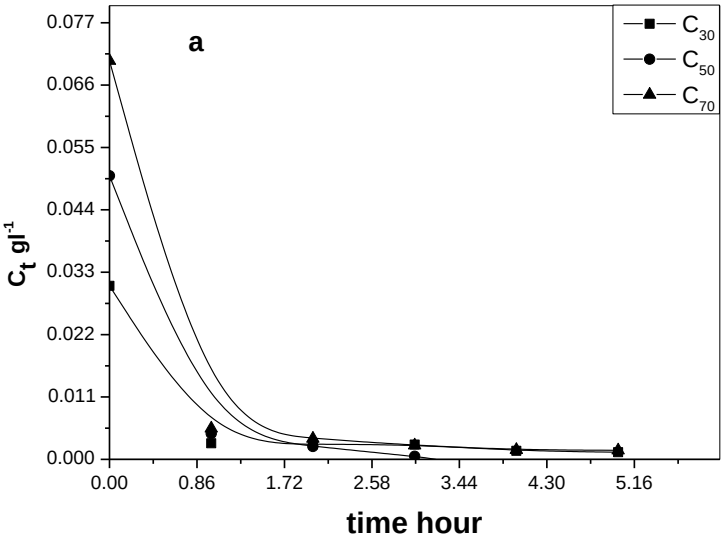

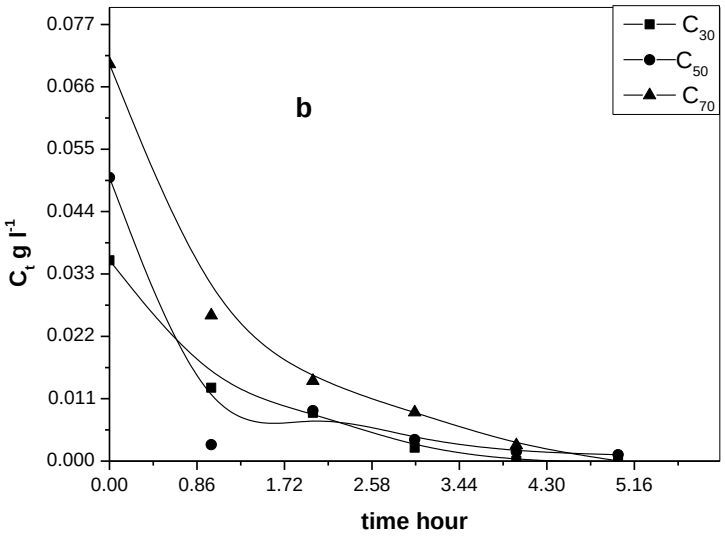

Fig. (46): Change of concentration methylene blue using (a) pure TiO_2 (b) TiO_2 sol-gel

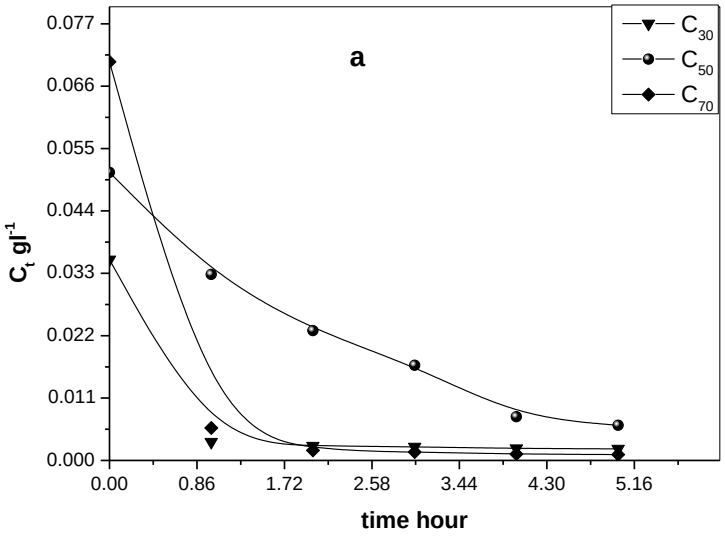

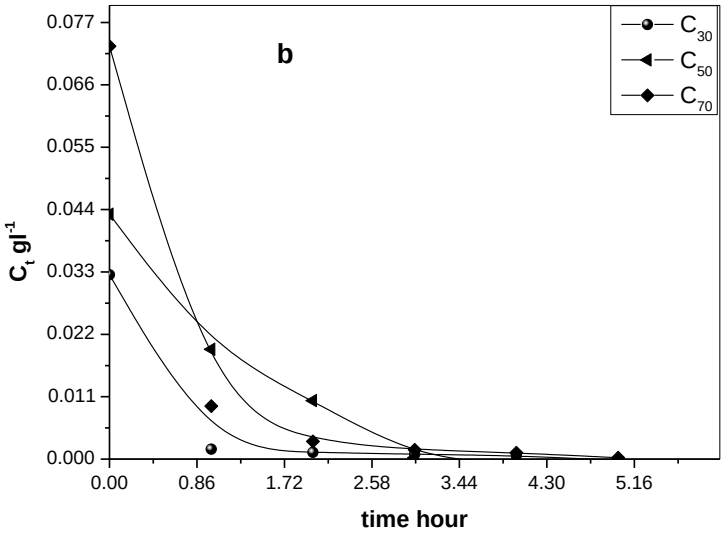

Fig. (47): Change of concentration tubantin blue using (a) pure TiO_2 (b) TiO_2 sol-gel

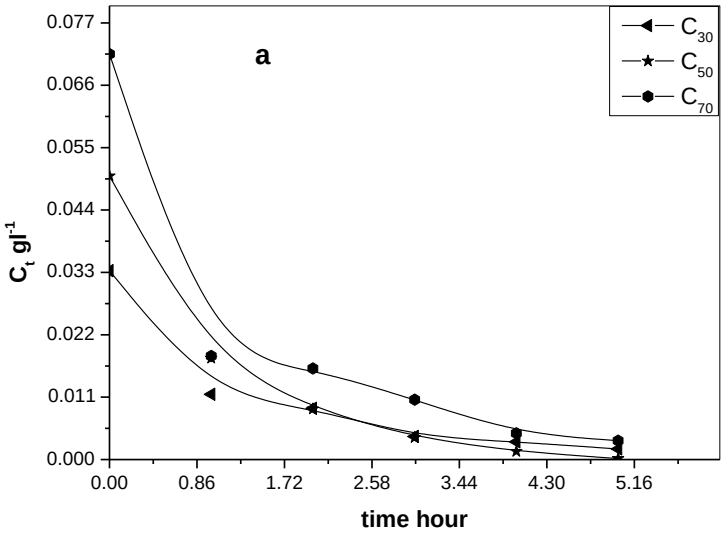

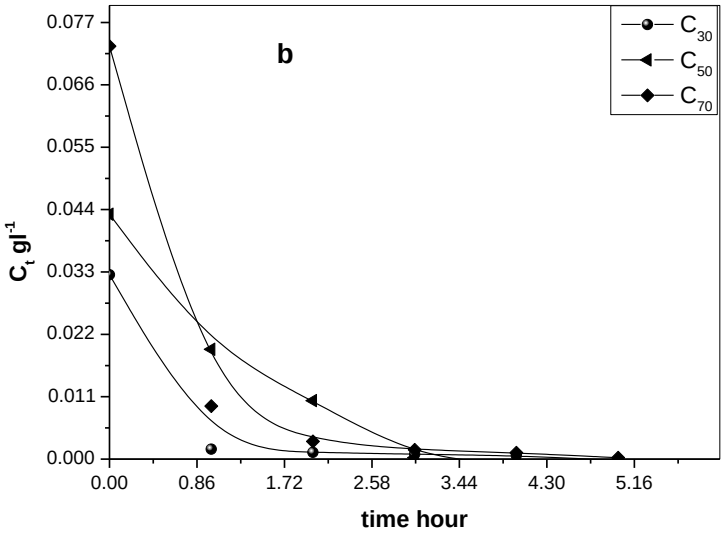

Fig. (48): Change of concentration tubantin red using (a) pure TiO_2 (b) TiO_2 sol-gel

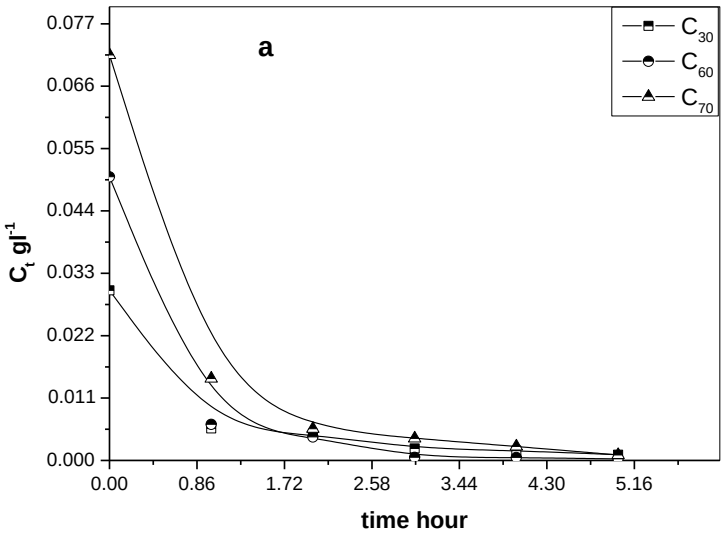

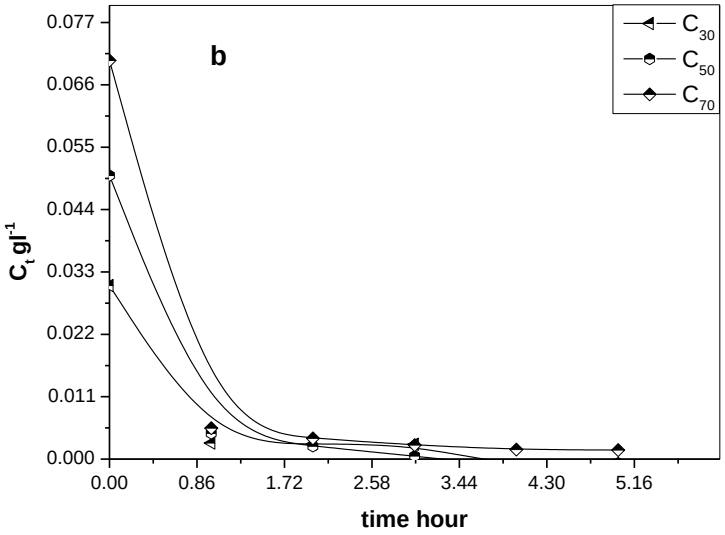

Fig. (49): Change of concentration reactive yellow using (a) pure TiO_2 (b) TiO_2 sol-gel

Tables (34-36) and Fig. (46-49) summarized the change of concentrations of the four dyes under study in different initial concentrations using two forms of photo-catalysts (pure TiO_2 and TiO_2 sol-gel) during photo-decolorization for five hours under solar radiation. It was observed that the photo-decolorization decreases with an increase in the initial concentration of dyes. (Rauf *et al*., 2009)

3.3.4. Photo-catalytic decolorization kinetic models

Table (37): First and second order kinetic model parameter k and the correlation coefficient (R^2) for photo-decolorization of four dyes in (C_{30}) using pure TiO_2

Kinetic Model	**Methylene blue**		**Tubantin blue**		**Tubantin red**		**Reactive yellow**	
	k	**R^2**	**k**	**R^2**	**k**	**R^2**	**k**	**R^2**
First order	0.0149	0.825	0.008	0.830	0.095	0.883	0.045	0.891
Second order	-0.033	0.826	-0.0268	0.826	-3.624	0.864	-1.711	0.889

Table (38): First and second order kinetic model parameter k and the correlation coefficient (R^2) for photo-decolorization of four dyes (C_{50}) using pure TiO_2

Kinetic Model	Methylene blue		Tubantin blue		Tubantin red		Reactive yellow	
	K	R^2	K	R^2	K	R^2	k	R^2
First order	0.202	0.4819	0.02249	0.8862	0.10457	0.7991	0.034	0.762
Second order	-2.884	0.555	-7.891	0.793	-2.589	0.748	-0.720	0.759

Table (39): First and second order kinetic model parameter k and the correlation coefficient (R^2) for photo-decolorization of four dyes (C_{70}) using pure TiO_2

Kinetic Model	Methylene blue		Tubantin blue		Tubantin red		Reactive yellow	
	k	R^2	k	R^2	k	R^2	k	R^2
First order	0.015	0.862	0.015	0.793	0.068	0.951	0.047	0.713
Second order	-0.213	0.857	-0.224	0.517	-1.132	0.864	-0.739	0.686

Table (40): First and second order kinetic model parameter k and the correlation coefficient (R^2) for photo-decolorization of four dyes (C_{30}) using TiO_2 sol-gel

Kinetic Model	Methylene blue		Tubantin blue		Tubantin red		Reactive yellow	
	K	R^2	K	R^2	K	R^2	k	R^2
First order	0.119	0.848	0.014	0.939	0.037	0.961	0.041	0.688
Second order	-4.179	0.819	-0.451	0.942	-1.171	0.958	-1.389	0.692

Table (41): First and second order kinetic model parameter k and the correlation coefficient (R^2) for photo-decolorization of four dyes (C_{50}) using TiO_2 sol-gel

Kinetic Model	Methylene blue		Tubantin blue		Tubantin red		Reactive yellow	
	k	R^2	k	R^2	k	R^2	k	R^2
First order	0.185	0.561	0.153	0.733	0.071	0.948	0.029	0.827
Second order	-5.769	0.491	-4.635	0.689	-1.619	0.938	-0.663	0.823

Table (42): First and second order kinetic model parameter k and the correlation coefficient (R^2) for photo-decolorization of four dyes (C_{70}) using TiO_2 sol-gel

Kinetic Model	Methylene blue		Tubantin blue		Tubantin red		Reactive yellow	
	k	R^2	k	R^2	k	R^2	k	R^2
First order	0.019	0.881	0.297	0.674	0.088	0.9478	0.015	0.861
Second order	-1.957	0.829	-0.436	0.658	-1.756	0.944	-0.217	0.857

Table (43): Langmuir Hinshelwood kinetic model parameter k and the correlation coefficient (R^2) for photo-decolorization of four dyes using pure TiO_2

Kinetic Model	**Methylene blue**		**Tubantin blue**		**Tubantin red**		**Reactive yellow**	
	k	**R^2**	**k**	**R^2**	**k**	**R^2**	**k**	**R^2**
Langmuir Hinshelwood	0.101	0.832	0.126	0.885	0.169	0.948	0.157	0.963

Table (44): Langmuir Hinshelwood kinetic model parameter k and the correlation coefficient (R^2) for photo-decolorization of four dyes using TiO_2 sol-gel

Kinetic Model	**Methylene blue**		**Tubantin blue**		**Tubantin red**		**Reactive yellow**	
	k	**R^2**	**k**	**R^2**	**k**	**R^2**	**k**	**R^2**
Langmuir Hinshelwood	0.214	0.998	0.146	0.778	0.163	0.945	0.176	0.998

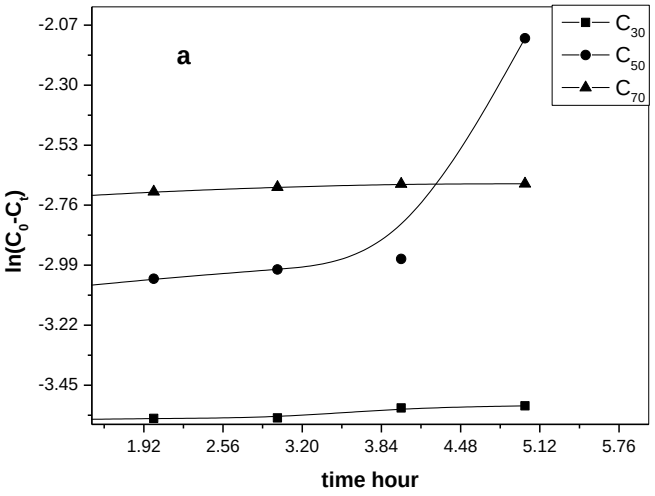

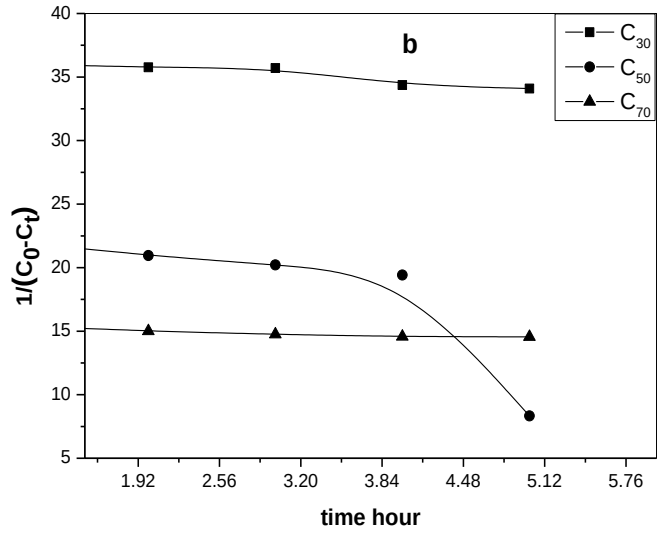

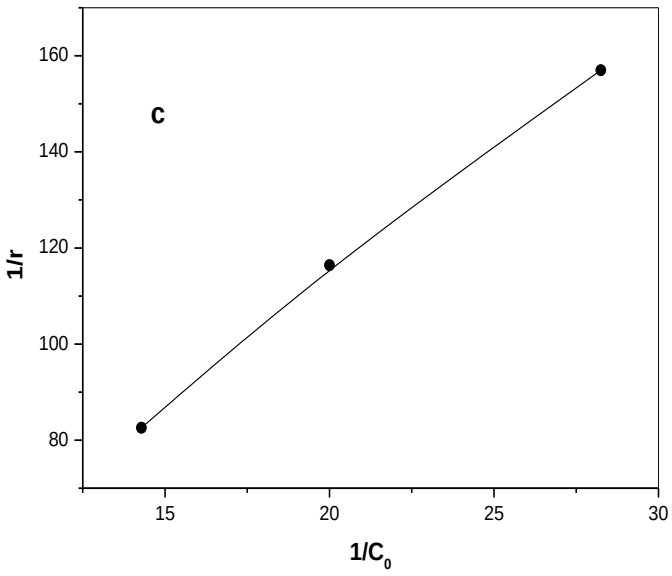

Fig. (50): Photo-decolorization of methylene blue using pure TiO_2 (a) first order kinetic, (b) second order kinetic and (c) Langmuir Hinshelwood kinetic

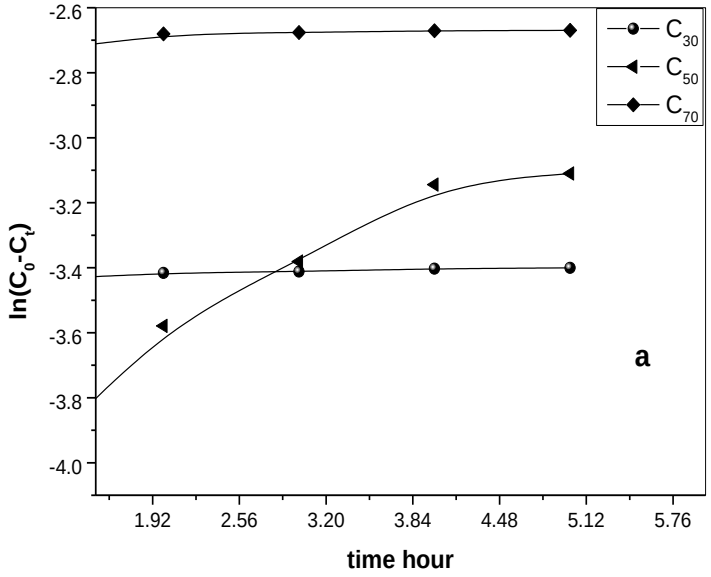

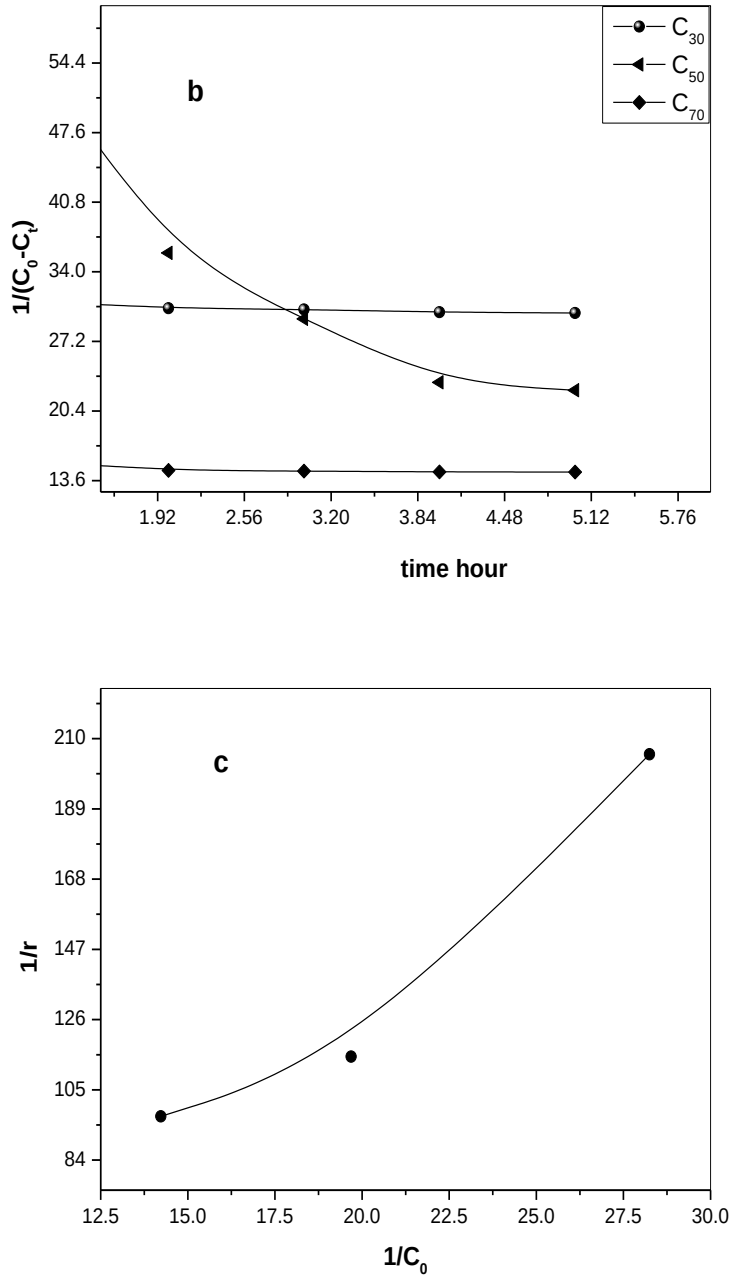

Fig. (51): Photo-decolorization of tubantin blue by using pure TiO_2 (a) first order kinetic, (b) second order kinetic and (c) Langmuir Hinshelwood kinetic

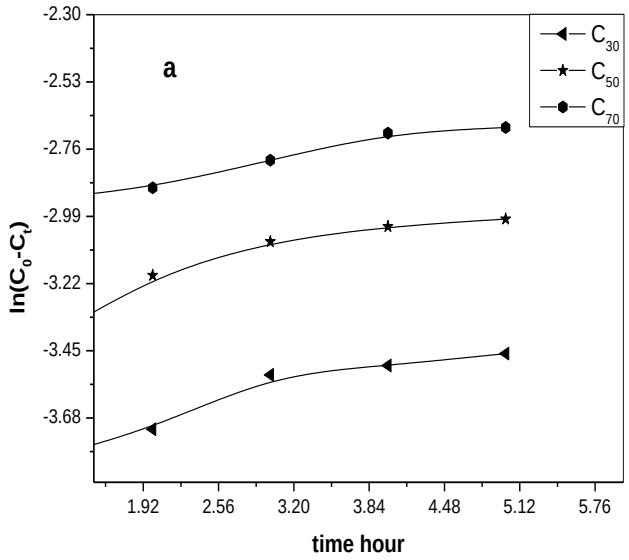
a
-2.30
-2.53
-2.76
-2.99
-3.22
-3.45
-3.68
ln(C0-Ct)
1.92
2.56
3.20
3.84
4.48
5.12
5.76
time hour
C30
C50
C70

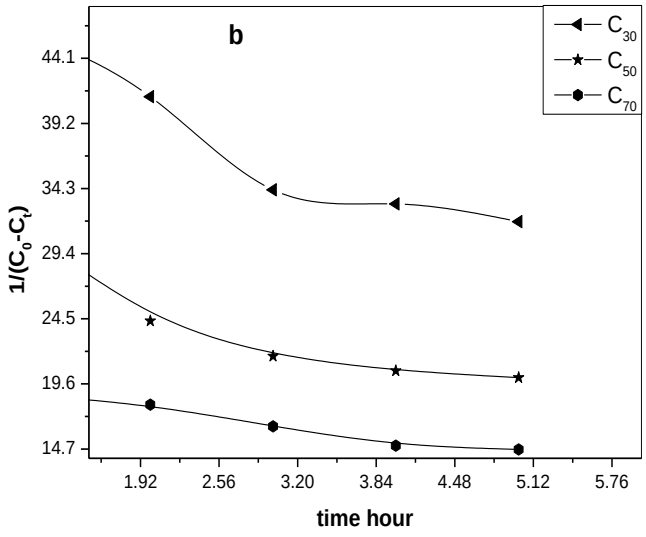
b
44.1
39.2
34.3
29.4
24.5
19.6
14.7
1/(C0-Ct)
1.92
2.56
3.20
3.84
4.48
5.12
5.76
time hour
C30
C50
C70

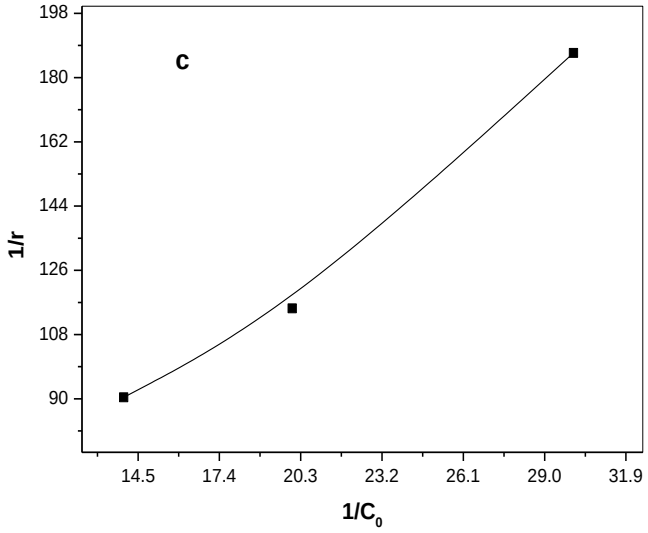

Fig. (52): Photo-decolorization of tubantin red by using pure TiO_2 (a) first order kinetic, (b) second order kinetic and (c) Langmuir Hinshelwood kinetic

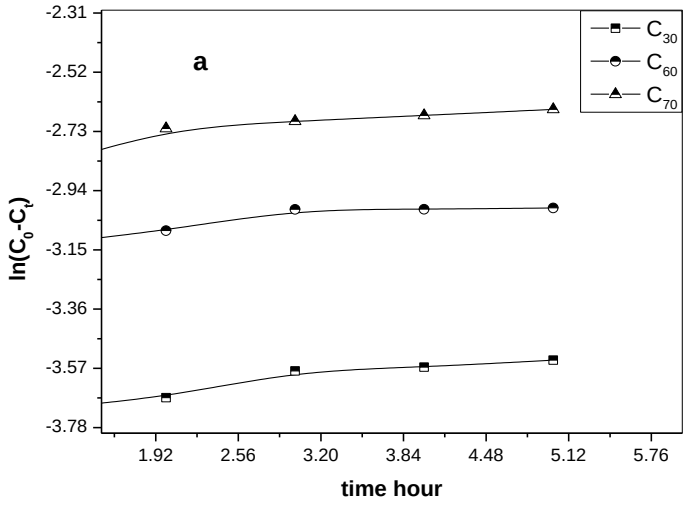

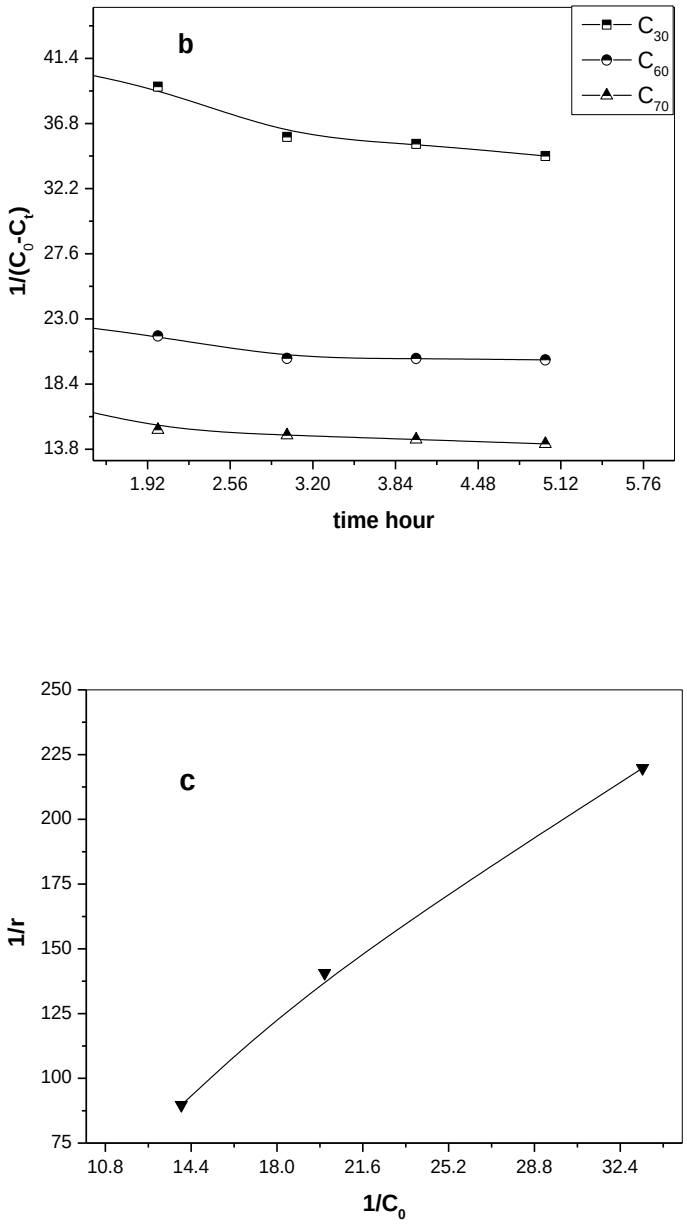

Fig. (53): Photo-decolorization of reactive yellow using pure TiO_2 (a) first order kinetic, (b) second order kinetic and (c) Langmuir Hinshelwood kinetic

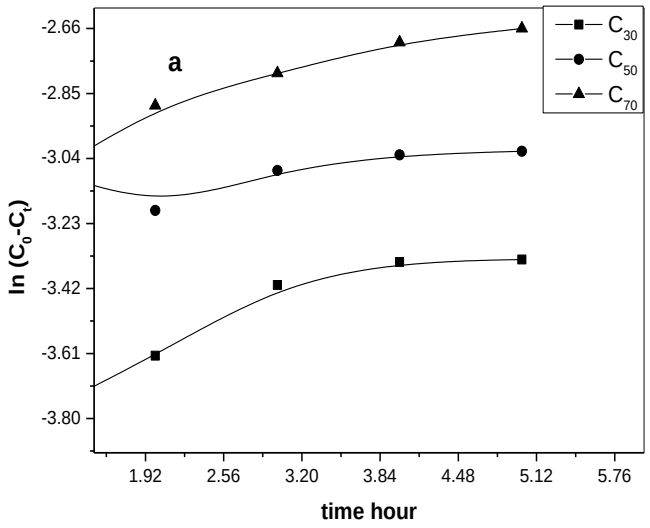
a
-2.66
-2.85
-3.04
-3.23
-3.42
-3.61
-3.80
ln (C0-Ct)
1.92
2.56
3.20
3.84
4.48
5.12
5.76
time hour
C30
C50
C70

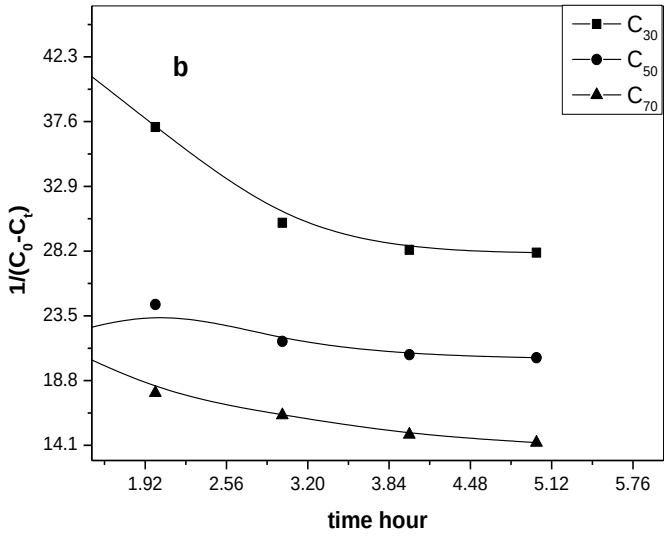
b
42.3
37.6
32.9
28.2
23.5
18.8
14.1
1/(C0-Ct)
1.92
2.56
3.20
3.84
4.48
5.12
5.76
time hour
C30
C50
C70

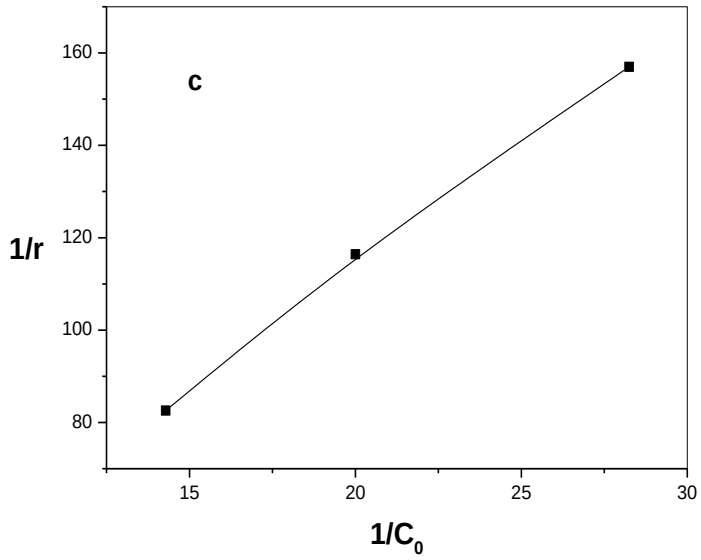

Fig. (54): photo-decolorization of methylene blue using TiO_2 sol-gel (a) first order kinetic, (b) second order kinetic and (c) Langmuir Hinshelwood kinetic

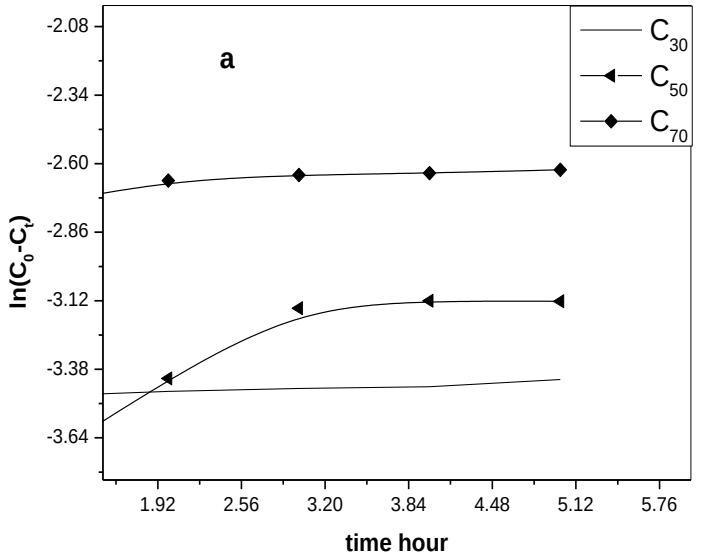

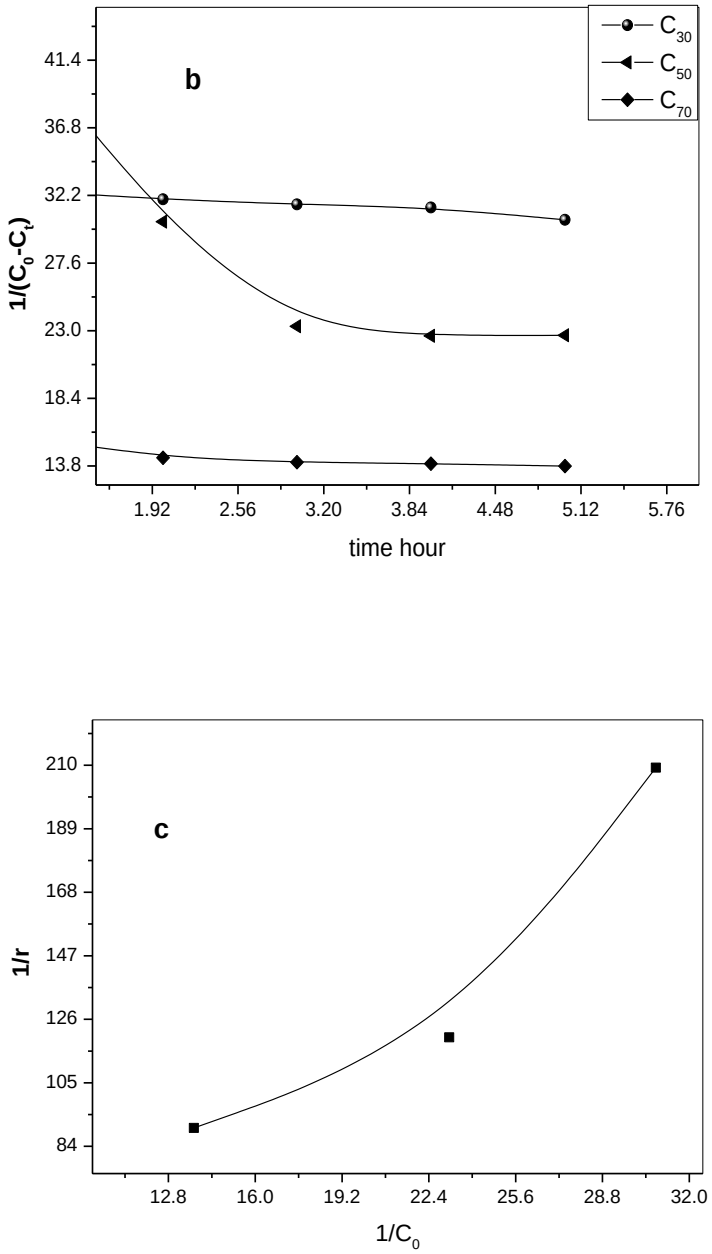

Fig. (55): Photo-decolorization of tubantin blue using TiO_2 sol-gel (a) first order kinetic, (b) second order kinetic and (c) Langmuir Hinshelwood kinetic

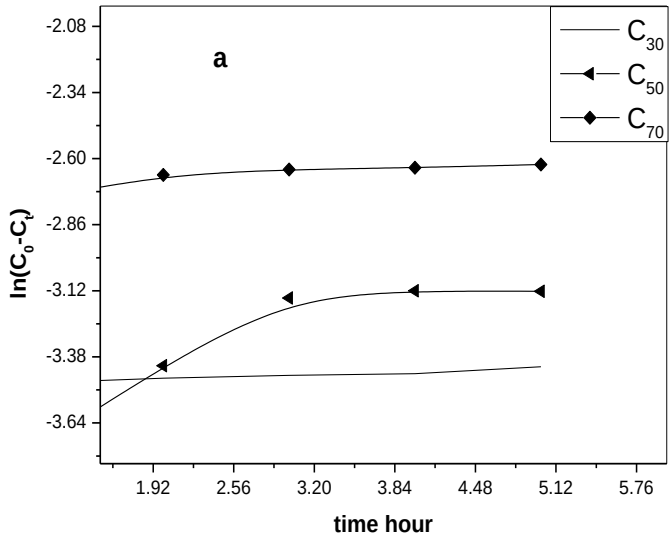
a
C30
C50
C70
-2.08
-2.34
-2.60
-2.86
-3.12
-3.38
-3.64
ln(C0-Ct)
1.92
2.56
3.20
3.84
4.48
5.12
5.76
time hour

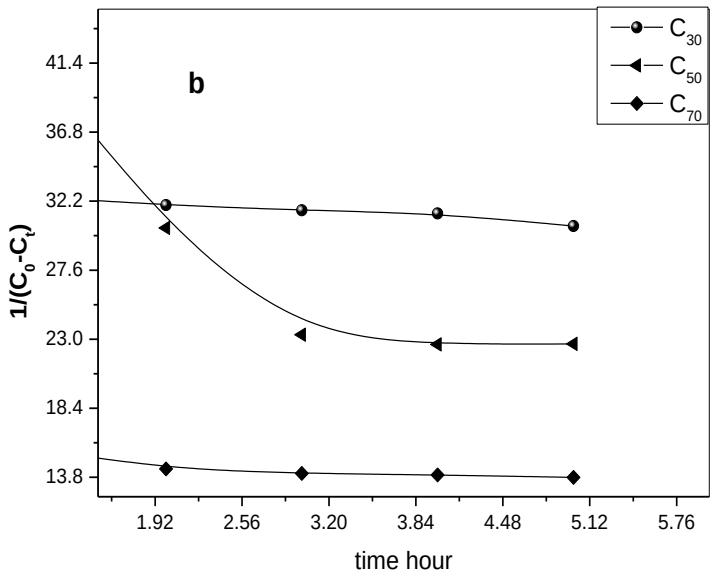
b
C30
C50
C70
41.4
36.8
32.2
27.6
23.0
18.4
13.8
1/(C0-Ct)
1.92
2.56
3.20
3.84
4.48
5.12
5.76
time hour

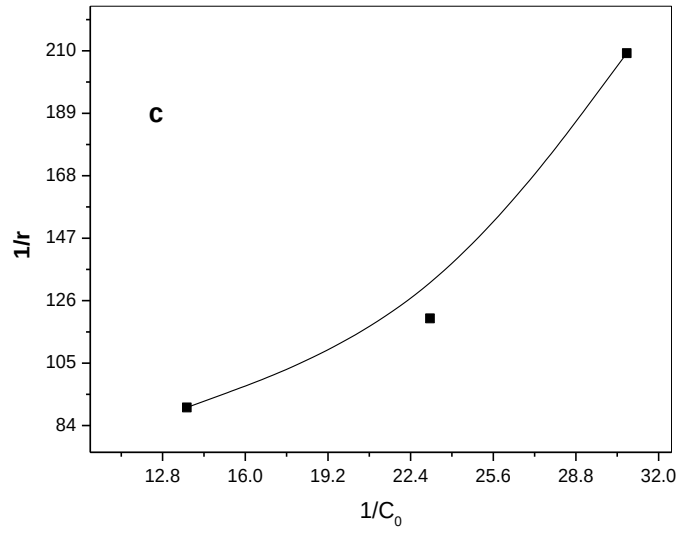

Fig. (56): Photo-decolorization of tubantin red using TiO_2 sol-gel (a) first order kinetic, (b) second order kinetic and (c) Langmuir Hinshelwood kinetic

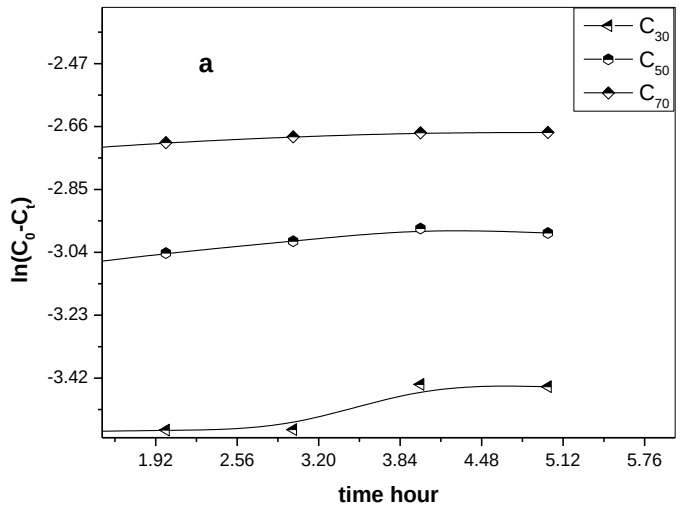

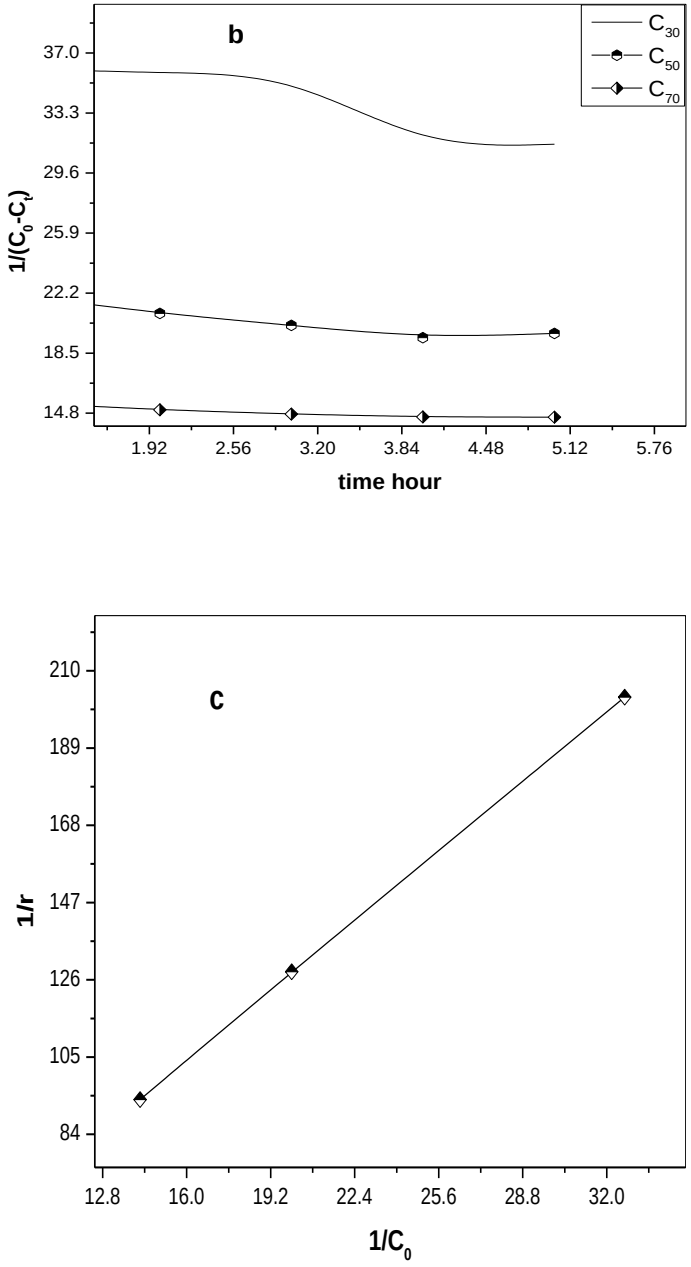

Fig. (57): Photo-decolorization of reactive yellow using TiO_2 sol-gel (a) first order kinetic, (b) second order kinetic and (c) Langmuir Hinshelwood kinetic

The experimental kinetic data were treated with three types of kinetic models (first-order, second order and Langmuir Hinshelwood model) to investigate the mechanism of successive adsorption and decolorization process. Tables (37-44) showed first, second order and Langmuir-Hinshelwood kinetic model parameter

(k) as well as the regression coefficient (R^2). Figs. (50-53) represented (first-order, second order and Langmuir Hinshelwood kinetic of photo-decolorization of four dyes (methylene blue, tubantin blue, tubantin red and yellow reactive) by using pure TiO_2 and Figs. (54-57) using TiO_2 sol-gel. It was observed that based on value of rate constant (k) regression coefficient (R^2) second order model ($k < 0$, R2 is low) does not fit to investigate the mechanism of the photo-decolorization for dyes at all initial dye concentration otherwise first order and Langmuir Hinshelwood ($k > 0$, R^2 is high) appropriate. The initial dye concentration effect on reaction rate i.e. in first order the effect of initial concentration is following order $C_{70} > C_{50} > C_{30}$. The rate of degradation relates to the probability of $OH^{\bullet}$ radicals formation on the catalyst surface and to the probability of $OH^{\bullet}$ radicals reacting with dye molecules (Konstantinou, and Albanis, 2004). The effect of dye type on reaction rate is following order methylene blue > tubantin red > tubantin blue > yellow reactive at both photo-catalysts, due their structures. This is in good accordance with the results of (Akpan and Hameed, 2011). The Langmuir-Hinshelwood model has been used to describe the photo-decolorization process kinetics that assumes automatically that reactions take place at the surface of the catalyst particles (Laoufi *et al.*, 2008). From analysis of Langmuir Hinshelwood kinetic model we can conclude that the adsorption properties of the substrate on the photo-catalyst surface, Figs. (50c-57c) showed the relation between 1/r and $1/C_0$ (r is reaction rate and C_0 is the initial concentration). The values of and K_{LH} ($dm^3\ mg^{-1}$), calculated from the intercept and the slope of the straight line (k_L ($mg\ dm^{-3}\ min^{-1}$) is reaction constant and K_{LH} is Langmuir Hinshelwood adsorption constant). Therefore, dark adsorption measurement is always required to compare with Langmuir Hinshelwood adsorption constant (K_{LH}). In this case, the classical Langmuir adsorption model has been applied to four dyes (methylene blue, tubantin blue, tubantin red and reactive yellow) in aqueous suspension according to eq. (10)

3.3.5. The dark adsorption

Table (45): The dark adsorption parameter maximum amount (Q_{max}), adsorption constant (K_{ad}) and regression coefficient (R^2) for four dyes on two types of photo-catalyst (pure TiO_2&TiO_2 sol-gel)

Dye	Pure TiO_2			TiO_2		
	Q_{max} gg^{-1}	K_{ad} dm^3g^{-1}	R^2	Q_{max} gg^{-1}	K_{ad} dm^3g^{-1}	R^2
Methylene blue	158.478	0.059	0.525	9.209	0.121	0.523
Tubantin blue	735.294	0.151	0.777	534.759	0.644	0.977
Tubantin red	1120.108	0.048	0.805	102.249	0.072	0.967
Reactive yellow	106.044	0.049	0.963	78.125	0.136	0.989

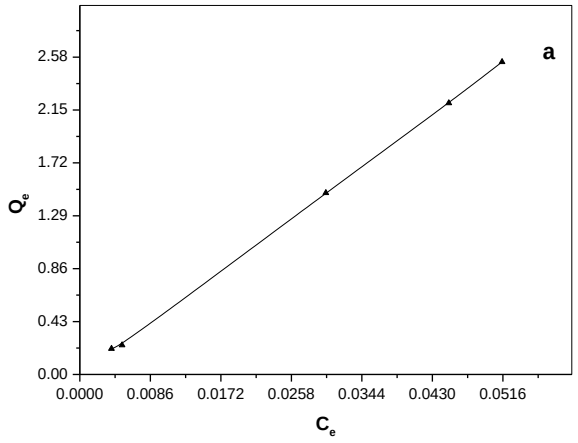

``

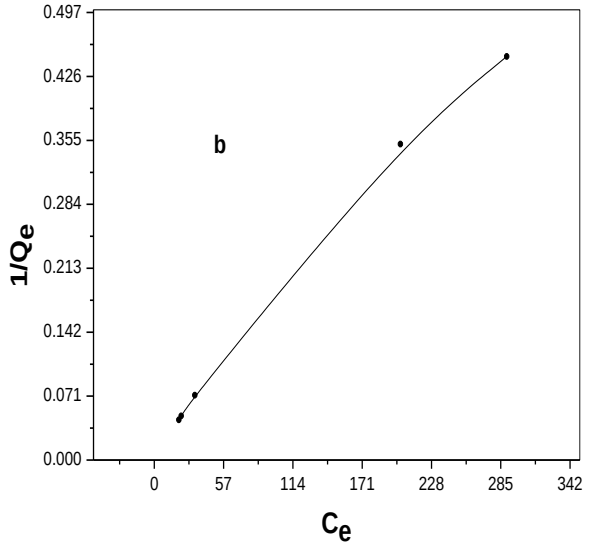

Fig (58): Adsorption isotherm of methylene blue on pure TiO_2, a. quantity adsorbed as a function of equilibrium concentration b. linear quantity adsorbed as a function of equilibrium quantity adsorbed as a function

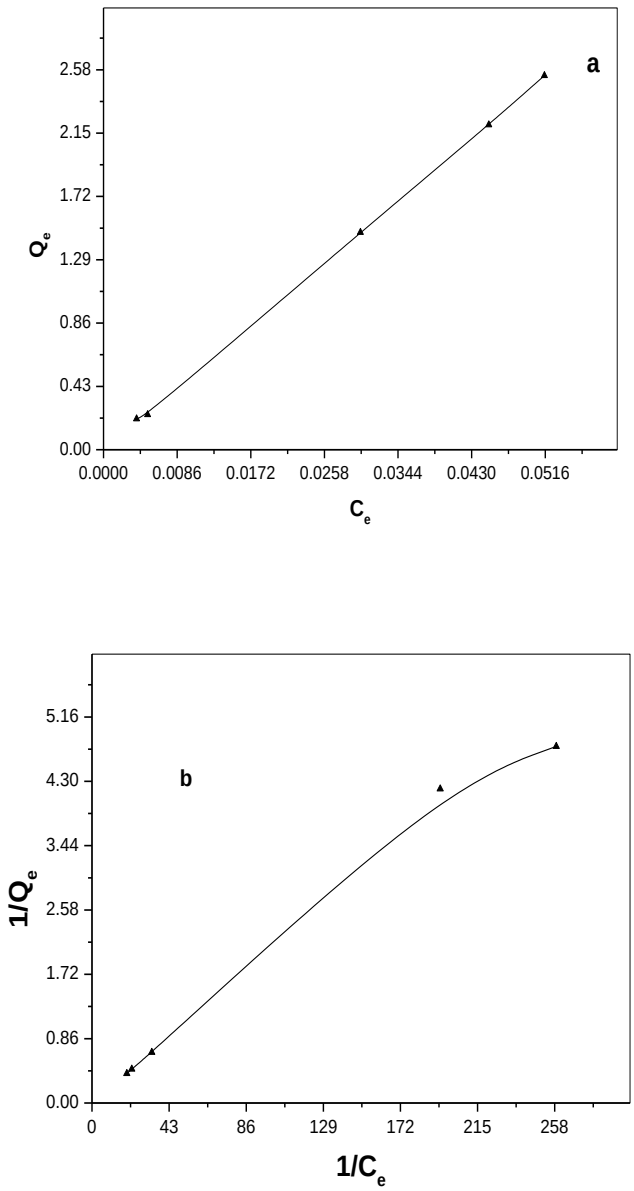

Fig (59): Adsorption isotherm of methylene blue on pure TiO_2, a. quantity adsorbed as a function of equilibrium concentration b. linear quantity adsorbed as a function of equilibrium quantity adsorbed as a function of equilibrium

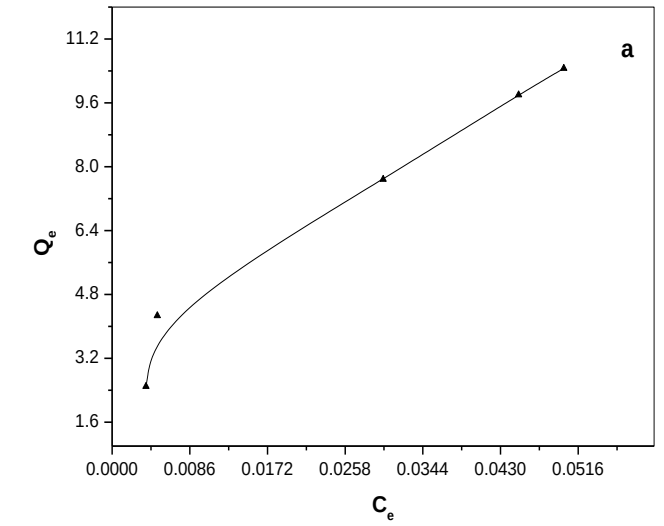

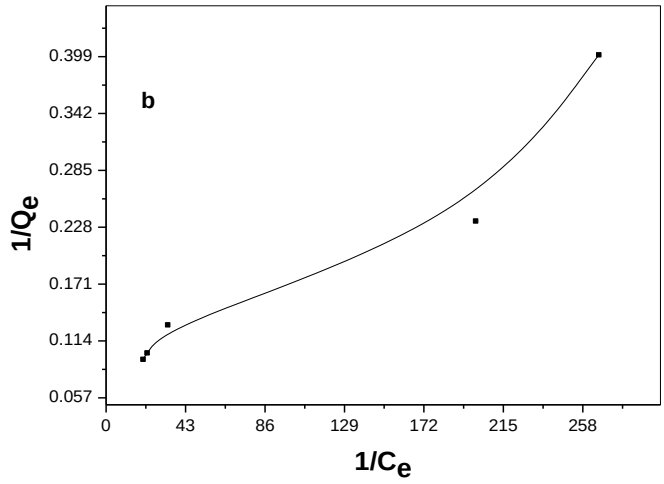

Fig (60): Adsorption isotherm of tubantin blue on pure TiO_2, a. quantity adsorbed as a function of equilibrium concentration b. linear quantity adsorbed as a function of equilibrium quantity adsorbed as a function of equilibrium

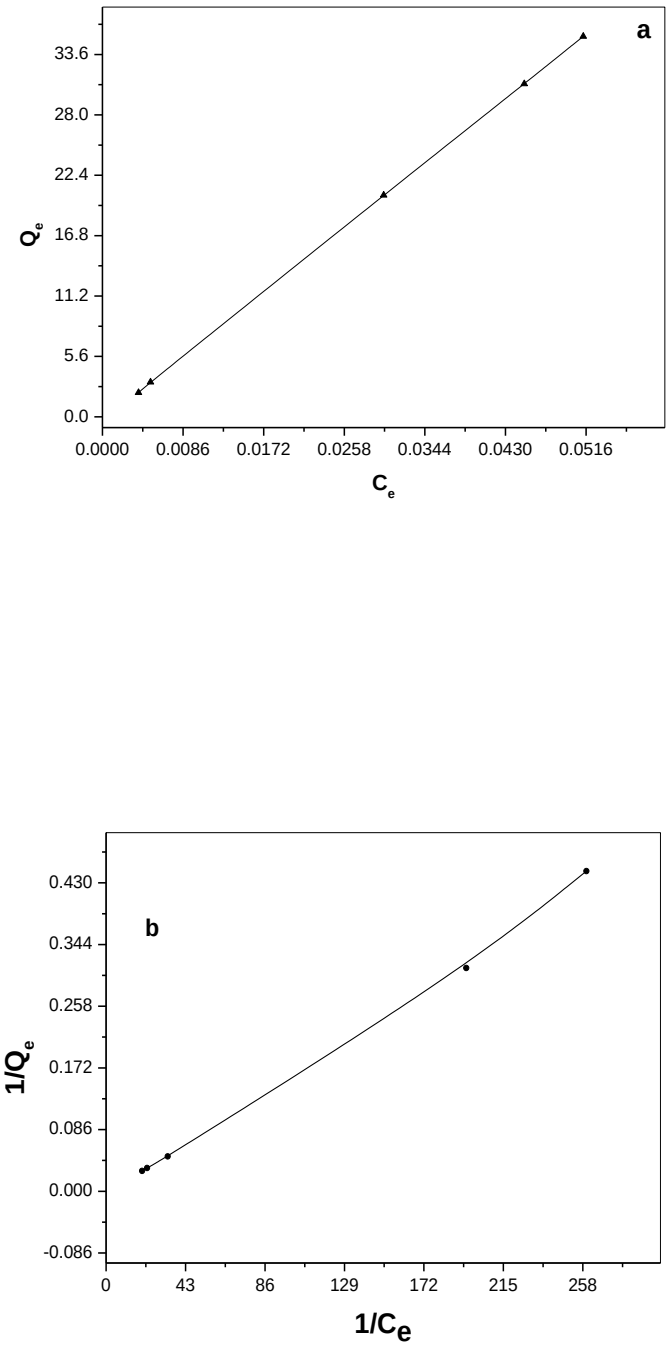

Fig (61): Adsorption isotherm of tubantin blue on TiO_2 sol-gel, a. quantity adsorbed as a function of equilibrium concentration b. linear quantity adsorbed as a function of equilibrium quantity adsorbed as a function of equilibrium

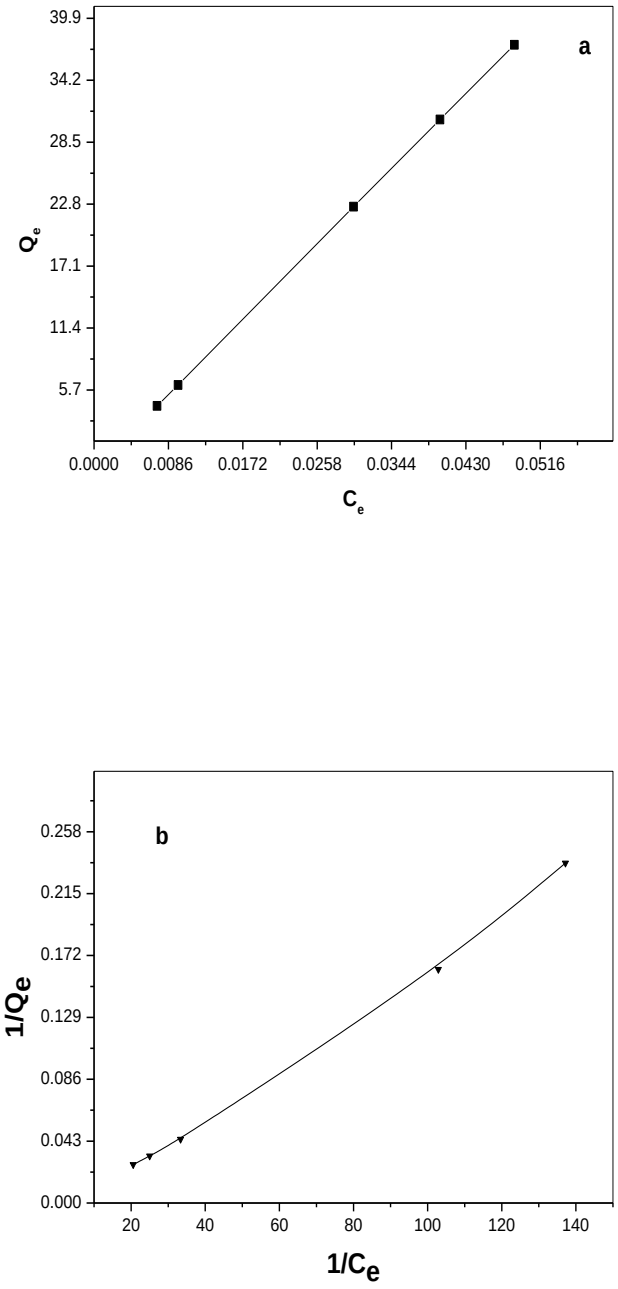

Fig (62): Adsorption isotherm of tubantin red on pure TiO_2, a. quantity adsorbed as a function of equilibrium concentration b. linear quantity adsorbed as a function of equilibrium quantity adsorbed as a function of equilibrium

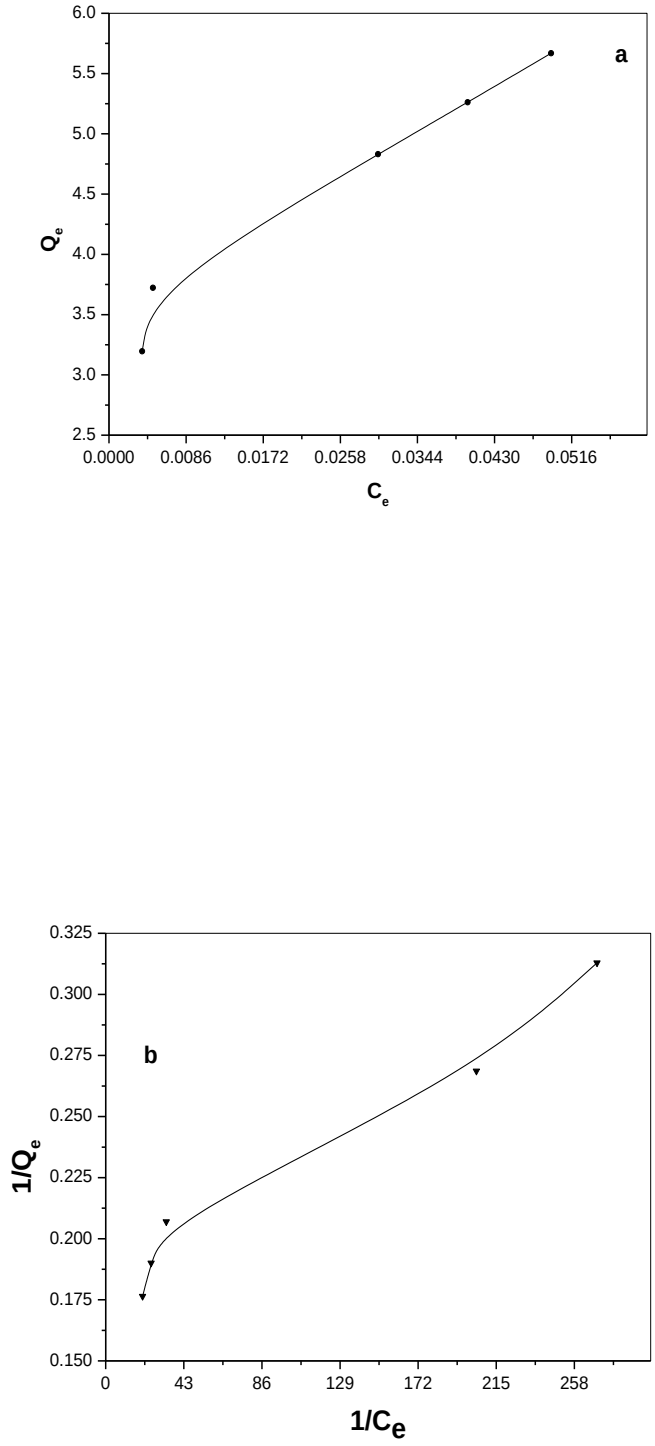

Fig (63): Adsorption isotherm of tubantin red on TiO_2 sol-gel, a. quantity adsorbed as a function of equilibrium concentration b. linear quantity adsorbed as a function of equilibrium quantity adsorbed as a function of equilibrium

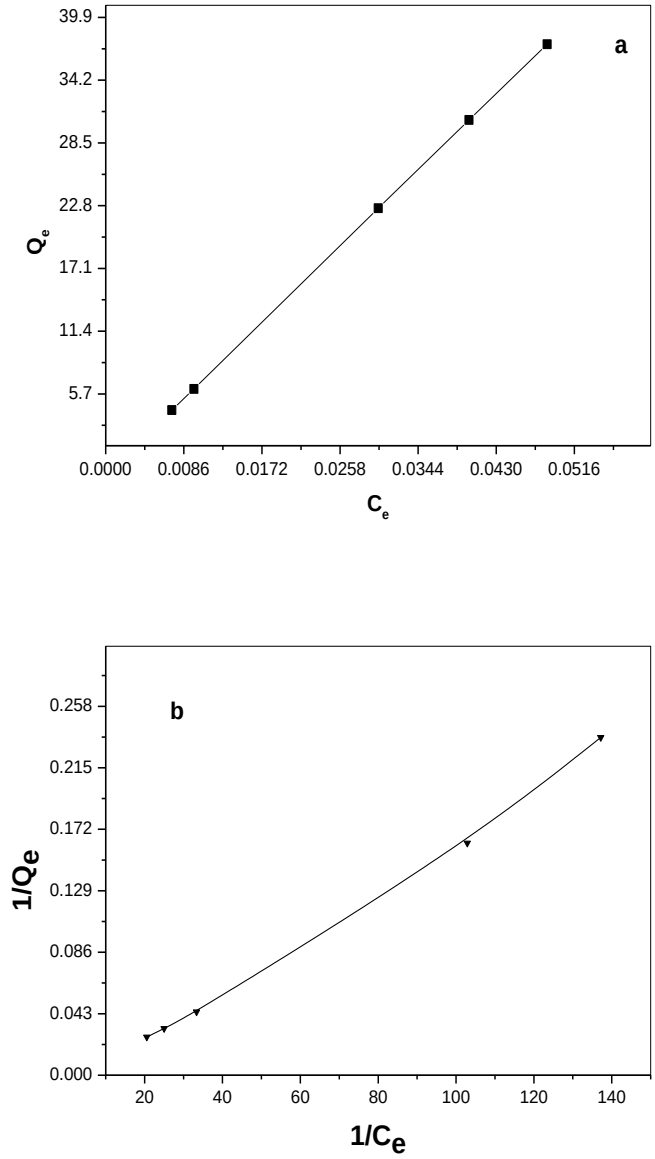

Fig (64): Adsorption isotherm of reactive yellow on pure TiO_2, a. quantity adsorbed as a function of equilibrium concentration b. linear quantity adsorbed as a function of equilibrium quantity adsorbed as a function of equilibrium

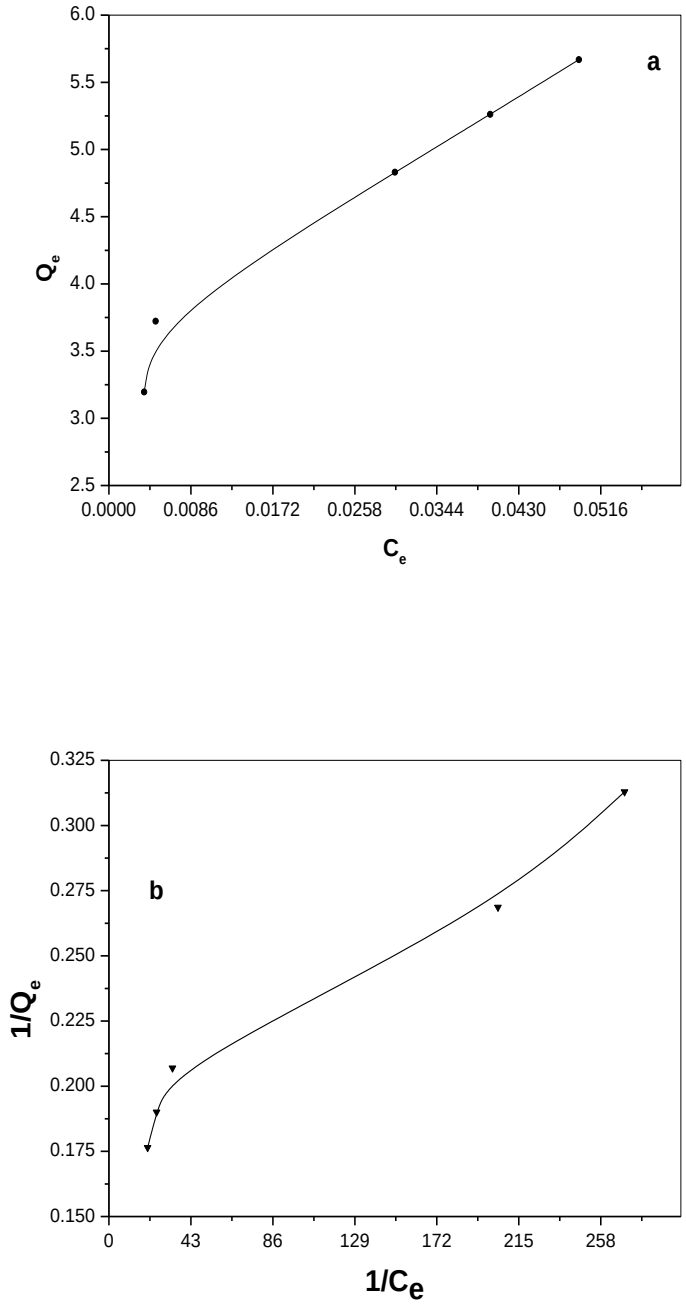

Fig (65): Adsorption isotherm of reactive yellow on TiO_2 sol-gel, a. quantity adsorbed as a function of equilibrium concentration b. linear quantity adsorbed as a function of equilibrium quantity adsorbed as a function of equilibrium

Figs. (58 & 65) shows the results for the dark adsorption of four dyes (methylene blue, tubantin blue, tubantin red and yellow reactive) on the two catalyst surface at different concentration range (30-70). According to (Khezrianjoo and Revanasiddappa, 2012) the adsorption behavior displayed by

the dye adsorbed molecules onto photo-catalyst with monolayer coverage of the catalyst surface following the Langmuir adsorption model at the low concentration range see eq.(12). K_{ad} adsorption constant, Q_{max} the maximum amount of dye adsorbed forming a complete monolayer were calculated from the intercept and the slope of the straight line as well as regression coefficient (R^2) which represented in Table (45)**.** It observed that all isotherms showed type L-shape, the L-shape of the isotherms means that there is no strong competition between the solvent and the adsorbate to occupy the adsorbent surface sites (Sauer et al., 2002). The adsorb-abilities of the dyes as well as the K_{ad} values decreased in the following order: tubantin blue > methylene blue > yellow reactive > tubantin red in using pure TiO_2 and tubantin blue > yellow reactive > methylene blue > tubantin red

Table (46): Average first-order rate constant, Langmuir Hinshelwood constant, Langmuir Hinshelwood adsorption constant and adsorption constant equilibrium

Dyes	**k_1 min^{-1}**		**k_L $mg\ dm^{-3}\ min^{-1}$**		**k_{L-H} $dm^3\ mg^{-1}$**		**K_{ad} $dm^3\ mg^{-1}$**	
	Pure TiO_2	**TiO_2 sol-gel**	**Pure TiO_2**	**TiO_2 sol-gel**	**Pure TiO_2**	**TiO_2 sol-gel**	**Pure TiO_2**	**TiO_2 sol-gel**
Methylene blue	0.077	0.108	0.188	0.214	0.648	0.080	0.059	0.121
Tubantin blue	0.015	0.763	0.126	0.146	0.306	1.376	0.151	0.644
Tubantin red	0.089	0.072	0.169	0.163	61.601	0.718	0.048	0.072
Reactive yellow	0.042	0.028	0.169	0.176	3.158	0.625	0.049	0.136

Table (46) show the average first-order rate constant, Langmuir Hinshelwood constant, Langmuir Hinshelwood adsorption constant and adsorption constant equilibrium. It is worth noting that the adsorption constant K_{ad} obtained from the dark adsorption isotherm is significantly different from the k_{L-H} determined by L–H equation, Similar results have been reported by (Sauer *et al*., 2002) showed the photo-adsorption and the fast photo-reaction of substrate on the TiO_2 surface making the observed k_{L-H} under irradiation conditions different from that K_{ad} in the dark

Chapter four

Conclusions and Recommendations

4.1. Conclusions

- Sol-gel is the best method for synthesis of TiO_2 nanoparticles with the best properties.
- Characterization of catalysts shows that two types are in anatase form, nanoparticles and they are best for photo-catalysis process under UV radiation (pure TiO_2 Eg =3.03eVand TiO_2 sol-gel E_g=3.23eV).
- Potassium ferrioxalate actinometry fit for determination of photon flux during TiO_2 photo-catalytic (λ_{max} 385).
- High Photo-decolorization percentage of Tubantin blue in take place basic solution. The Photo-decolorization percentage increased as a function of amount of catalyst and irradiation time, decrease as concentration of dyes increase.
- The photo-decolorization percentage of the four dyes under study differs is government depending on the type of catalyst and dyes.
- The daily photon flux was nearly constant during the experiments, when using pure TiO_2. The increase of solution temperature varies depending on the catalyst type.
- The photo-decolorization decreases with an increase in the initial concentration of dyes.
- Second-order model does not fit to investigate the mechanism of the photo-decolorization for dyes at all initial dye concentration otherwise first order and Langmuir-Hinshelwood.
- Photo-decolorization rate reaction influence by initial dye concentration and type of dye and catalyst.

4.2. Recommendations

The following recommendation can be proposed taking into account of results of this research:

- It is recommended to improve the titanium dioxide activity through synthesis in difference nanoparticles shape and doping form with different metal to shift its absorbance in visible radiation instead of UV radiation.
- It is recommended to solve the separation problem used immobilize catalyst model rather than slurry model or by using adsorbents materials such as activated carbon or zeolites.
- It is recommended to apply the titanium photo-catalytic process for degradation of other organic compounds.
- It is recommended to apply the results of operation condition to treat industrial wastewater that contains dyes.
- It is recommended to use HPLC technique to follow the change of dye concentration rather than spectrophotometer.
- It is recommended to use GC/MS to monitor intermediate products during the titanium dioxide photo-catalytic process.
- It recommended todetermine the total organic carbon (TOC) using TOC analyzer for photo-catalytic kinetic study due to it is simplified kinetic model.

Appendices

Appendix A: Change in dyes colour during solar photocatalytic by using pure TiO_2 and TiO_2 sol-gel

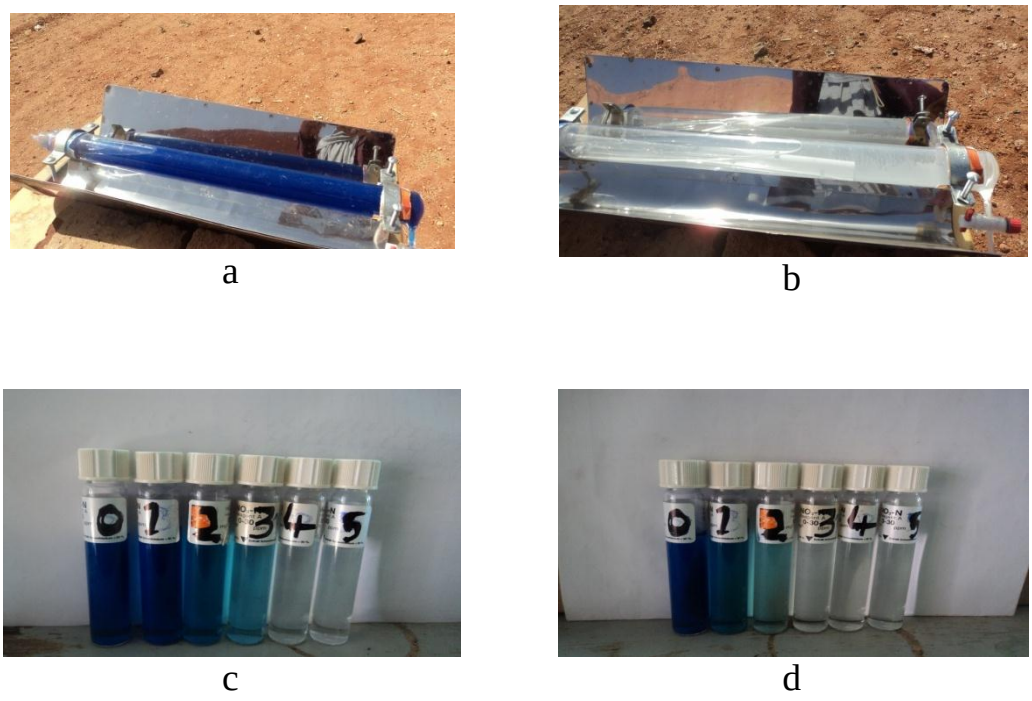

Fig. (A-1): Change mthylene blue colour (a) at first hour (b) after five hour (c) treatment by using pure TiO_2 (d) treatment by using TiO_2 sol-gel

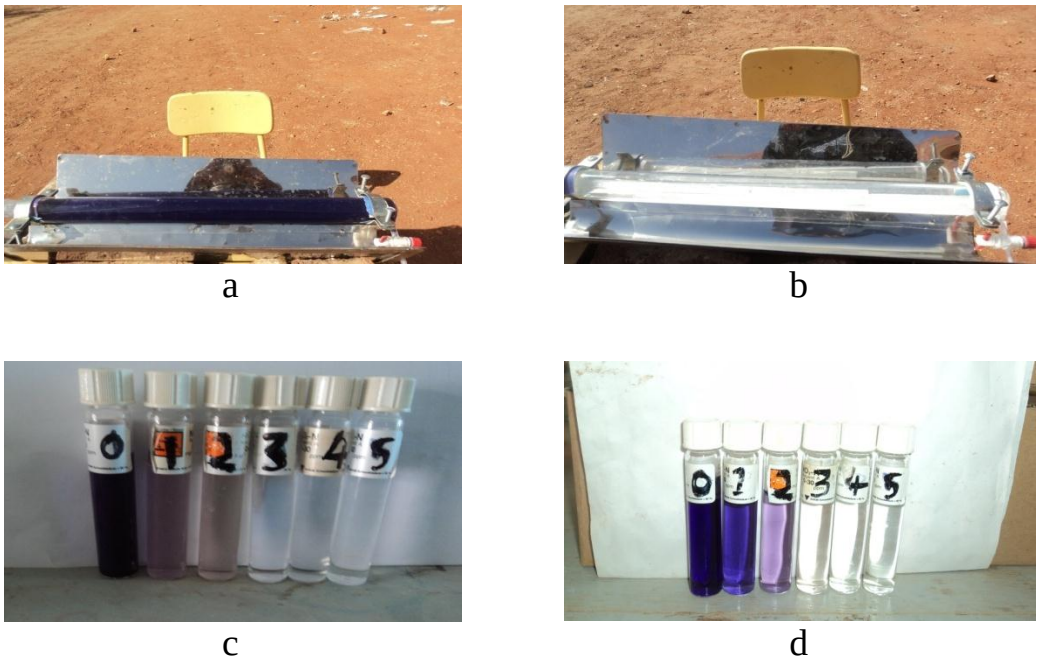

Fig . (A-2): Change tubantin blue colour (a) at first hour (b) after five hour (c) treatment by using pure TiO_2 (d) treatment by using TiO_2 sol-gel

a

b

c

d

Fig. (A-3): Change tubantin red colour (a) at first hour (b) after five hour (c) treatment by using pure TiO_2 (d) treatment by using TiO_2 sol-gel

A

b

C

d

Fig. (A-4): Change reactive yellow colour (a) at first hour (b) after five hour (c) treatment by using pure TiO_2 (d) treatment by using TiO_2 sol-gel

Appendix B:The pictures of in struments

Fig. B-1:PANalytical's X-ray diffractometer

Fig. B-2:UV-visible spectrophotometer

Fig. B-3: Fourier transform infrared (FTIR) spectroscop

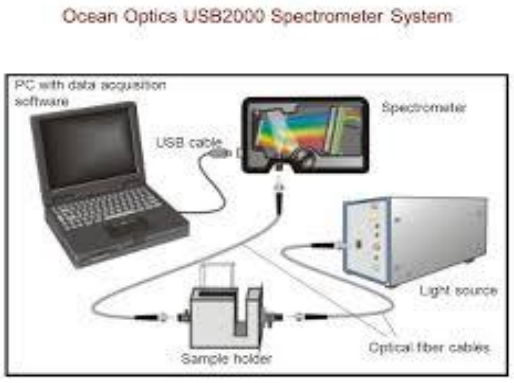

Fig. B-4: Ocean optio USB2000 Spectrometer

Fig. B-5: Micrometric gas adsorption analyzer

Fig. B-6: UV-visible spectrophotometer Aquanova

References:

1. Abbasi, M. and Asl, N.R., 2008. Sonochemical degradation of Basic Blue 41 dye assisted by nanoTiO_2 and H_2O_2. *Journal of hazardous materials*, 153(3), pp.942-947.
2. Ajona, J.I. and Vidal, A., 2000. The use of CPC collectors for detoxification of contaminated water: design, construction and preliminary results. *Solar energy*, 68(1), pp.109-120.
3. Akpan, U.G. and Hameed, B.H., 2009. Parameters affecting the photocatalytic degradation of dyes using TiO_2-based photo-catalysts: a review. *Journal of hazardous materials*, 170(2), pp.520-529.
4. Aleboyeh, A., Daneshvar, N. and Kasiri, M.B., 2008. Optimization of CI Acid Red 14 azo dye removal by electrocoagulation batch process with response surface methodology. *Chemical Engineering and Processing: Process Intensification*, 47(5), pp.827-832.
5. Alfano, O.M. and Cassano, A.E., 2008. Photoreactor modeling: applications to advanced oxidation processes. *International Journal of Chemical Reactor Engineering*, 6(1).
6. Alinsafi, A., Evenou, F., Abdulkarim, E.M., Pons, M.N., Zahraa, O., Benhammou, A., Yaacoubi, A. and Nejmeddine, A., 2007. Treatment of textile industry wastewater by supported photocatalysis. *Dyes and Pigments*, *74*(2), pp.439-445.
7. Alvarez-Corena, J.R., Bergendahl, J.A. and Hart, F.L., 2016. Advanced oxidation of five contaminants in water by UV/TiO_2: reaction kinetics and byproducts identification. *Journal of environmental management*, 181, pp.544-551.
8. Amini, M., Arami, M., Mahmoodi, N.M. and Akbari, A., 2011. Dye removal from colored textile wastewater using acrylic grafted nanomembrane. *Desalination*, 267(1), pp.107-113.

9. Bafana, A., Jain, M., Agrawal, G. and Chakrabarti, T., 2009. Bacterial reduction in genotoxicity of Direct Red 28 dye. *Chemosphere*, 74(10), pp.1404-1406.
10. Bakshi, D.K. and Sharma, P., 2003. Genotoxicity of textile dyes evaluated with Ames test and rec-assay. *Journal of environmental pathology, toxicology and oncology*, 22(2).
11. Baur, W.H., 1961. Atomabstände und bindungswinkel im brookit, TiO2. *Acta Crystallographica*, 14(3), pp.214-216.
12. Baydoğan, N., Ozdurmusoglu, T., Cimenoglu, H. and Tugrul, A.B., 2013. Refractive Index and Extinction Coefficient of ZnO: Al Thin Films Derived by Sol-Gel Dip Coating Technique. In Defect and Diffusion Forum (Vol. 334, pp. 290-293). *Trans Tech Publications*.
13. Bhatkhande, D.S., Pangarkar, V.G. and Beenackers, A.A., 2002. Photo-catalytic degradation for environmental applications–a review. *Journal of Chemical Technology and Biotechnology*, 77(1), pp.102-116.
14. Blanco, J., Malato, S., Fernandez, P., Vidal, A., Morales, A., Trincado, P., Oliveira, J.C., Minero, C., Musci, M., Casale, C. and Brunotte, M., 2000. Compound Parabolic Concentrator Technology Development to Commercial Solar Detoxification Application. pp. 427-436.
15. Burda, C., Chen, X., Narayanan, R. and El-Sayed, M.A., 2005. Chemistry and properties of nano-crystals of different shapes. *Chemical reviews*, 105(4), pp.1025-1102.
16. Buitron, G., Quezada, M. and Moreno, G., 2004. Aerobic degradation of the azo dye acid red 151 in a sequencing batch biofilter. *Bioresource technology*, 92(2), pp.143-149.

17. Carp, O., Huisman, C.L. and Reller, A., 2004. Photo-induced reactivity of titanium dioxide. *Progress in solid state chemistry*, 32(1), pp.33-177.
18. Chaleshtori, M.Z., Hosseini, M., Edalatpour, R., Masud, S.S. and Chianelli, R.R., 2013. New porous titanium–niobium oxide for photocatalytic degradation of bromocresol green dye in aqueous solution. *Materials Research Bulletin*, 48(10), pp.3961-3967.
19. Chatterjee, S., Lee, D.S., Lee, M.W. and Woo, S.H., 2009. Enhanced adsorption of congo red from aqueous solutions by chitosan hydrogel beads impregnated with cetyl trimethyl ammonium bromide. *Bioresource Technology*, 100(11), pp.2803-2809.
20. Chen, J.Q., Wang, D., Zhu, M.X. and Gao, C.J., 2007. Photo-catalytic degradation of dimethoate using nanosized TiO2 powder. Desalination, 207(1-3), pp.87-94.
21. Chen, J., Wang, H., Wei, X. and Zhu, L., 2012. Characterization, properties and catalytic application of TiO 2 nanotubes prepared by ultrasonic-assisted sol-hydrothermal method. *Materials Research Bulletin*, 47(11), pp.3747-3752.
22. Chen, X. and Mao, S.S., 2007. Titanium dioxide nano-materials: synthesis, properties, modifications, and applications. *Chemical. Review*, 107(7), pp.2891-2959.
23. Chen, Y., Lin, A. and Gan, F., 2006. Preparation of nano-TiO_2 from TiCl 4 by dialysis hydrolysis. *Powder Technology*, 167(3), pp.109-116.
24. Chong, M.N., Jin, B., Chow, C.W. and Saint, C., 2010. Recent developments in photo-catalytic water treatment technology: a review. *Water research*, 44(10), pp.2997-3027.

25. Crini, G., 2005. Recent developments in polysaccharide-based materials used as adsorbents in wastewater treatment. *Progress in polymer science*, 30(1), pp.38-70.
26. Crini, G. and Badot, P.M., 2008. Application of chitosan, a natural aminopolysaccharide, for dye removal from aqueous solutions by adsorption processes using batch studies: a review of recent literature. *Progress in polymer science*, 33(4), pp.399-447.
27. Cromer, D.T. and Herrington, K., 1955. The structures of anatase and rutile. *Journal of the American Chemical Society*, 77(18), pp.4708-4709.
28. Daneshvar, N., Salari, D. and Khataee, A.R., 2003. Photo-catalytic degradation of azo dye acid red 14 in water: investigation of the effect of operational parameters. *Journal of Photochemistry and Photobiology A: Chemistry*, 157(1), pp.111-116.
29. de Alvarenga, J.M., Fideles, R.A., da Silva, M.V., Murari, G.F., Taylor, J.G., de Lemos, L.R., Rodrigues, G.D. and Mageste, A.B., 2015. Partition study of textile dye Remazol Yellow Gold RNL in aqueous two-phase systems. *Fluid Phase Equilibria*, 391, pp.1-8.
30. De Lasa, H.I., Serrano, B. and Salaices, M., 2005. Photo-catalytic reaction engineering (p. 193). New York: *Springer*.
31. Demas, J.N., Bowman, W.D., Zalewski, E.F. and Velapoldi, R.A., 1981. Determination of the quantum yield of the ferrioxalate actinometer with electrically calibrated radiometers. *The Journal of Physical Chemistry*, *85*(19), pp.2766-2771.
32. Diebold, U., 2003. The surface science of titanium dioxide. *Surface science reports*, 48(5), pp.53-229.
33. Domínguez, J.R., Beltrán, J. and Rodríguez, O., 2005. Vis and UV photo-catalytic detoxification methods (using TiO_2, TiO_2/H_2O_2, TiO_2/O_3, $TiO_2/S_2O_8^{2-}$, O_3, H_2O_2, $S_2O_8^{2-}$, Fe^{3+}/H_2O_2 and

$Fe^{3+}/H_2O_2/C_2O_4^{2-}$) for dyes treatment. *Catalysis today*, 101(3), pp.389-395.

34. Eckenfelder, W.W., 2000. Industrial water pollution control. *McGraw-Hill.*
35. Esplugas, S., Gimenez, J., Contreras, S., Pascual, E. and Rodríguez, M., 2002. Comparison of different advanced oxidation processes for phenol degradation. *Water research*, 36(4), pp.1034-1042.
36. Fan, L., Zhou, Y., Yang, W., Chen, G. and Yang, F., 2008. Electrochemical degradation of aqueous solution of Amaranth azo dye on ACF under potentiostatic model. *Dyes and Pigments*, 76(2), pp.440-446.
37. Foo, K.Y. and Hameed, B.H., 2010. An overview of dye removal via activated carbon adsorption process. *Desalination and Water Treatment*, 19(1-3), pp.255-274.
38. Fox, M.A. and Dulay, M.T., 1993. Heterogeneous photo-catalysis. *Chemical reviews*, 93(1), pp.341-357.
39. Fujishima, A. and Honda, K., 1972. Electrochemical photolysis of water at a semiconductor electrode. *Nature*, 238(5358), pp.37-38.
40. Fujishima, A. and Zhang, X., 2006. Titanium dioxide photo-catalysis: present situation and future approaches. *Comptes Rendus Chimie*, 9(5), pp.750-760.
41. Gaya, U.I. and Abdullah, A.H., 2008. Heterogeneous photo-catalytic degradation of organic contaminants over titanium dioxide: a review of fundamentals, progress and problems. *Journal of Photochemistry and Photobiology C: Photochemistry Reviews*, 9(1), pp.1-12.
42. Gernjak, W., Krutzler, T., Glaser, A., Malato, S., Caceres, J., Bauer, R. and Fernández-Alba, A.R., 2003. Photo-Fenton treatment of water containing natural phenolic pollutants. *Chemosphere*, 50(1), pp.71-78.

43. Ghaly,A.E., Ananthashankar, R., Alhattab, M.V.V.R., and Ramakrishnan, V.V., 2014. Production, Characterization and Treatment of Textile Effluents: A Critical Review. *Journal of Chemical Engineering & Process Technology*, 5(1) p1
44. Gomez, V., Larrechi, M.S. and Callao, M.P., 2007. Kinetic and adsorption study of acid dye removal using activated carbon. *Chemosphere*, 69(7), pp.1151-1158.
45. Govindaraj, R., Pandian, M.S., Murugan, G.S., Ramasamy, P. and Mukhopadhyay, S., 2015. Synthesis of porous titanium dioxide nanorods/nanoparticles and their properties for dye sensitized solar cells. *Journal of Materials Science: Materials in Electronics*, 26(4), pp.2609-2613.
46. Grujić-Brojčin, M., Šćepanović, M., Dohčević-Mitrović, Z. and Popović, Z.V., 2006. Infrared study of nonstoichiometric anatase TiO2 nanopowders. *Science of Sintering*, 38(2), pp.183-189.
47. Guimarães, J.R., Maniero, M.G. and de Araujo, R.N., 2012. A comparative study on the degradation of RB-19 dye in an aqueous medium by advanced oxidation processes. *Journal of environmental management*, 110, pp.33-39.
48. Gupta, V.K., Jain, R. and Varshney, S., 2007. Electrochemical removal of the hazardous dye Reactofix Red 3 BFN from industrial effluents. *Journal of Colloid and Interface Science*, 312(2), pp.292-296.
49. Habibi, M.H., Hassanzadeh, A. and Mahdavi, S., 2005. The effect of operational parameters on the photo-catalytic degradation of three textile azo dyes in aqueous TiO_2 suspensions. *Journal of Photochemistry and Photobiology A: Chemistry*, 172(1), pp.89-96.
50. Han, F., Kambala, V.S.R., Srinivasan, M., Rajarathnam, D. and Naidu, R., 2009. Tailored titanium dioxide photo-catalysts for the

degradation of organic dyes in wastewater treatment: a review. *Applied Catalysis A: General*, 359(1), pp.25-40.

51. Han, H. and Bai, R., 2009. Buoyant photo-catalyst with greatly enhanced visible-light activity prepared through a low temperature hydrothermal method. *Industrial & Engineering Chemistry Research*, 48(6), pp.2891-2898.
52. Harrelkas, F., Azizi, A., Yaacoubi, A., Benhammou, A. and Pons, M.N., 2009. Treatment of textile dye effluents using coagulation–flocculation coupled with membrane processes or adsorption on powdered activated carbon. *Desalination*, 235(1-3), pp.330-339.
53. Hayle, S.T. and Gonfa, G.G., 2014. Synthesis and characterization of titanium oxide nano-materials using sol-gel method. *American Journal of Nano-science and Nanotechnology*, 2(1), pp.1-7.
54. Herrmann, J.M., 1999. Heterogeneous photo-catalysis: fundamentals and applications to the removal of various types of aqueous pollutants. *Catalysis today*, 53(1), pp.115-129.
55. Hoffmann, M.R., Martin, S.T., Choi, W. and Bahnemann, D.W., 1995. Environmental applications of semiconductor photo-catalysis. *Chemical reviews*, 95(1), pp.69-96.
56. Houas, A., Lachheb, H., Ksibi, M., Elaloui, E., Guillard, C. and Herrmann, J.M., 2001. Photocatalytic degradation pathway of methylene blue in water. *Applied Catalysis B: Environmental*, 31(2), pp.145-157.
57. Hsing, H.J., Chiang, P.C., Chang, E.E. and Chen, M.Y., 2007. The decolorization and mineralization of Acid Orange 6 azo dye in aqueous solution by advanced oxidation processes: A comparative study. *Journal of Hazardous Materials*, 141(1), pp.8-16.
58. Hu, A., Liang, R., Zhang, X., Kurdi, S., Luong, D., Huang, H., Peng, P., Marzbanrad, E., Oakes, K.D., Zhou, Y. and Servos, M.R., 2013.

Enhanced photo-catalytic degradation of dyes by TiO_2 nanobelts with hierarchical structures. *Journal of Photochemistry and Photobiology A: Chemistry*, 256, pp.7-15.

59. Huang, M., Xu, C., Wu, Z., Huang, Y., Lin, J. and Wu, J., 2008. Photo-catalytic decolorization of methyl orange solution by Pt modified TiO_2 loaded on natural zeolite. *Dyes and Pigments*, 77(2), pp.327-334.
60. Jawad, A.H., Mubarak, N.S.A., Ishak, M.A.M., Ismail, K. and Nawawi, W.I., 2016. Kinetics of photo-catalytic decolorization of cationic dye using porous TiO 2 film. *Journal of Taibah University for Science*, 10(3), pp.352-362.
61. Kar, A., Smith, Y.R. and Subramanian, V., 2009. Improved photocatalytic degradation of textile dye using titanium dioxide nanotubes formed over titanium wires. *Environmental science & technology*, 43(9), pp.3260-3265.
62. Karunakaran, C., Senthilvelan, S., Karuthapandian, S. and Balaraman, K., 2004. Photo-oxidation of iodide ion on some semiconductor and non-semiconductor surfaces. *Catalysis Communications*, 5(6), pp.283-290.
63. Kerkez-Kuyumcu, Ö., Kibar, E., Dayıoğlu, K., Gedik, F., Akın, A.N. and Özkara-Aydınoğlu, Ş., 2015. A comparative study for removal of different dyes over M/TiO_2 (M= Cu, Ni, Co, Fe, Mn and Cr) photocatalysts under visible light irradiation. *Journal of Photochemistry and Photobiology A: Chemistry*, 311, pp.176-185.
64. Khan, R. and Fulekar, M.H., 2016. Biosynthesis of titanium dioxide nanoparticles using Bacillus amyloliquefaciens culture and enhancement of its photo-catalytic activity for the degradation of a sulfonated textile dye Reactive Red 31. *Journal of colloid and interface science*, 475, pp.184-191.

65. Khataee, A.R., Fathinia, M. and Aber, S., 2010. Kinetic modeling of liquid phase photocatalysis on supported TiO_2 nanoparticles in a rectangular flat-plate photo-reactor. Industrial & Engineering *Chemistry Research*, 49(24), pp.12358-12364.
66. Khataee, A.R. and Kasiri, M.B., 2010. Photo-catalytic degradation of organic dyes in the presence of nanostructured titanium dioxide: influence of the chemical structure of dyes. *Journal of Molecular Catalysis A: Chemical*, 328(1), pp.8-26.
67. Khezrianjoo,S. and Revanasiddappa. H.D., 2012. Langmuir-Hinshelwood Kinetic Expression for the Photo-catalytic Degradation of Metanil Yellow Aqueous Solutions by ZnO Catalyst. Chemical *Science Journal*.
68. Konstantinou, I.K. and Albanis, T.A., 2004. TiO_2-assisted photo-catalytic degradation of azo dyes in aqueous solution: kinetic and mechanistic investigations: a review. *Applied Catalysis B: Environmental*, 49(1), pp.1-14.
69. Kuhn, H.J., Braslavsky, S.E. and Schmidt, R., 2004. Chemical actinometry (IUPAC technical report). *Pure and Applied Chemistry*, 76(12), pp.2105-2146.
70. Kumar, K.V., Porkodi, K. and Selvaganapathi, A., 2007. Constrain in solving Langmuir–Hinshelwood kinetic expression for the photocatalytic degradation of Auramine O aqueous solutions by ZnO catalyst. *Dyes and Pigments*, 75(1), pp.246-249.
71. Kuo, W.S. and Ho, P.H., 2006. Solar photocatalytic decolorization of dyes in solution with TiO_2 film. *Dyes and Pigments*, 71(3), pp.212-217.
72. Latroche, M., Brohan, L., Marchand, R. and Tournoux, M., 1989. New hollandite oxides: TiO_2 (H) and K0. 06TiO_2. *Journal of Solid State Chemistry*, 81(1), pp.78-82.

73. Lee, J., Kim, J. and Choi, W., 2007. Ferrioxalate-polyoxometalate system as a new chemical actinometer. *Environmental science & technology*, 41(15), pp.5433-5438.
74. Liu, B., Wen, L. and Zhao, X., 2007. The photoluminescence spectroscopic study of anatase TiO_2 prepared by magnetron sputtering. *Materials Chemistry and Physics*, 106(2), pp.350-353.
75. Mahmoodi, N.M. and Arami, M., 2006. Bulk phase degradation of Acid Red 14 by photo-catalysis using immobilized titanium (IV) oxide nano-particles. *Journal of Photochemistry and Photobiology A: Chemistry*, 182(1), pp.60-66.
76. Marugán, J., van Grieken, R., Cassano, A.E. and Alfano, O.M., 2008. Intrinsic kinetic modeling with explicit radiation absorption effects of the photo-catalytic oxidation of cyanide with TiO_2 and silica-supported TiO_2 suspensions. *Applied Catalysis B: Environmental*, 85(1), pp.48-60.
77. Marugán, J., Van Grieken, R., Pablos, C., Satuf, M.L., Cassano, A.E. and Alfano, O.M., 2013. Modeling of a bench-scale photo-catalytic reactor for water disinfection from laboratory-scale kinetic data. *Chemical engineering journal*, 224, pp.39-45.
78. Metivier-Pignon, H., Faur, C. and Le Cloirec, P., 2007. Adsorption of dyes onto activated carbon cloth: Using QSPRs as tools to approach adsorption mechanisms. *Chemosphere*, 66(5), pp.887-893.
79. Metcalf & Eddy, Burton, F.L., Stensel, H.D. and Tchobanoglous, G., 2003. Wastewater engineering: treatment and reuse. McGraw Hill.
80. Minero, C., Pelizzetti, E., Malato, S. and Blanco, J., 1993. Large solar plant photo-catalytic water decontamination: Degradation of pentachlorophenol. *Chemosphere*, 26(12), pp.2103-2119.

81. Mo, S.D. and Ching, W.Y., 1995. Electronic and optical properties of three phases of titanium dioxide: Rutile, anatase, and brookite. *Physical Review B*, 51(19), p.13023.
82. Moawad, H., El–Rahim, W.M.A. and Khalafallah, M., 2003. Evaluation of biotoxicity of textile dyes using two bioassays. *Journal of basic microbiology*, 43(3), pp.218-229.
83. Mohan, S.V., Ramanaiah, S.V. and Sarma, P.N., 2008. Biosorption of direct azo dye from aqueous phase onto Spirogyra sp. I02: Evaluation of kinetics and mechanistic aspects. *Biochemical Engineering Journal*, 38(1), pp.61-69.
84. Moon, J., Yun, C.Y., Chung, K.W., Kang, M.S. and Yi, J., 2003. Photo-catalytic activation of TiO_2 under visible light using Acid Red 44. *Catalysis Today*, *87*(1), pp.77-86.
85. Mukherjee, P.S. and Ray, A.K., 1999. Major challenges in the design of a large-scale photo-catalytic reactor for water treatment. *Chemical Engineering and Technology*, 22(3), p.253.
86. Muscat, J., Swamy, V. and Harrison, N.M., 2002. First-principles calculations of the phase stability of TiO_2. *Physical Review B*, 65(22), p.224112.
87. Muschaweck, J., Spirkl, W., Timinger, A., Benz, N., Dörfler, M., Gut, M. and Kose, E., 2000. Optimized reflectors for non-tracking solar collectors with tubular absorbers. *Solar energy*, 68(2), pp.151-159.
88. Neamtu, M., Yediler, A., Siminiceanu, I., Macoveanu, M. and Kettrup, A., 2004. Decolorization of disperse red 354 azo dye in water by several oxidation processes—a comparative study. *Dyes and pigments*, 60(1), pp.61-68.
89. Neppolian, B., Choi, H.C., Sakthivel, S., Arabindoo, B. and Murugesan, V., 2002. Solar light induced and TiO_2 assisted

degradation of textile dye reactive blue 4. *Chemosphere*, 46(8), pp.1173-1181.

90. Ohenoja, K., Illikainen, M. and Niinimäki, J., 2013. Effect of operational parameters and stress energies on the particle size distribution of TiO_2 pigment in stirred media milling. *Powder technology*, 234, pp.91-96.
91. Ollis, D.F., 2005a. Kinetic disguises in heterogeneous photo-catalysis. Topics in catalysis, 35(3-4), pp.217-223.
92. Ollis, D.F., 2005b. Kinetics of liquid phase photo-catalyzed reactions: an illuminating approach. *The Journal of Physical Chemistry B*, 109(6), pp.2439-2444.
93. Patel, H. and Vashi, R.T., 2012. Removal of Congo Red dye from its aqueous solution using natural coagulants. *Journal of Saudi Chemical Society*, 16(2), pp.131-136.
94. Paxton, A.T. and Thien-Nga, L., 1998. Electronic structure of reduced titanium dioxide. *Physical Review B*, 57(3), p.1579
95. Pera-Titus, M., García-Molina, V., Baños, M.A., Giménez, J. and Esplugas, S., 2004. Degradation of chlorophenols by means of advanced oxidation processes: a general review. *Applied Catalysis B: Environmental*, 47(4), pp.219-256.
96. Prigione, V., Tigini, V., Pezzella, C., Anastasi, A., Sannia, G. and Varese, G.C., 2008. Decolourisation and detoxification of textile effluents by fungal biosorption. *Water Research*, 42(12), pp.2911-2920.
97. Prieto, O., Fermoso, J., Nuñez, Y., Del Valle, J.L. and Irusta, R., 2005. Decolouration of textile dyes in wastewaters by photo-catalysis with TiO 2. *Solar Energy*, 79(4), pp.376-383.

98. Puma, G.L. and Brucato, A., 2007. Dimensionless analysis of slurry photo-catalytic reactors using two-flux and six-flux radiation absorption–scattering models. *Catalysis Today*, 122(1), pp.78-90.

99. Rafatullah, M., Sulaiman, O., Hashim, R. and Ahmad, A., 2010. Adsorption of methylene blue on low-cost adsorbents: a review. *Journal of hazardous materials*, 177(1), pp.70-80.

100. Qamar, M., Saquib, M. and Muneer, M. 2005. Photocatalytic degradation of two selected dye derivatives, chromotrope 2B and amido black 10B, in aqueous suspensions of titanium dioxide. *Dyes and Pigments* 65 (1), pp. 1-9.

101. Rauf, M.A. and Ashraf, S.S., 2009. Fundamental principles and application of heterogeneous photo-catalytic degradation of dyes in solution. *Chemical engineering journal*, 151(1), pp.10-18.

102. Rodrıguez, S.M., Gálvez, J.B., Rubio, M.M., Ibáñez, P.F., Padilla, D.A., Pereira, M.C., Mendes, J.F. and De Oliveira, J.C., 2004. Engineering of solar photo-catalytic collectors. *Solar Energy*, 77(5), pp.513-524.

103. Rodríguez, S.M., Richter, C., Galvez, J.B. and Vincent, M., 1996. Photocatalytic degradation of industrial residual waters. *Solar Energy*, 56(5), pp.401-410.

104. Sachdeva, S. and Kumar, A., 2009. Preparation of nanoporous composite carbon membrane for separation of rhodamine B dye. *Journal of Membrane Science*, 329(1), pp.2-10.

105. Saquib, M., Tariq, M.A., Haque, M.M. and Muneer, M., 2008. Photo-catalytic degradation of disperse blue 1 using UV/TiO_2/H_2O_2 process. *Journal of environmental management*, 88(2), pp.300-306.

106. Saquib, M., Tariq, M.A., Faisal, M. and Muneer, M., 2008. Photo-catalytic degradation of two selected dye derivatives in aqueous suspensions of titanium dioxide. *Desalination*, 219(1-3), pp.301-311.

107. Sarioglu, M. and Atay, U.A., 2006. Removal of methylene blue by using biosolid. *Global Nest* J, 8(2), pp.113-120.

108. Sauer, T., Neto, G.C., Jose, H.J. and Moreira, R.F.P.M., 2002. Kinetics of photo-catalytic degradation of reactive dyes in a TiO_2 slurry reactor. *Journal of Photochemistry and Photobiology A: Chemistry*, 149(1), pp.147-154.

109. Sen, T.K., Afroze, S. and Ang, H.M., 2011. Equilibrium, kinetics and mechanism of removal of methylene blue from aqueous solution by adsorption onto pine cone biomass of Pinus radiata. *Water, Air, & Soil Pollution*, 218(1-4), pp.499-515.

110. Seyyedi, K. and Jahromi, M.A.F., 2014. Decolorization of azo dye CI Direct Black 38 by Photo-catalytic method using TiO_2 and optimizing of process. *Apcbee Procedia*, 10, pp.115-119.

111. Sikorska, E., Khmelinskii, I.V., Bourdelande, J.L., Worrall, D.R., Jasiewicz, B. and Sikorski, M., 2003. Diffuse reflectance spectroscopy in photochemistry of opaque food products-methods and applications. *Polish journal of food and nutrition sciences*, 12(Suppl. 2), pp.100-107.

112. Simons, P.Y. and Dachille, F., 1967. The structure of TiO_2II, a high-pressure phase of TiO2. *Acta Crystallographica*, 23(2), pp.334-336.

113. Sonune, A. and Ghate, R., 2004. Developments in wastewater treatment methods. *Desalination*, 167, pp.55-63.

114. Suarez-Parra, R., Hernandez-Perez, I., Rincon, M.E., Lopez-Ayala, S. and Roldan-Ahumada, M.C., 2003. Visible light-induced degradation of blue textile azo dye on TiO_2/CdO–ZnO coupled nano-porous films. *Solar energy materials and solar cells*, 76(2), pp.189-199.

115. Su, C., Tseng, C.M., Chen, L.F., You, B.H., Hsu, B.C. and Chen, S.S., 2006. Sol–hydrothermal preparation and photocatalysis of titanium dioxide. *Thin Solid Films*, 498(1), pp.259-265.

116. Szaciłowski, K., Macyk, W., Drzewiecka-Matuszek, A., Brindell, M. and Stochel, G., 2005. Bioinorganic photochemistry: frontiers and mechanisms. *Chemical reviews*, 105(6), pp.2647-2694.

117. Tan, I.A.W., Ahmad, A.L. and Hameed, B.H., 2008. Adsorption of basic dye on high-surface-area activated carbon prepared from coconut husk: Equilibrium, kinetic and thermodynamic studies. *Journal of hazardous materials*, 154(1), pp.337-346.

118. Tanaka, K., Capule, M.F. and Hisanaga, T., 1991. Effect of crystallinity of TiO2 on its photo-catalytic action. *Chemical Physics Letters*, 187(1-2), pp.73-76.

119. Thompson, T.L. and Yates, J.T., 2006. Surface science studies of the photo-activation of TiO2 new photochemical processes. *Chemical Reviews*, 106(10), pp.4428-4453.

120. Touati, A., Hammedi, T., Najjar, W., Ksibi, Z. and Sayadi, S., 2016. Photo-catalytic degradation of textile wastewater in presence of hydrogen peroxide: Effect of cerium doping titania. *Journal of Industrial and Engineering Chemistry*, 35, pp.36-44.

121. Van Well, M., Dillert, R.H., Bahnemann, D.W., Benz, V.W. and Mueller, M.A., 1997. A novel non-concentrating reactor for solar water detoxification. *Journal of solar energy engineering*, 119(2), pp.114-119.

122. Wang, J., Mao, B., Gole, J.L. and Burda, C., 2010. Visible-light-driven reversible and switchable hydrophobic to hydrophilic nitrogen-doped titania surfaces: correlation with photo-catalysis. *Nanoscale*, 2(10), pp.2257-2261.

123. Wunderlich, W., Oekermann, T., Miao, L., Hue, N.T., Tanemura, S. and Tanemura, M., 2004. Electronic properties of nono-porous TiO_2 and ZnO then films comparison of simulations and experiments. *Journal of Ceramic Processing & Research*, 5(4), pp.343-354.

124. Wyness, P., Klausner, J.F., Goswami, D.Y. and Schanze, K.S., 1994. Performance of non-concentrating solar photo-catalytic oxidation reactors: Part I—Flat-plate configuration. *Journal of Solar Energy Engineering*, 116(1), pp.2-7.

125. Wyness, P., Klausner, J.F., Goswami, D.Y. and Schanze, K.S., 1994. Performance of Non-concentrating Solar Photo-catalytic Oxidation Reactors: Part II—Shallow Pond Configuration. *Journal of solar energy engineering*, 116(1), pp.8-13.

126. Xu, L., Zhao, H., Shi, S., Zhang, G. and Ni, J., 2008. Electrolytic treatment of CI Acid Orange 7 in aqueous solution using a three-dimensional electrode reactor. *Dyes and Pigments*, 77(1), pp.158-164.

127. Yakuphanoglu, F., Cukurovali, A. and Yilmaz, I., 2004. Determination and analysis of the dispersive optical constants of some organic thin films. *Physica B: Condensed Matter*, 351(1), pp.53-58

128. Yang, Y., Wang, G., Wang, B., Li, Z., Jia, X., Zhou, Q. and Zhao, Y., 2011. Biosorption of Acid Black 172 and Congo Red from aqueous solution by nonviable Penicillium YW 01: Kinetic study, equilibrium isotherm and artificial neural network modeling. *Bioresource technology*, 102(2), pp.828-834.

129. Yao, Z., Wang, L. and Qi, J., 2009. Biosorption of methylene blue from aqueous solution using a bioenergy forest waste: Xanthoceras sorbifolia seed coat. *Clean–soil, Air, Water*, 37(8), pp.642-648.

130. Zangeneh, H., Zinatizadeh, A.A.L., Habibi, M., Akia, M. and Isa, M.H., 2015. Photocatalytic oxidation of organic dyes and pollutants in wastewater using different modified titanium dioxides: a comparative review. *Journal of Industrial and Engineering Chemistry*, 26, pp.1-36.
131. Zhang, Q., Gao, L. and Guo, J., 2000. Effects of calcination on the photocatalytic properties of nanosized TiO_2 powders prepared by $TiCl_4$ hydrolysis. *Applied Catalysis B: Environmental*, 26(3), pp.207-215.
132. Zhang, R. and Gao, L., 2001. Effect of peptization on phase transformation of TiO_2 nanoparticles. *Materials research bulletin*, 36(11), pp.1957-1965.
133. Zhang, T., ki Oyama, T., Horikoshi, S., Hidaka, H., Zhao, J. and Serpone, N., 2002. Photo-catalyzed N-demethylation and degradation of methylene blue in titania dispersions exposed to concentrated sunlight. *Solar energy materials and solar cells*, 73(3), pp.287-303.
134. Zhang, X., Chen, W., Lin, Z., Yao, J. and Tan, S., 2011. Preparation and photo-catalysis properties of bacterial cellulose/TiO_2 composite membrane doped with rare earth elements. *Synthesis and Reactivity in Inorganic, Metal-Organic, and Nano-Metal Chemistry*, 41(8), pp.997-1004.
135. Zonoozi, M.H., Moghaddam, M.A. and Arami, M., 2009. Coagulation/flocculation of dye-containing solutions using polyaluminium chloride and alum. *Water science and technology*, 59(7), pp.1343-1351.
136. https://wikipedia.org/wiki/Wastewater
137. https://wikipedia.org/wiki/Ultraviolet
138. http://www.nrel.gov/solar/spectra/am1.5
139. www.solargis.com/products/maps-and-gis-data
140. https://pubchem.ncbi.nlm.nih.gov/compound/.